The Hong Kong Polytechnic University

Department of Building Services Engineering

Effective Energy Simulation and Optimal Design of Side-lit Buildings with Venetian Blinds

Tian Cheng

A thesis submitted in partial fulfilment of the requirements for the degree of Doctor of Philosophy

August, 2010

CERTIFICATE OF ORIGINALITY

I hereby declare that this thesis is my own work and that, to the best of my knowledge and belief, it reproduces no material previously published or written, nor material that has been accepted for the award of any other degree or diploma, except where due acknowledgement has been made in the text.

Tian Cheng

Department of Building Services Engineering

The Hong Kong Polytechnic University

Hong Kong SAR, China

August, 2010

ABSTRACT

Venetian blinds are popularly used in buildings to control the amount of incoming daylight for improving visual comfort and reducing heat gains in air-conditioning systems. Studies have shown that the proper design and operation of window systems could result in significant energy savings in both lighting and cooling. However, there is no convenient computer tool that allows effective and efficient optimization of the envelope of side-lit buildings with blinds now. Three computer tools, Adeline, DOE2 and EnergyPlus widely used for the above-mentioned purpose have been experimentally examined in this study. Results indicate that the two former tools give unacceptable accuracy due to unrealistic assumptions adopted while the last one may generate large errors in certain conditions. Moreover, current computer tools have to conduct hourly energy simulations, which are not necessary for life-cycle energy analysis and optimal design, to provide annual cooling loads. This is not computationally efficient, particularly not suitable for optimal designing a building at initial stage because the impacts of many design variations and optional features have to be evaluated. A methodology is therefore developed for efficient and effective thermal and daylighting simulations and optimal design of buildings with blinds.

Based on geometric optics and radiosity method, a mathematical model is developed to reasonably simulate the daylighting behaviors of venetian blinds. Indoor illuminance at any reference point can be directly and efficiently

computed. They have been validated with both experiments and simulations with Radiance. Validation results show that indoor illuminances computed by the new models agree well with the measured data, and the accuracy provided by them is equivalent to that of Radiance. The computational efficiency of the new models is much higher than that of Radiance as well as EnergyPlus.

Two new methods are developed for the thermal simulation of buildings. A fast Fourier transform (FFT) method is presented to avoid the root-searching process in the inverse Laplace transform of multilayered walls. Generalized explicit FFT formulae for calculating the discrete Fourier transform (DFT) are developed for the first time. They can largely facilitate the implementation of FFT. The new method also provides a basis for generating the symbolic response factors. Validation simulations show that it can generate the response factors as accurate as the analytical solutions. The second method is for direct estimation of annual or seasonal cooling loads without the need for tedious hourly energy simulations. It is validated by hourly simulation results with DOE2. Then symbolic long-term cooling load can be created by combining the two methods with thermal network analysis. The symbolic long-term cooling load can keep the design parameters of interest as symbols, which is particularly useful for the optimal design and sensitivity analysis.

The methodology is applied to an office building in Hong Kong for the

optimal design of building envelope. Design variables such as window-to-wall ratio, building orientation, and glazing optical and thermal properties are included in the study. Results show that the selected design values could significantly impact the energy performance of windows, and the optimal design of side-lit buildings could greatly enhance energy savings. The application example also demonstrates that the developed methodology significantly facilitates the optimal building design and sensitivity analysis, and leads to high computational efficiency.

ACKNOWLEDGEMENT

I am especially grateful to my supervisor, Dr. Chen Tingyao, for making this research project possible, and for his indispensable guidance, constant support, and continuous encouragement throughout the course of my research work.

This project was funded by the Research Grant Council (RGC) of the Hong Kong SAR government under project No. RGEN and A-PJ11. The support of the RGC is gratefully acknowledged.

I also wish to dedicate this thesis to my mother and my wife for their patience, understanding, moral support and encouragement.

TABLE OF CONTENTS

LIST OF FIGURES

LIST OF TABLES

NOMENCLATURE

a	thermal diffusivity, m^2/hr
A	area, m^2
B	Final luminous exitance, Lux
b	z-transfer function coefficients, $W/(m^2℃)$
d	z-transfer function coefficients
D	depth, m
DF	daylight factor
EA	effective aperture
E_{en}	annual energy consumption related with building envelope, kWh
EI	electricity intensity used for the require illuminance intensity, kWh/m^2
E_l	energy conversation due to the utilization of daylighting, kWh
H	height, m
IL	illuminance, Lux
j	imaginary operator defined by $j^2 = -1$.
l	thickness, m
L	width of the blinds slat, m
M	transmission matrix
n	node
p_b	ratio of the slat area that can receive beam light to the entire slat area
q	heat flow, W/m^2
Q_c	cooling load, kWh
r_{ab}	solar absorpance of the window
r_t	solar transmittance of the window
R	thermal resistance, $m^2℃/W$
R_b	ratio of beam light on the blinds slat to the diffuse illuminance on the outdoor unobstructed horizontal plane
s	Laplace transform variable

S	heat source
SL	sky luminance distribution model
t	time, hr
T	temperature, ℃
T_v	window optical transmittance
U	heat transfer coefficient, W/(m^2℃)
V	volume, m^3
VDF	vertical daylight factor
VF	view factor
VIL	illuminance on the outside vertical surface of the blinds, Lux
W	width of window, m
y	convective thermal conductance, W/(m^2℃)
Y	response factor, W/(m^2℃)
Y_{RTS}	radiant time series, W/(m^2℃)
z^{-1}	backward operator
Z	thermal impedance, ℃/W

GREEK

α	altitude, °
β	slat tilt angle, °
γ	azimuth, °
ε	emissivity
η	efficiency
θ	incident angle, °
λ	thermal conductivity, W/(m℃)
ρ	reflectance
σ	Stefan-Boltzmann constant
φ	incident angle, °
ω	frequency, rad/hr

SUBSCRIPTS

a	indoor air
ac	air-conditioning system
b	beam sunlight
bl	blinds
dif	diffuse skylight
en	building envelope
gl	glazing
gr	ground
i	the *i*th variable
in	indoor
inf	infiltration
j	the *j*th variable
mea	measured value
o	outdoor air
p	power station
sim	simulated value
slat	blinds slat
sky	sky
sol	solar
r	multi-reflections on the interior surfaces of a room
ref	reference point
rm	room
win	window

CHAPTER 1

INTRODUCTION

Designing a building with the aim to minimize the life-cycle or long-term energy use and cost of buildings involves detailed evaluation of the impacts of many design variations and optional features. The effect of each option and each combination of these options needs to be evaluated so as to determine the most effective combination for adoption. This may only be practically handled by using an accurate and efficient building energy simulation model.

Detailed energy simulation programs such as DOE2 are widely used in current building optimal design. Most of these programs are based on hourly calculation. However, many cases, such as preliminary building design, optimal building design, and life cycle energy analysis only need to determine the annual cooling load. The utilization of hourly calculation in optimal design may lead to unnecessary calculation and long time-consumption.

For buildings with side windows, daylighting should be considered in the optimal design as it can reduce both the cooling and lighting energy. Venetian blinds are widely used to properly adjust the amount of incoming daylight for energy savings and to deal with glare for visual comfort. The daylighting simulation with venetian blinds is quite complicated. Some detailed lighting simulation programs such as Radiance can reasonably predict the indoor

illuminance with venetian blinds. However, the calculation with Radiance requires long time consumption because of the low efficiency of ray-racing method. This problem greatly hinders the utilization of Radiance in long-term daylighting simulation because there are thousands of working hours should be considered. To simplify the calculation, some other simulation programs, such as DOE2 and Adeline, adopted different assumptions for the long-term daylighting simulation with venetian blinds. However, the experimental validation results presented in chapter 4 indicate that these assumptions may result in large errors.

The main objective of this thesis is to develop accurate and efficient model for daylighting and thermal simulation. It consists of several techniques including discrete Fourier transform, fast Fourier transform, and symbolic analysis of buildings with generalized thermal network.

The main contributions of this these are the following:

(1) The accuracy of daylighting simulation results given by Adeline and DOE2 without and with blinds have been examined against measured data collected in a full-scale classroom. The results show that when the window is shaded with venetian blinds, Adeline and DOE2 cannot give acceptable results.

(2) An efficient and accurate model is developed for the simulation of indoor daylight illuminance when windows are shaded by venetian blinds. Algebraic

equations have been derived for computing different daylight factors and optical transmittances through the blinds, based on the geometric optics and radiosity method. The equations contain all the primary design variables that impact the efficiency and effectiveness of daylighting, and significantly enhance the computational efficiency of daylighting modeling. Hence, the model is particularly suitable for long-term daylighting simulation, optimal building design, and parametric analysis. The model has been validated against experimental results and the simulation results of Radiance. Validation results show that indoor illuminances computed by the model agree well with the measured data, and its accuracy is equivalent to that of Radiance.

(3) A new method has been developed for the direct and rigorous calculation of response factors of multilayered slabs. This method uses FFT, and hence does not need to numerically search for the poles of the image function of solutions to heat conduction through multilayered slabs. Calculating analytical response factors in each harmonics, the FFT method can generate response factors as accurate as the analytical solutions. Z-transfer coefficients have been generated by the least square method from accurate response factors. Validation results show that z-transfer coefficients obtained by this method are much more accurate than those by the conventional method.

(4) A novel method has been developed for the direct calculation of life-cycle, annual or seasonal cooling loads without the need for hourly simulations. The method is primarily based on the principle of superposition and symbolic transfer function. The principle of the method has been presented and applied to a simple example in Hong Kong. The new method can generate symbolic long-term cooling load, which keep important design parameters as symbols. Validation with DOE2 shows that the new model has high accuracy.

The remainder of this thesis is organized into nine chapters.

In the next chapter, a literature review is given. Topics covered include current methods for building optimal design, daylighting simulation with venetian blinds, generation of response factor and z-transfer coefficients of multi-layered wall and long-term building thermal simulations.

Chapter 3 represents a methodology for the development of accurate and efficient simulation models, which include daylighting simulation model with venetian blinds; method for rigorous calculation of response factors of multi-layered walls and model for direct calculation of long-term cooling load without hourly calculation.

In Chapter 4, the accuracy of daylighting simulation results given by

Adeline and DOE2 with and without venetian blinds have been examined against measured data collected in a full-scale classroom. The simulation results by Radiance are also presented for reference comparison to those data computed by the above two programs.

In Chapters 5 and 6, an accurate and efficient method for the calculation of indoor daylight illuminance with venetian blinds is developed. The new model considers the different features of daylights passing through blinds in their optical transfer process. The light transmissions are reasonably describes by algebraic equations based on the geometric optics and radiosity method. The new model has been validated with both experiments and Radiance.

In Chapter 7, a direct numerical method is developed for the rigorous calculation of response factors of multi-layered walls. This method is based on discrete Fourier transform. The Fast Fourier transform (FFT) is utilized to reduce the time consumption of the calculation. Through the least square method, the accurate response factors are then transformed to more accurate and reliable z-transfer coefficients as compared to other available methods. The whole method has been validated with theoretical results.

Chapter 8 represents a novel thermal simulation method is developed for the direct calculation of life-cycle, annual or seasonal cooling loads without

hourly calculation. The method is primarily based on the principle of superposition and symbolic transfer function. The Fourier transform method developed in chapter 7 is employed to generate the symbolic response factors. The new thermal simulation method has been applied to a typical room in Hong Kong and the simulation results are validated with DOE2.

In Chapter 9, an application example is given to show the advantages of the new daylighting and thermal simulation models in optimal design and parameter analysis. The optimization is based on an office building in Hong Kong. The aim of the optimization is to reduce the annual energy consumption related with room envelope, which include cooling, lighting and embodied energy. The hill-climbing and numeration methods are used in the optimization.

Finally, conclusions and recommendations for further work are presented in Chapter 10.

CHAPTER 2

LITERATURE REVIEW

2.1 Methods for building optimal design

Energy use in buildings accounts for a large percentage of the energy consumption world wide. In Canada, residential and commercial/institutional buildings consume about 30% of the total secondary energy use and also responsible for nearly 29% of CO_2 equivalent greenhouse gas emissions (Energy efficiency trends in Canada, 2003). A similar situation is also observed in the United States, where buildings account for 39% of the total primary energy consumption and 70% of the electricity consumption (Building energy data book, 2003). As the environmental impacts of buildings are acknowledged, there is a growing concern about the design of energy efficient buildings.

The successful design of energy efficient buildings requires that special attention is paid to the conceptual stage when many potential design alternatives can be generated and evaluated to obtain the most promising solution (Cofaigh *et al*., 1999). There are many design parameters influence the building energy performance. The combinations of these design parameters may lead to numerous design alternatives. Although many sophisticated energy simulation program such as DOE2 and Energy-Plus are available to study the impact of design parameters on building performance, the large number of design

alternative makes it virtually impossible to calculate all design alternatives to find the optimal combination of design parameters.

By now, the most popular method used in the optimal building design is based on the coupling of an optimization program or algorithms with an energy simulation program. The amount of calculations can be great reduced in this way. For example, Wang *et al*. (2005) coupled multi-objective genetic algorithm and a simulation program based on the ASHRAE toolkit to minimize the life cycle cost and life cycle environmental impact of an office building. The considered parameters include orientation, window-to-wall ratio, wall and roof type, and floor shape. Daylighting was not considered in the optimization. The optimization results suggest that the window area should be kept at its lower limit to save cost. Ouarghi and Krarti (2006) coupled neural network and genetic algorithm with DOE2 to optimizing the office building shape. The considered parameters include window-to-wall ratio, glazing type and the insulation of wall and roof. Daylighting and the embodied energy are not considered. The optimized window areas were not provided in the optimization results. Tuhus-Dubrow and Krarti (2010) coupled genetic algorithm and DOE2 to optimize building shape and building envelope features to minimize the energy use and life cycle energy cost for residential buildings. Optimization results show that small window area should be adopted for all orientations to save energy.

Although the utilization of optimization algorithm greatly reduced the amount of calculations, the optimization process is still time-consuming. It may take from several minutes (Ouarghi and Krarti, 2006) to more than a day (Wang *et al*., 2005), depending on the number of design alternatives. Additionally, due to the inherent randomness of some optimization algorithms, the optimization process may need to be repeated several times to get a reliable result (Wang *et al*., 2005), which further increases the computing effort. We cannot solve this problem by reducing the number of design alternatives because too few design alternatives may lead to inaccurate optimization results. Therefore, there should be a trade-off between the computing effort and the number of design alternatives.

Commercial buildings are generally occupied during daytime. So daylighting can be utilized to replace the artificial lighting. Daylighting has great energy-saving potential; especially for cooling-dominated commercial buildings because it can reduce the energy use in both lighting and cooling (Tian et al., 2010). The utilization of daylighting can also reduce the peak cooling load (Choi et al., 1984). All these make daylighting an indispensable part of the optimal design of buildings. However, the energy savings from daylighting are ignored in many previous optimization works (Wang *et al*., 2005; Ouarghi and Krarti, 2006; Tuhus-Dubrow and Krarti, 2010). The optimization results with daylighting may differ a lot from those without daylighting. For example, daylighting is ignored

in Wang et al. (2005) and Duhus-Dubrow and Krarti (2010)'s work. Their optimization results show that the window is an energy consumer and should be as small as possible. However, with the utilization of daylighting, the windows can be either energy consumer or energy saver, which depends on the window-to-wall ratio; and there is an optimal window area where the maximum energy can be saved (Chisi and Tinker, 2005; Tian et al., 2010).

Sensitivity analysis is widely performed at early stage of the building design process, where it can give important information about which design parameters to focus on in the next phases of design as well as information about the unimportant design parameters that only have a minor impact on building performance (Heiselberg *et al*., 2009). Lam et al. (2008) applied sensitivity analysis to analyze different design parameters' influence on the electricity use characteristics of 10 air-conditioned office buildings in Hong Kong. The design parameters include building envelope, HVAC system and HVAC refrigeration plant. DOE-2.1E was used for the energy simulation. 3-5 discrete values were used for each design parameter and the influence of each design parameter was evaluated by mean influence coefficient. The lighting energy saving from daylighting is not included in the analysis. Analysis results show that the electricity use is more sensitive to equipment load, lighting load, cooling set point. As daylighting was not considered, the window-to-wall ratio has positive influence coefficient, which means the increase of window area will increase the

electricity use. Tavares and Martins (2007) applied sensitivity to analyze the influence of different design parameters on heat and cooling load, and annual electric energy. VisualDOE was used for the building energy simulation. The design parameters include wall and roof type, window frames, air change rate HVAC system and thermostat set-point. The analysis was based on one base case and the sensitivity was evaluated by the perceptual difference to the base case. Analysis results show that the heating load is more sensitive to design parameters than cooling load and annual electric energy. Among all considered design parameters, roofing, HVAC system and thermostat set-point are more influential. In the work of Heiselberg et al. (2009), a sensitivity analysis was performed to identify the important design parameters to reduce the total building energy use for heating, ventilation, cooling and lighting, which was calculated by the software program BE06. Daylighting was considered in the analysis. 3 discrete values were used for each design parameter to represent the whole parameter range. The sensitivity of total energy use to design parameter was evaluated by the mean and standard deviation of the elementary effects. Analysis results show that for most of design parameters the influence on energy uses is nearly linear, meaning the impact is almost the same in the whole parameter range. Lighting control and lighting power are more influential than other design parameters.

As pointed by Heiselberg *et al*.(2009), the main barrier for application of sensitivity analysis in building performance assessment is the increase in

calculation time and complexity (Heiselberg *et al*., 2009). Ideally, the sensitivity analysis needs a continuous change of each design parameters within a reasonable range to acquire sufficient information for quantitative assessment of the influence of each parameter. However, this demands tremendous computing efforts. Even if advanced and efficient methods are used, a large amount of calculations may be needed for the investigation of a few variables. Therefore, only a few discrete values are often considered in the sensitivity analysis to represent the whole range. As mentioned previously, 3 values were used for each design parameter in the analysis of Heiselberg *et al*. (2009); and 3-5 values were used for each design parameters in the work of Lam *et al*. (2008). Fewer values can reduce the computational effort. However, if the design parameters have sharply changing influence on the output over the whole parameter ranges, too few discrete values may lead to wrong results.

2.2 Daylighting simulation methods with venetian blinds

Venetian blinds are widely used in commercial buildings to adjust the amount of incoming daylight, minimize the glare problem and reduce the solar heat gain through the windows. Although the blinds can deal with glare, it may reduce the indoor daylight illuminance by 10-40% when its tilt angles are between 45° upward and 45° downward (Galasiu et al., 2004). The optimal design and use of venetian blinds for maximizing energy savings in both lighting

and cooling requires computationally efficient and relatively accurate computer tools for long-term daylighting simulation.

Computer simulation tools have been widely adopted for the analysis of daylighting as well as building cooling loads due to solar heat gains through windows. Among them, Radiance (Ward and Shakespeare, 1998) is the most popular one used by designers (Reinhart and Fitz, 2006) for analysis of lighting distribution. It is an advanced lighting simulation program that can simulate complex geometries with flexible reflection and transmittance material, using a mixed stochastic, deterministic backward ray-tracing algorithm (Ward and Rubinstein, 1988; Ward and Shakespeare, 1998).

Radiance has been validated using the exterior sky conditions generated by either the sky scanner or the sky model in the simulations. Mardaljevic pursued studies (Mardaljevic, 1995; Mardaljevic, 2000) using the BRE-IDMP data set (Mardaljevic, 2001) to validate Radiance under real sky conditions. This data set consists of 'simultaneous measurements of the sky luminance distribution, the direct normal illumiannce and internal illuminance in a full-size mock office (together with other measurements)'(Mardaljevic, 2000). In 1995, Mardaljevic (1995) verified Radiance with measured interior illuminance based on sky scanner data that was collected simultaneously. Clear glazing and two types of light shelf were tested. Validation results show that Radiance is capable of

reliably modeling interior illumiannces under both clear and overcast sky conditions. The mean error was 5.6%. Mardaljevic's later work (Mardaljevic, 2001) indicates that daylight-coefficient-based Radiance is of with high accuracy for simulating rooms with bare window. Higher relative errors, which are greater than ±50%, occur more frequently at the reference point near the window.

The sky model has been used as well in the validation of Radiance. Freewan et al. (2008) used CIE standard clear sky model (CIE, 1973) in their Radiance simulation to examine the performance of light shelf Their Radiance simulation results are in good agreement with measured values under the clear sky. The relative error ranges from 2% to 28%. Gallasiu and Atif (2002) investigated the accuracy of Radiance in simulating daylight illuminance distribution in an atrium building. They concluded that Radiance can generate accurate results in overcast sky and diffuse daylight. Although they found large errors, which may be as much as 100%, in simulations of direct sunlight, they believed that these errors are primarily caused by the inaccurate modeling of the fenestration of the atrium. Reinhart and Walkenhorst (2001) used the Perez sky model (Perez et al., 1993) to validate a Radiance-based daylight coefficient approach with measured data. The façade of the test office featured a double glazing and external venetian binds. The researchers found that daylight autonomies could be predicted with a relative error below 2% points, where simulation errors stem with roughly equal parts from the Radiance algorithm and the Perez sky model. Reinhart and Andersen

(2006) demonstrated that the combination of Perez model and a Radiance-based daylight coefficient approach can satisfactorily simulate interior illuminance with translucent panel. The overall mean bias error (MBE) and root mean square error (RMSE) are below 9% and 19%, respectively.

Radiance is not an appropriate choice for annual daylighting simulation in buildings primarily due to two reasons. First, the simulation of venetian blinds with Radiance is quite complicated. As there are thousands of working hours in annual simulation, great amount of time is needed for the simulation in one year. Second, the tilt angle of the blinds should be variables to respond to time-varying outdoor weather conditions. Therefore, many Radiance models with different tilt angles should be created and Radiance has to select the appropriate model in each hour in simulation based on current condition, which is difficult to be realized.

DOE2 and Adeline could be suitable computer simulation tools for long-term daylighting analysis because they are computationally efficient and can be conveniently used in practice.

Adeline is popular in long-term daylighting analysis and design (Adeline, 1994; Galasiu and Atif, 2002; Bodart and Herde, 2002; Tian et al., 2010), and consists of Radiance and several other programs. It includes Scribe, a

CAD-program used to describes the geometry of the space using 3D-modeling; Plink, a program used to assign material properties; Superlite, a daylighting simulation programs based on the radiosity method; Radlink and Superlink. The last two programs can link Radiance and Superlite with other energy simulation programs, respectively, to evaluate long-term energy performance of daylighitng based on hourly weather data. Both Radlink and Superlink have high efficiency in long-term simulation. However, the assumption behind their simulation is not explicitly described. Their accuracy in shading simulation has not been examinated.

DOE2 is an hourly building energy simulation program that can be used for both building heat transfer and daylighting simulations (Winkelmann and Selkowitz, 1985). It has been widely used in dayligting analysis and design (Choi et al., 1984; Lee and Selkowitz, 1995; Krarti et al., 2005). The user can specify one or two reference points in a space for daylighting analysis. DOE2 then uses standard CIE clear (CIE, 1973) and overcast sky (Moon and Spencer, 1942) models at 20 different solar positions to predict daylight illuminance at the reference points based on hourly exterior irradiance data. In DOE2, the entire shading device is assumed as perfect diffuser (Winkelmann and Selkowitz, 1985). DOE2 was verified for daylighting simulations without shading (Winkelmann and Selkowitz, 1985). It was found that DOE2 can provide satisfactory simulation results for most places throughout the room except the places near the

window and far away from the window. The reason is that DOE2 uses the split-flux method for calculating the internally reflected illuminance, which gives overestimated results in the area far away from the window and underestimated values in the area near the window (Winkelmann and Selkowitz, 1985).

EnergyPlus can also be used for daylighting simulation. The basic simulation method is derived from DOE2, with three major differences. Firstly, EnergyPlus considers four sky types – clear, clear turbid, intermediate and overcast. Secondly, in Energyplus, the clear sky daylight factor are calculated for hourly sun-path sun positions several times a year whereas in DOE2 these daylight factors are calculated for a set of only 20 sun positions. Thirdly, EnergyPlus uses radiosity method for blinds simulation. Like DOE2, EnergyPlus can only use up to 2 reference points for each zone (EnergyPlus Engineering Reference, 2011).

The above literature review shows that venetian blinds are popularly used as shading device to deal with glare and to control the solar heat gain through the windows. Long-term daylighting simulations are usually needed for the optimal design of windows, including window size, optical properties orientation, etc. Although Radiance has been extensively validated in different buildings and optical devices, it is not suitable for long-term simulations. Due to the high computational efficiency of DOE2 and Adeline, they have been popularly used

for the long-term daylighting analysis of buildings, even though they have not been validated for daylighting simulations with venetian blinds until now. Therefore, there is really the need for the examination of these two programs and the assumptions used by them. This will ensure that the published data generated by them will not mislead the readers and will provide confidence for researchers and engineers to use the two programs for the mentioned purpose in the future.

Some models have been provided for the simulation of light transmittance through blinds. Pfrommer et al (1996) developed optical blinds models for both specular- and diffuse-reflecting surfaces. The model takes into account both the reflections between adjacent slats and the reflections between the blinds and the glazing. However, only two reflections between slats are considered by this model, which may lead to underestimation of the shading transmittance the blinds (Chantrasrisalai and Fisher, 2004). Breitenbach et al. (2001) provided a model for the simulation of light passing through blinds with and without reflection on slat surfaces. This model divides the incident light into several groups based on number of reflections they will experience among slats. Then the overall transmittance of the blinds can be obtained by multiplying the fractions of light in each group by corresponding transmittances. This model can be applied to both pecular- and diffuse-reflecting surfaces. However, the reflection between blinds and glazing is ignored. Kotey and Wright assumed the slat reflect diffusely any incident radiation. Then a simplified radiosity method is used to calculate the light transmittance and reflection of blinds. However,

similar to the model of Breitenbach et al.(2001), the reflection of glazing is not taken into consideration.

Although some models have been generated for simulation of venetian blinds, most of them do not consider the reflections on glazing. And the reflections between the internal surface of the room and blinds are ignored by all the models mentioned above. In addition, all these model only aim at the calculation of shading transmittance, which is not adequate for daylight simulation. For example, as observed from our experimental results (shown in Chapter 4), the light directly reflected from blinds slats may contribute a lot to the room illuminance, especially when the slats are in nearly vertical position and obstruct most of the incident light. This is difficult to simulate if only the shading transmittance is available.

2.3 Calculation of response factor and z-transfer coefficients of multi-layered wall

The heat transfer through building constructions is one of the principal components of space cooling/heating load and energy requirements of a building. For the purpose of detail evaluation of energy consumption and dynamic simulation of HVAC system, it is necessary to conduct transient thermodynamic analysis for heat flow in building construction. Many methods have been developed for the solving of heat transfer problem. Based on their approaches for

solving the one-dimensional heat conduction equation, these methods may be categorized into four groups: (1) numerical methods; (2) harmonic methods; (3) response factor methods and (4) z-transfer function method.

The harmonic method can be used to solve the heat conduction problem if the boundary conditions are periodic and can be approximated by the coefficients of Fourier series. The thermal characteristic of wall is determined by the admittance transfer functions (magnitude and phase lag angle), which are function of frequency, thermal properties and geometry. Each selected harmonic then can be processed separately and modified by admittance transfer functions appropriate to its frequency. For inputs with more than one harmonic, the total thermal response of the wall may be obtained by superposition of the individual response of all harmonics. The accuracy of this method is determined by the number of harmonics. In practical, people usually use a limited number of Fourier series coefficients to simplify the calculation. In this condition, larger error many be introduced if too few harmonics are used.

The response factor method and z-transfer function method are widely used in many computer programs for solving the heat conduction problems. For example, DOE2, a detailed building energy simulation program, uses response factor to calculate heat gains and losses by conduction through building constructions (LBNL, 1982). BLAST used both methods for the analysis of

transient heat conduction through walls (Hittle 1979). HVACSIM$^+$ (Park et al., 1986), TRNSYS (Klein et al., 1994) and EnergyPlus (Strand et al., 1999) use z-transfer function method in their thermal calculation. The major advantages of these two methods are that they are not numerical in the sense of finite difference techniques, and they do not require the heat conduction boundary condition be periodic.

Traditionally, the Laplace transform is used in the calculation of response factors. First, the temperature inputs are approximated as overlapping triangular pulses. Each pulse can be transformed into frequency domain by the use of Laplace transform. Multiplying the Laplacian of a unit triangular pulse with appropriate transfer function of the wall, we can obtain the response of the wall to this pulse in frequency domain. The unit triangular pulse response is finally transformed back to the time domain by inverse Laplace transforms and the time-series representation of the response in time domain are response factors.

However, the series of response factor may be very long, especially for walls with high mass. In this case, Mitalas and Stephenson (1971) subsequently developed the z-transfer function method based on the response factor method. Unlike response factor method, the calculation of heat transfer through a wall by z-transfer function needs not only temperature but also heat flux at previous time steps. Then the heat flow can be calculated from very short series of z-transfer

function coefficients, which are Z-transform of the responding response factors. Harris and McQuiston (1988) published the z-transfer function coefficients for 41 wall and 42 roof constructions. These coefficients are given in the 1993 and 1997 ASHRAE Handbook of Fundamentals.

Both response factors and z-transfer coefficients were originally calculated using the inverse Laplace transforms. The inverse can be achieved by the method of residues. In this method, a number of roots of the transfer have to be found first. Then the same number of derivatives and residues at these roots must be calculated. For single-layered slabs, the analytic solution of the inverse can be readily obtained by this method. However, for most constructions with more than one layer, finding the roots is very cumbersome and tedious because the transfer functions are complex hyperbolic functions. As there are risks to miss several roots in numerically search, especially where two adjacent roots lying close together (Hittle and Bishop, 1983), roots of the transfer function must be searched by numerical iteration with very fine increment. The number of roots required increases as $(\text{time-step})^{-0.5}$, which will certainly increase the time consumption of the calculation.

As the root-finding process is computationally inefficient and may lead to miscalculation due to missing several roots in numerically searching, many methods have been developed to improve the calculation. Hittle and Bishop

(1983) proposed a method to improve the root-finding procedure. Unfortunately, this method is quite complicated and is difficult to program. Some new methods were later developed, which can avoid the root-finding procedure. These include the state space method (Ouyang and Haghighat, 1991) and time-domain method (Davies, 1996; Davies, 1997). The state space method is similar to finite difference techniques (Strand *et al*., 1999). Its accuracy, computation speed and stability depend on its time step and space step. Large time and space step may cause instability and poor accuracy. Some measures must be taken to improve its convergence. Contrarily, small time and space step means long time consumption for iterative computation. The computation of decay times in time-domain methods is essentially the same thing as numerically searching for the roots of the hyperbolic characteristic equation, and is also a time-consuming iteration.

2.4 Methods for long-term building thermal simulations.

Many simulation methods and computer programs (Kerrisk *et al*., 1981; Rabl and Riahle, 1992; Sowell and Hittle, 1995; ASHRAE Handbook, 2001; Al-Homoud, 2001; Crawkey et al., 2001) have been developed for calculating operation energy in the past four decades. Building energy analysis techniques may be classified into three categories, namely simplified energy estimation, inverse modeling and detailed energy simulation (ASHRAE Handbook, 2001). The long-established degree-day and modified degree-day methods are useful for estimating energy use in buildings where heat loss is mainly due to

indoor/outdoor temperature difference. However, the methods do not account for the effects of solar radiation and humidity, thermal mass of the fabric, etc. Whereas the bin and modified bin methods can overcome some of the shortcomings, they are still unable to accurately reflect the effects of solar gains and thermal mass (Al-Homoud, 2001).

Inverse models have been used primarily in empirical studies of building thermal systems. Black-box modeling and grey-box modeling are the two approaches commonly used (Al-Homoud, 2001). Black-box modeling focuses simply on the relation between the system inputs and outputs and ignores the physic processes of the system. Unlike the black-box approach, a grey-box model is derived based on the physical principles that govern the response of the system to exogenous inputs (Rabl and Riahle, 1992). This makes a grey-box model more efficiently applied in building energy analysis. However, existing grey-box building models predict cooling loads simply based on steady heat balance, which provides accuracy no better than the modified bin method.

Until now, accurate modeling of the dynamic behaviors of buildings requires the use of a detailed hourly building energy simulation program, such as DOE2, TRNSYS or EnergyPlus (Kerrisk *et al*., 1981; Sowell and Hittle, 1995; Al-Homoud, 2001; Crawkey et al., 2001). Nearly all such programs are based on either one of two types of simulation techniques. Time domain techniques such

as finite difference and state-space methods are used to numerically solve a set of non-linear and time-dependent heat balance equations, to yield reasonably accurate predictions. For such numerical models in general, some internal temperatures of no interest have to be calculated. These are the major reasons that models based on this type of methods are significantly less efficient compared to those that are based on the transfer function methods. The latter type of models, however, needs an assumption that heat transfer processes in buildings are approximately linear and time-invariant. Some popular building energy simulation programs, such as DOE2, adopt this assumption.

Obviously, there is a gap between the detailed hourly simulation method and the modified bin method for building energy analysis. Many cases, such as preliminary building design, optimal building design, and life cycle energy analysis only need to determine the annual cooling load. However, detailed hourly simulations have to be performed now because there is no an effective analysis method available.

2.5 Objectives

The specific objectives of this thesis are the following:

(1) The accuracy of daylighting simulations with venetian blinds by DOE2 and Adeline and the assumptions adopted by them will be validated by experiments conducted in a full-scale classroom.

(2) An accurate and efficient daylighting simulation model will be developed for prediction of indoor daylight illuminance with venetian blinds. The model should include the primary design parameters that impact the daylighting performance. This is particularly useful for optimal design and parametric analysis.

(3) A novel thermal simulation model will be proposed for the accurate and efficient calculation of long-term cooling load. The development of the model consists of two steps. First, the method for the rigorous calculation of response factor of multi-layered wall will be developed. This method can be used to generate symbolic response factor from symbolic transfer functions obtained from thermal network analysis. Next, method for the direct calculation of long-term cooling load without hourly calculation will be developed.

CHAPTER 3

METHODOLOGY

A methodology is presented for the development of accurate and efficient models for long-term daylighting and thermal simulations. The methodology consists of four parts. The first part is a model for the simulation of indoor daylight illuminance with venetian blinds. The second part is a method for the rigorous calculation of response factors of multi-layered walls. The third part is a method for the direct calculation of long-term cooling load without hourly simulation. The last part presents a method for the generation of symbolic long-term cooling load.

The methodology consists of the following steps:

(1) The indoor daylight factor with venetian blinds consists of three parts: the daylight factor due to diffuse light passing through gaps between blind slats and direct reaching the reference point; the daylight factor due to multi-reflections among the different interior surfaces of walls, ceiling and floor, and the daylight factor due to reflection directly from the blinds slats. The first one can be calculated by integration. The second daylight factor is calculated by either radiosity method or regression equations obtained by more detailed computer tools such as Radiance. The calculation of the second and third daylight factors needs luminous exitances on corresponding surfaces, which are computed by radiosity method.

(2) Based on a principle that different transfer functions should be equivalently transformable, discrete Fourier transform is utilized to rigorously calculate the response factors of multi-layered slabs. The fast Fourier transform (FFT) is utilized to reduce the time consumption of the calculation. The least square method is used to generate z-transfer coefficients from accurate response factors.

(3) The heat transfer processes in a building is approximately treated as linear and time-independent. Then the method for the direct evaluation of dynamic long-term cooling load without the need for hourly thermal simulation is developed primarily based on the principle of superposition. The method can be applied to both continuous and intermittent operation schedules. For intermittent operation, the hourly cooling loads in steady and continuous operation schedule may be imagined as convectively supplied heat during unoccupied hours, which will result in additional cooling load during occupied hours.

(4) The method developed at step (2) does not need to change the format of the original Laplace transfer function. Therefore, symbolic long-term cooling load can be created by combining the new methods developed in steps (2) and (3) with thermal network analysis.

All components of this methodology will be developed and discussed in detail in the following chapters.

CHAPTER 4

EXPERIMENTAL AND SIMULATING EXAMINATION OF COMPUTER TOOLS, RADLINK AND DOE2, FOR DAYLIGHTING AND ENERGY SIMULATION WITH VENETIAN BLINDS

Venetian blinds are widely used to properly adjust the amount of incoming daylight for energy savings in lighting and cooling and to deal with glare for visual comfort. Two computer tools, Radlink in Adeline and DOE2, have been popularly used for long-term daylighting simulation with venetian blinds because they are computationally efficient and relatively convenient for use. Unlike Radiance, DOE2 and Radlink simplify the simulation by adopting some assumptions for high computational efficiency. However, the two tools and the assumptions adopted by them for the simulation of venetian blinds have not been validated until now. Therefore, indoor illuminances with and without venetian blinds were measured in a full-scale classroom under variant sky conditions, and were used to examine them. Experimental and simulated results show that without blinds, both DOE2 and Adeline with Radiance can accurately predict indoor daylight distribution, except that DOE2 gives relatively large errors near and far away from windows. With blinds, the root mean square error (RMSE) between the measured illuminances and those computed by Radlink and DOE2 are 80% and 48% under overcast sky, respectively, and 68 and 75 under clear sky.

Analysis of the results shows that it is the assumptions used in Radlink and DOE2 that result in large simulation errors and unrealistic indoor illuminance distribution. These errors could lead to largely misestimated energy use in both lighting and cooling, and hence should not be acceptable. Therefore, more accurate and efficient computer tools need to be developed for the simulation of venetian blinds. The analysis also reveals that any assumption that does not take into account the different features of daylight passing through blinds in their optical transfer process could result in significant computation errors.

4.1 Experimental set-up

Experiments were carried out in a full-scale classroom in the campus of the Hong Kong Polytechnic University. The internal dimensions of the classroom are 8.9m (width) × 8.9m (depth) × 2.6m (height) and the window is integrated on the façade facing 10 degrees east of south. The window has the same width as that of the room and the height of its upper and lower edges is 2.2 m and 1.1 m, respectively. Figure 4.1-(a) indicates the dimension of the classroom and the dimension and position of the window on the façade. The window is glazed with clear glass whose measured optical transmittance is 0.78. The width of window bars was 10 cm and the width of glazing panes was 90 cm. The floor is covered with textile carpet, the walls are painted, and the ceiling is equipped with plasterboard. Figure 4.1-(b) shows the position of 6 reference points at which the indoor daylight illuminance is measured. All the reference points were located

along the centre line of the test room because these places are usually used as reference points in daylighting simulations (Mardaljevic, 1995; Krarti et al., 2005). The reference points are 1.3 m apart, starting at 1.1 m away from the window. Daylight illiminance was measured at 0.75 m from the floor surface. The classroom was on the fifth floor. The nearest building was about 150m in front of the classroom and that building was about 15 m higher than the window of the classroom. Hence, external obstructions to the window of the classroom should be negligible.

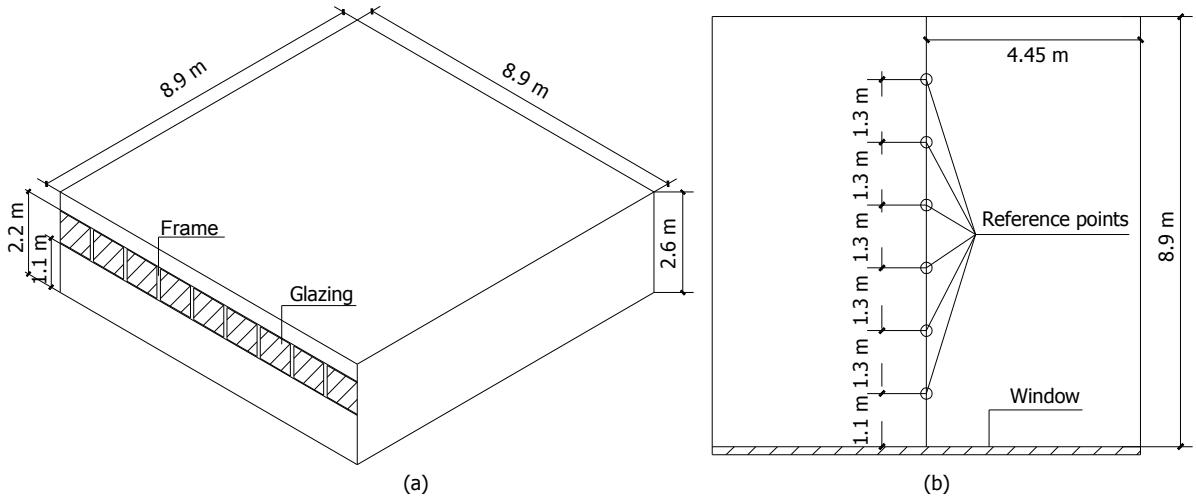

Figure 4.1. Schematic diagram of the classroom,
(a) room dimensions, (b) floor plan.

Venetian blinds with horizontal painted slats were suspended and the middle surface of the blind slats was 2.5 cm in parallel to the interior surface of the window glass. The slats were slightly curved (shown in Figure 4.2) and their thickness was 0.4 mm. All slats were arranged 2.3 cm apart. The tilt angle, as shown in Figure 4.3, could be set to any value between 90° and -90°, with zero on horizontal, anti-clockwise positive and clockwise negative. The title angle

was respectively set to -60°, -30°, 0°, 30° and 60°, in the experiments.

Lux meters (DL-202) with accuracy of ±6% were used for the measurement of indoor and outdoor illuminances. A Kipp&Zonen shadow ring was used to measure the horizontal diffuse illuminance. The horizontal beam illuminance can be calculated by substracting the diffuse illuminance from the global illuminance. All measurements were taken at the time interval of 15 minutes, from 9 am to 5 pm. Experiments were carried out from January 2007 to March 2008. The outdoor daylight illuminance and diffuse illuminance at the outside surface of the window, and the indoor horizontal daylight illuminance at the reference points were simultaneously measured each time. The sky was considered as overcast when the ratio between beam illuminance and global illuminance is less than 0.5%. The whole set of measured data was discarded when the global illuminance is less than 1000 Lux.

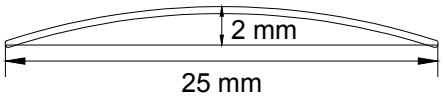

Figure 4.2 Geometric shape of individual slat

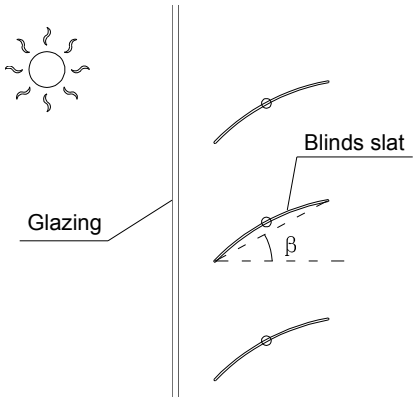

Figure 4.3. Sketch of blind slats at the tilt angle of β.

4.2 Examination approach

The CIE Technical Committee 3.33 and the Subtask C of the IEA SHC Task 31 proposed the benchmarks consisting of a set of reference test cases against which the accuracy of different lighting programs can be fairly and independently assessed in various aspects (CIE, 2004). The primary principle of the proposed validation approach is to design a test with a minimum number of independent parameters so as to minimize uncertainty due to errors caused by different influence parameters or sources. This also allows us to make the objective comparisons among lighting programs and to identify the weaknesses and strengths of them. Users can understand the limitation of individual programs based on validation results, and properly select the most suitable tool according their needs.

Hence, this experimental study will only follow the principle of recommended approach, i.e. to minimize uncertainties in the study by reducing the number of influence sources or variables. Daylight illuminances without and

with blinds in the same room will be measured and compared. This will help to estimate how much error is caused primarily by blinds rather than by bare glazing system. Ideally, experiments should be carried out in the both back and normal surfaces of the classroom to isolate the illuminance caused by internally-reflected daylight among the interior surfaces from the other daylight. To reduce the time of experiments and to overcome the limitation of resources, however, an alternative approach was adopted to identify factors causing the error. In addition to the above-mentioned experiments, simulation analyses will be carried out with Radiance to identify the implicit assumptions adopted in Radlink, and to determine the errors caused by the assumptions in the two programs. Although the computer tools to be examined are DOE2 and Radlink, simulation results by Radiance will also be presented for comparison to the data computed by the other two programs.

4.2.1 Exterior illuminance models

Exterior daylighting illuminances used as input to the computer tools are fundamental data, which are also very important to obtain the reliable simulation results. There are two primary types of models for describing them: the sky scanner and the sky model. The sky scanner measures the sky luminance distribution by scanning the sky dome. The collected sky luminance data reflect the real sky conditions. They can help to assess the intrinsic accuracy of the simulation programs under different real sky conditions because the errors

possibly caused by sky models can be eliminated. On the other hand, the sky scanner data is scarce and generally not publicly available. It requires a great amount of efforts to produce it locally, which may not be so practical. This makes researchers and engineers to use a practical alternative, i.e. the sky model. The sky model is much simpler as it only requires exterior direct and diffuse illuminance inputs, which may be directly computed from locally available solar irradiance records. The use of the simple sky model will inevitably introduce errors because the sky model produces exterior illuminances somehow different from more realistic data given by the sky scanner. Fortunately, previous studies have showed that the use of the sky model in simulations can generate relatively accurate results as compared to those by the use of the sky scanner (Freewan et al., 2008; Galasiu and, Atif, 2002; Reinhart and Walkenhorst, 2001; Reinhart and Andersen, 2006).

Several sky models, such as Perez sky model (Perez et al., 1993), are available currently. The CIE standard clear (CIE, 1973) and overcast (Moon and Spencer, 1942) sky models are most widely used now. Adeline (1994) and DOE2 (Winkelmann and, Selkowitz, 1985) use the CIE standard sky models as the default models, and Radiance also has an option for using these models. Hence, they will be adopted in the simulations.

4.2.2 Model properties

The reflection on the slat surfaces is highly determined by the coating. Andersen et al. (2005) experimentally studied the reflective properties of blind slats and found that the reflectance of painted slats is very diffuse and can be seen as Lambertian surface. However, the reflection of slats with mirror coating may have highly directional properties (Andersen et al., 2005). For these surfaces, the incident angle of the light has to be considered as it determines the number of reflections between slats (Breitenbach et al., 2001), thus influencing the shading transmittance. 2-D ray-tracing technique can be used for the simulation of specular reflecting surfaces (Parmelee and Aubele, 1952; Pfrommer et al., 1996).

For Radiance, users need to input the geometry of a space, and the characteristics of surface materials and light sources. The program can then generate photo-realistic color images showing the predicted daylight levels at any points in a room. Only painted slats are considered in the examination, which are assumed as Lambertian surface (perfect diffusers) in the Radiance simulation. The reflectances of the internal surfaces of the classroom and the blind slats were determined according to (Zhao, 1984) and (Rea, 2000). They are listed in Table 4.1. The built-in *Gensky* program and measured exterior illuminances were used to generate the sky conditions. The blinds were modeled with the *mkillum* program, which is the recommended approach for treating blinds (Ward and Shakespeare, 1998). Table 4.2 presents a list of utilized Radiance simulation

parameters.

Table 4.1 Reflectance of the interior surfaces of different room components.

Name	Description	Reflectance (%)
Wall	Painted with yellow color	57
Ceiling	Equipped with white plasterboard	30
Floor	Covered with texture carpet	10
Blinds slats	Painted with white color	60

Table 4.2 Input parameters to Radiance simulation.

Ambient bounces	Ambient division	Ambient sampling	Ambient accuracy	Ambient resolution	Direct threshold	Direct sampling	*-s* (*mkillum*)	*-d* (*mkillum*)
7	4096	1024	0.1	128	0.03	0.02	64	96

Radlink requires shading coefficient for shading simulation. Since there is not any assumption explicitly described in Radlink, we analyzed daylight illuminances computed by Radlink with and without blinds. Examination of these results indicates that the computed illuminances with blinds are strictly proportional to the computed results with bare glazing. This implies that Radlink actually adopts an assumption that the incoming daylight would not change its direction when passing through the shading device, and its intensity decreases proportionally to the shading coefficient. In other words, the shading coefficient actually acts as the optical transmittance in Radlink.

DOE2 and Radlink do not consider the real properties of the slat surfaces because they use assumptions for blinds. As many fixed settings are predetermined by these two programs, we only need to input shading

transmittance and whether or not the shading device is used. In Radlink, two shading system types were used. The first one is "*None"*, which means there is no shading device. Another one is "*Fixed*", which means the shading device is always utilized. We only need to input the shading transmittance under "*Fixed*" system type. For DOE2, the utilization of shading device is controlled by *Shading Schedule*. There is no shading if the schedule value is 0; and the shading is used if a shading transmittance value is input to the schedule.

Both Radlink and DOE2 require the user to input the transmittance of shading device. It is defined as the ratio between the vertical illuminances after and before the blinds. The value generally cannot be obtained directly, and may be determined by either calculation with an accepted computer program or experiment (Aleo et al., 1994; Athienitis and Tzempelikos, 2002). Obviously, it should be more convenient to use the former way in practice. In this study, the transmittances of the blinds were first determined by both experiments and Radiance simulations. Two Lux meters were used for the determination of shading transmittance. One measures the vertical illuminance between the window glazing and blinds. Another meter measures the vertical illuminance right after the blinds. The ratio between two measures is the shading transmittance from experiments. Radiance can not explicitly compute the shading transmittance. Therefore, the shading transmittance is determined in a similar way. Two reference points are created in the Radiance simulation model, which

are placed before and after the blinds. The ratio between the simulated illuminances on these two points is the shading transmittance from Radiance simulation.

Figure 4.4 represents the measured and computed transmittances at the different title angles of the slat for overcast sky. It can be seen that a good agreement between the computed and measured transmittances can be achieved. Under clear sky, the transmittance of the blinds is a function of both slat tilt angle and solar incident angle. Similar to the cases under overcast sky, we found that the computed transmittances agree well with experimental results under different tilt angles and solar incident angles. Then the computed transmittances were used in Radlink and DOE2 simulations.

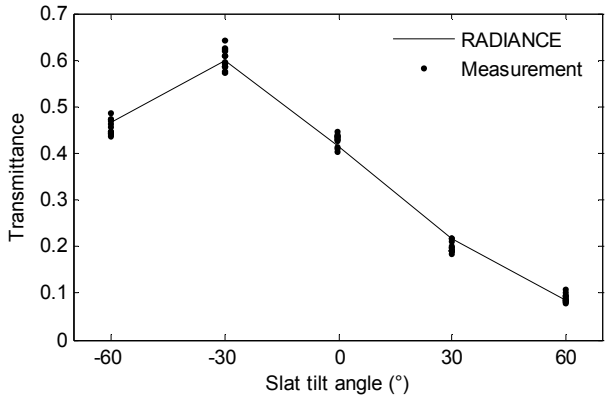

Figure 4.4. Measured and calculated transmittance of the blinds, overcast sky.

4.2.3 Conversion of measured outdoor illuminance to inputs required by the computer tools

The three computer programs may require the different types of inputs and provide the different types of outputs, which may be also different from the type of measured data. A key to reasonable comparison is to have a comparable basis. Hence, some inputs to computer programs may need to be pre-treated while outputs post-treated in order to generate the comparable simulated results in the same sky condition as those in the corresponding experiments.

Radiance requires outdoor beam and diffuse irradiances as inputs, which are converted to outdoor illuminance with a luminous efficacy model (Ward, 1998). Users should use the built-in *Gensky* program to define the sky types. The ratio of outdoor solar irradiance to illuminance was first determined based on Radiance simulation results. Then, this ratio and the measured outdoor illuminances were used to calculate the outdoor beam and diffuse irradiance required for inputs to Radiance. The outdoor illuminances converted from the input solar irradiances were compared to the original measured outdoor illuminance data. It was found that the measured outdoor illuminances and those values computed by Radiance are exactly equal.

DOE2 requires hourly outdoor beam and diffuse irradiances, and fractions of the skydome covered with clouds (*CR*) as inputs. The hourly *CR* data are used to

discriminate different sky types. Clear and overcast skies are represented by $CR \leq 0.2$ and $CR = 1.0$, respectively. Similar to Radiance, the input beam and diffuse irradiances are converted to outdoor beam and diffuse illuminance through a luminous efficacy model (Winkelmann and Selkowitz, 1985). The input data to DOE2 should make sure that it uses the same outdoor illuminances and the sky conditions as those in the experiment. Therefore, these outdoor illuminances in the Input Function provided by DOE2 were replaced by the measured values, and the real CR was input to DOE2 as well.

Radlink requires monthly atmospheric turbidity and hourly sunshine probability (*SSP*) data as inputs. Similar to the *CR* data in DOE2, the hourly *SSP* data are used to discriminate different sky types. Clear and overcast skies are represented by $SSP = 1.0$ and $SSP = 0.0$, respectively (Szermann and Stoffel, 1999). Radlink does not directly generate indoor illuminances, but the daylight factors in the space under both clear and overcast skies. Hence, SSP was input to Radlink first according to the real sky conditions in the experiment. The output results, i.e. daylight factors at different reference points, from Radlink were post-treated by multiplying them with the measured outdoor illuminances so as to obtain the indoor illuminances.

4.2.4 Comparison indexes

The accuracy of the simulation tools was quantified by mean bias error

(MBE) and root mean square error (RMSE). MBE indicates the average bias deviation between the computed results and measured values while RMSE shows the statistically absolute deviation between the two values. MBE and RMSE are expressed by

$$MBE = \frac{\sum_{i=1}^{n} \frac{E_{i,s} - E_{i,m}}{E_{i,m}}}{n} \tag{4.1}$$

$$RMSE = \sqrt{\frac{\sum_{i=1}^{n} \left(\frac{E_{i,s} - E_{i,m}}{E_{i,m}} \right)^2}{n}} \tag{4.2}$$

where $E_{i,s}$ and $E_{i,m}$ are corresponding simulated and measured indoor illuminance (Lux), respectively; and n is the number of a pair of simulated and measured data.

4.3 Measured and simulated results with bare glazing

At each solar position, 5 measurements were taken at each reference point to minimize the random errors in the experiment. This implies that the averaged value is obtained by filtering the measurement random noises. Figure 4.5-(a) shows the measured indoor illuminances at all the 6 reference points against the corresponding average measured value under overcast and clear skies. It can be seen that all measured data are close to the corresponding averaged value at each reference point in the given sky conditions, which reflects the good repeatability of measurements. The average measured illuminances were used for examination of the accuracy of the illuminances computed by the three computer tools.

Adeline 3.0 and DOE2.1e were used in simulations. Figure 4.5-(b), (c) and (d) show a comparison between measured and simulated indoor illuminances without blinds. The solid line indicates the averaged measured illuminace while the dots in Figure 4.5-(b), (c) and (d) represent the values calculated by Radiance, Radlink in Adeline and DOE2.

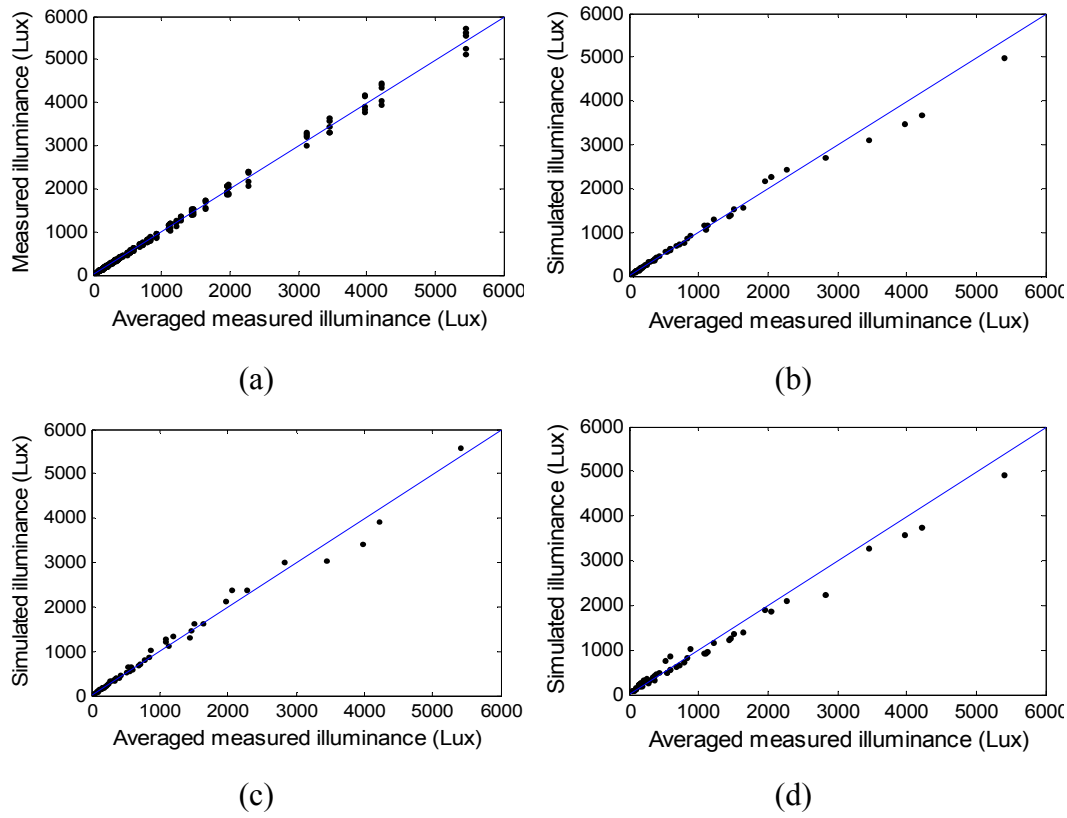

Figure 4.5. Measured and simulated indoor illuminances without blinds.
(a) measured indoor illuminances vs. the average measured illuminance.
(b) Illuminances simulated by Radiance vs. the average measured value.
(c) Illuminances simulated by Radlink vs. the average measured value.
(d) Illuminances simulated by DOE2 vs. the average measured value.

It can be observed from Table 3 that the MBE and RMSE computed by Radiance and Radlink are slightly different. Radiance asks users to input the values of these parameters, while Radlink may use their predetermined values. This may result in these minor differences.

Figure 4.6 presents the measured and simulated indoor illuminances at different reference points without blinds. Table 4.3 summaries that the MBEs and RMSEs of Radiance, Radlink and DOE2 in simulations without blinds under overcast and clear skies. It can be observed from Figure 4.5, Figure 4.6 and Table 4.3 that the daylight illuminaces generated by Radiance, Radlink and DOE2 generally agree well with the measured values. However, DOE2 produced relatively large errors at reference points far away from the windows. The MBE of its computed results could be as large as 46% at the reference point 7.6m from the window. The illuminance error distribution generated by DOE2 confirms the comparison results given by Winkelmann and Selkowitz (1985). These errors are mainly caused by the split-flux method for calculating the internally reflected illuminance. The split-flux method assumes that the inter-reflection of daylight in a room can be handled by the theory of the integrating sphere. As a room is not a sphere, errors must arise. Another reason is that the split-flux method only calculates the average value of the internally reflected illuminance in the room (Hopkinson et al., 1966). It is assumed that the internally reflected illuminance would be uniformly distributed throughout the room. The error caused by the method may be negligible in a top-lit room. However, large errors may result from it in a room with a side window.

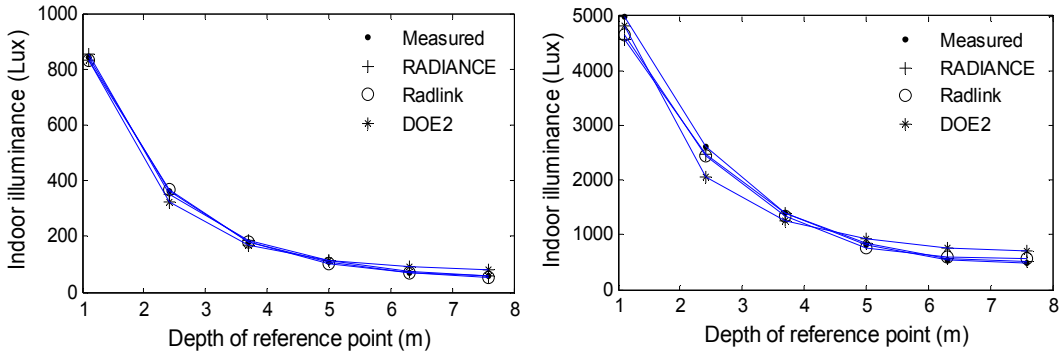

(a) (b)

Figure.4.6. Measured and simulated indoor illuminances under overcast sky without blinds, (a) Overcast sky; (b) Clear sky, solar altitude = 40°, solar azimuth = 50° west of south.

Table 4.3 Summary of MBE and RMSE for bare glazing under clear and overcast skies (%).

	Sky type	Radiance	Radlink	DOE2
MBE	Overcast	2	2	11
	Clear	5	5	14
RMSE	Overcast	6	6	23
	Clear	7	7	28

To further demonstrate this point, we calculated the internally reflected illuminances with Radiance and then compared them with the results calculated by the split-flux method. Figure 4.7 presents the results computed by the two programs. It can be easily seen that the internally reflected illuminance decreases with the depth of the reference point. Since the split-flux method assumes that the internally reflected illuminance is evenly distributed throughout the room, it overestimates the internally reflected illuminance at the rear part of the room and underestimates the illuminance at the area near window.

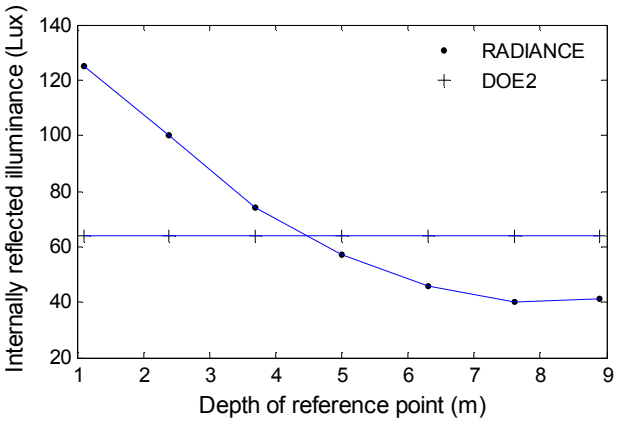

Figure 4.7. Internally reflected illuminances generated by Radiance and DOE2.

4.4 Examination of simulation results for window with venetian blinds

Radlink and DOE2 use some assumptions to simplify the simulation of venetian blinds. Their simulation results, as well as those computed by Radiance, are examined in this section.

Figure 4.8 shows a sample of the illuminance distribution generated by Radiance at the tilt angle of -30° under clear sky. Figure 4.9-(a) shows the measured indoor illuminances against the corresponding averaged values (the solid line) at each given condition and each reference point under overcast and clear skies. Figures 4.9-(b) through (d) show simulated indoor illuminance and averaged measured values represented by the solid lines.

Figure 4.8. A Radiance rendering of the classroom under clear sky,
tilt angle = -30°, solar altitude = 60°, solar azimuth = 50° west of south.

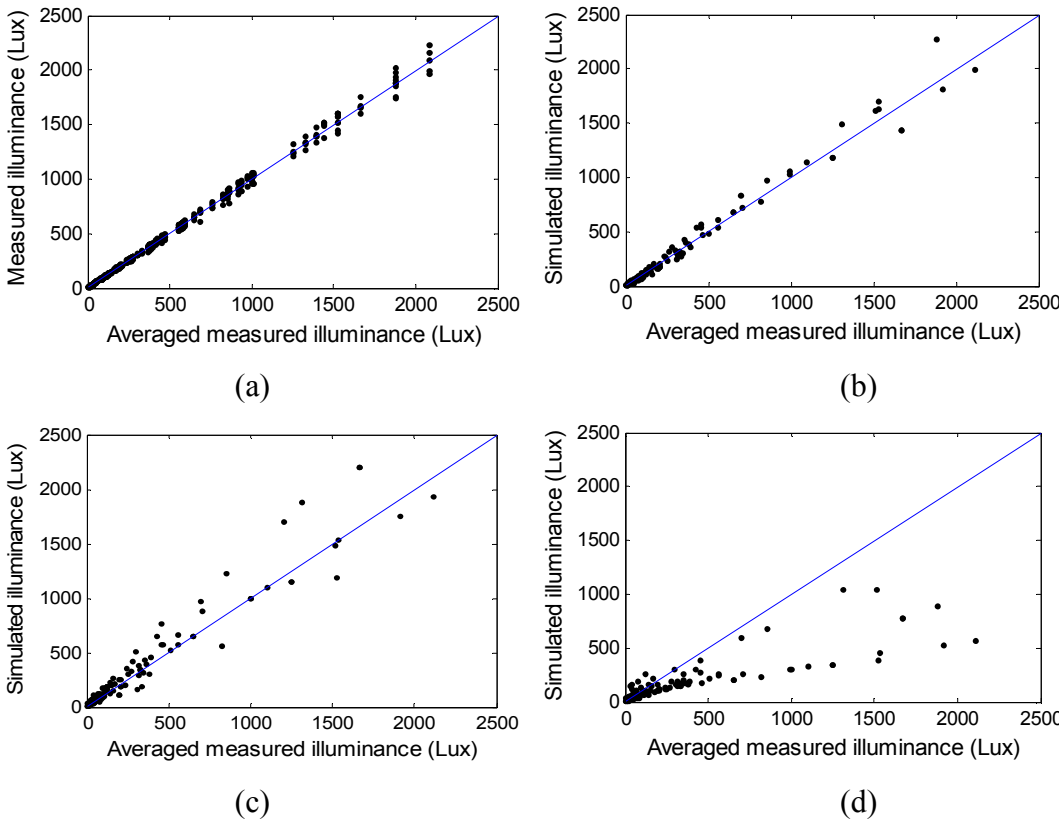

Figure 4.9. Measured and simulated indoor illuminances with blinds.
(a) measured indoor illuminances vs. the average measured illuminance.
(b) Illuminances simulated by Radiance vs. the average measured value.
(c) Illuminances simulated by Adeline vs. the average measured value.
(d) Illuminances simulated by DOE2 vs. the average measured value.

Figure 4.10 presents measured and simulated indoor illuminances at different reference points under overcast sky. It can be observed that the tilt angle strongly impacts the distribution of indoor illuminance throughout the room. Among the

three simulation tools, only Radiance can accurately predict the indoor illuminance under different tilt angles. It is also noteworthy to mention that large errors from Radiance are usually at places close to the window where daylight illuminance varies significantly. For example, the maximum MBE, 34%, occurs at the reference point 1.1 meter from the window at the tilt angle of 0°.

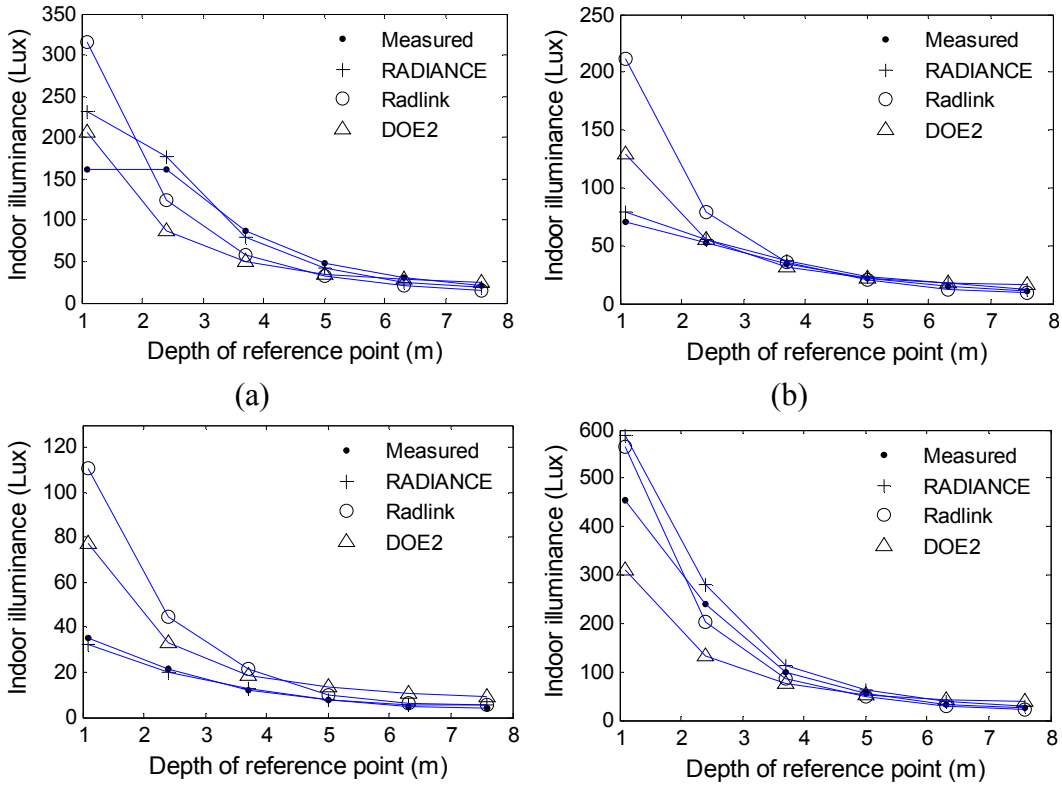

Figure 4.10. Measured and simulated indoor daylight illuminances under overcast sky, (a) tilt angle = 0°; (b) tilt angle = 30°; (c) tilt angle = 60°; (d) tilt angle = -30°.

Table 4.4 summaries the MBEs and RMSEs of the three computer tools in daylighting simulations for windows with blinds at different tilt angles under overcast sky. The tilt angle of 60° is seldom used under overcast sky because daylight is not enough for required lighting intensity. Hence, this angle is not considered in this study. Results show that Radiance slightly overestimates the

indoor illuminance in most of the cases. Radlink largely overestimates the illuminance at the positive tilt, especially at reference points near the window. As mentioned previously, Radlink assumes the blinds system does not affect the direction of incident light passing through blinds, which results in a great amount of the direct skylight that could directly reach the reference points without experiencing the internal multi-reflections. The realistic process is that the blinds system obstructs most of the incoming lights and reflects them to other directions. After multi-reflections and absorptions on the internal surface of the room, only a very small fraction of them could reach the reference points. Therefore, the real daylight illuminances should be much lower than those values predicted by Radlink at the positive tilt angle. Radlink has relatively better performance at the tilt angle of 0° and -30° because the daylight is much less blocked by blinds at these angles, and more incident daylight can directly pass through blinds without reflections. This is relatively close to the assumption made by Radlink. In contrast with Radlink, DOE2 assumes the blinds as perfect diffusers, and therefore completely ignores the influence of direct skylight and the light directly reflected from the slats. Most of the light has to experience multi-reflections on indoor room surfaces before reaching the reference point. As a result, it greatly underestimates the overall indoor daylight illuminance at the tilt angles of 0° and -30°. Moreover, DOE2 overestimates the illuminance at the reference point far from the window, even at the tilt angles of 0° and -30°, due to the limitation of the split-flux method. The above analysis shows that the simulated errors at

different conditions can be well explained by the effect of assumptions adopted by Radlink and DOE2.

Table 4.4 Summary of MBE and RMSE for windows with blinds under overcast sky (%).

	Tilt angle	Radiance	Radlink	DOE2
MBE	-30°	17	-3	-18
	0°	1	6	-25
	30°	11	33	6
	60°	9	89	69
	Overall	9	32	8
RMSE	-30°	18	14	35
	0°	21	38	35
	30°	12	98	27
	60°	19	119	77
	Overall	18	80	48

Figure 4.11 presents measured and simulated indoor illuminances at different reference points under the clear sky. Table 4.5 summaries the MBEs and RMSEs between measured and simulated illuminances for windows with blinds under clear sky. When the tilt angle is -30°, the indoor illuminance near the window can be higher than 2000 Lux, which will cause glare problem. Since the tilt angle at -30° is not likely to be used in practice, this angle was not included in the analysis. The presence of beam light makes the simulation more complicated, resulting in the deteriorated accuracy of Adeline and DOE2. Radiance generally underestimates the indoor illuminances. Its overall MBE error is -6.8%, which is much smaller than those of Adeline and DOE2. The maximum MBE of Radiance is 36.1%, which occurs at the reference point 1.1 meter from the window at the tilt angle of 0°. The overall MBE of Randlink and DOE2 is 37% and 23%,

respectively, while the overall RMSE of them is 68% and 75%.

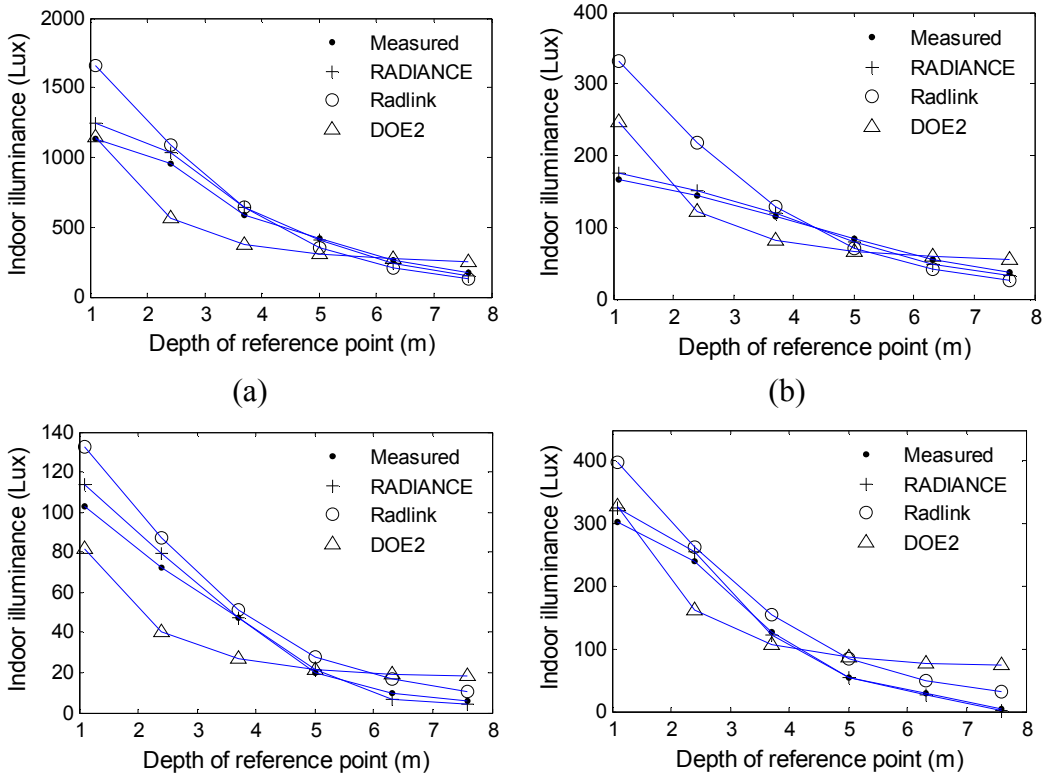

Figure 4.11. Measured and simulated indoor daylight illuminances under clear sky, solar altitude = 40°, solar azimuth = 50° west of south,
(a) tilt angle = 0°; (b) tilt angle = 30°; (c) tilt angle = 60°; (d) tilt angle = -60°.

Reinhart and Walkenhorst (2001) used the Radiance-based daylight simulation method DAYSIM to compute the indoor illuminances with external blinds. They compared the simulated illuminances with the measured data when windows were not equipped with the external blinds and when windows were shaded with the horizontal slats and the fully closed blinds. The overall MBE and RMSE with the horizontal slats under both clear and overcast skies are 6% and 29% in their study, as compared to -3% and 19%, respectively, under the same conditions in this study.

Comparison between the MBE and RMSE with bare glazing and those corresponding values with blinds generated by Radiance, Radlink and DOE2 shows that the calculated errors with blinds should primarily result from the inaccurate simulation of blinds.

Table 4.5 Summary of MBE and RMSE for windows with blinds under clear sky (%).

	Tilt angle	Radiance	Radlink	DOE2
MBE	-60°	-7	58	60
	0°	-4	15	-21
	30°	-7	26	16
	60°	-10	33	37
	Overall	-7	37	23
RMSE	-60°	15	88	101
	0°	16	26	33
	30°	16	62	32
	60°	28	85	100
	Overall	20	68	75

4.5 Summary

The accuracy of daylighting simulation results given by Radlink in Adeline and DOE2 without and with blinds have been examined against measured data collected in a full-scale classroom. The simulation results by Radiance are also presented for reference comparison to those data computed by the above two programs. The results show that when the window has only bare glazing, Radiance and Radlink give the similar results. They can accurately predict indoor illuminance under variant sky conditions while DOE2 may generate large errors at places near and far away from a window. The reason is that the split-flux

method underestimates the illuminance near the window, but overestimates the internally reflected illuminance far away from the window. When a window is shaded with venetian blinds, Radiance can reasonably predict accurate indoor iluminance distribution. Its MBEs are within ±10% in most tilt angles. Under overcast sky, the overall MBE and RMSE of Radiance are 10% and 18%, respectively. With blinds, Adeline and DOE2 cannot give acceptable results. The overall MBE and RMSE of Radlink with Radlink under overcast sky are 32% and 80%. The overall MBE and RMSE of DOE2 are 8% and 48%. Under clear sky, the presence of solar beam light makes the simulations much more complicated and the accuracies of all three programs generally deteriorate. The MBE of Radiance, Radlink and DOE2 are -7%, 37% and 23% while the RMSE are 20%, 68% and 75%, respectively. Larger errors generated by Radiance primarily occur at places near the window where the daylight illuminance rapidly decays. This actually makes accurate daylighting simulation at these places much more difficult. However, the error should have little effect on energy savings in lighting drawn from daylighting simulations because the daylight illuminance is usually enough near a window under clear sky.

Long-term daylighting simulations combined with cooling and heating load calculations are essential for the energy analysis of buildings. A trade-off between computational efficiency and accuracy has to be made in the simulation programs for the energy analysis. Comparison and analysis of experimental and

simulated results indicates that the errors computed with blinds are primarily caused by the assumptions adopted in Radlink and DOE2. Daylight that can reach the reference point may be roughly divided into two parts. The one is directly from the area of blinds while the other comes from all the interior surfaces of a space after internal multi-reflections among these surfaces. Examination of experimental and computed data reveals that any assumption that does not take into account the different features of daylight passing through blinds in their optical transfer process would result in significant computation errors. This is because only a very small fraction of the latter can actually reach the reference point due to the absorption of the interior surfaces in the multi-reflection process. The former, on the other hand, can easily reach the place without further optical loss. It should be noted that accurately predicting the absolute daylight illuminance distribution is essential for reasonably estimating the energy savings. The same average daylight illuminances in a space may not lead to the same energy savings if the daylight distributions are different. Obviously, the more uniform daylight distribution could save much more energy than the rapidly changed daylight distribution. However, the need for adopting the relatively realistic assumptions has been largely ignored.

Radlink and DOE2 generate large errors at most points, particularly at those points where the daylight illuminance is not high enough for the required illuminance. This will unreasonably overestimates the energy savings. Therefore,

researchers and engineers should cautiously use the currently available data produced by Radlink and DOE2 and avoid using the two programs for daylighting and energy simulations with blinds.

Since Radiance is not suitable for long-term daylighting simulations, more accurate and efficient computer tools need to be developed for the simulation of venetian blinds.

CHAPTER 5

MODEL FOR DAYLIGHTING SIMULATION WITH VENETIAN BLINDS

Two primary types of methods are currently used for daylighting simulations with venetian blinds. The ray tracing method used by Radiance can generate accurate daylight distributions, but is time-consuming and user-unfriendly for long-term simulations. The other type of methods, used by Adeline and DOE2, simplifies daylighting calculations by assuming different daylight distributions from venetian blinds. Although it significantly enhances the computational efficiency, it also greatly deteriorates simulation accuracy due to the unrealistic assumptions, as shown in the last chapter. A method is therefore developed for the accurate and efficient simulations with venetian blinds. Daylight through venetian blinds is divided into three parts. A part of daylight may be incident on the reference point from sky directly. The second part passes through venetian blinds by multi-reflections among the slats, glazing and indoor room surfaces, and then reaches the reference point directly from blinds slats. For the last part, the daylight passing through the blinds experience multi-reflection among indoor room surfaces before they can reach the reference point. The first part of daylight can be calculated by integration. The second and third parts involve the multi-reflection among different surfaces. To study the multi-reflection among slats with curved and specular-reflecting surfaces,

geometrical analysis often need to be conducted to calculate the number of reflections of light with different incident angles before the light can pass through the blinds (Breitenbach et al., 2001). The new method assumes the slat surfaces are flat and perfect diffusers. Therefore, the multi-reflections among slats, glazing and indoor room surfaces can be easily calculated by radiostiy method. To enhance the computational efficiency, the multi-reflection among indoor room surfaces is calculated by fitting equations obtained from simulation results of Radiance. The model is of high computational efficiency, and includes the primary design parameters that impact the daylighting performance. This is particularly useful for optimal design and parametric analysis. This chapter describes the theory of this model. The implementation and validation of this method is presented in Chapter 6.

5.1 Overall daylighting model

Two assumptions are adopted for the model to simplify modeling and enhance the computational efficiency. First, it is assumed that the blinds slat surfaces are perfect diffusers (Lambertian surface). This assumption is true for painted slats, according to the findings by Andersen et al. (2005). The slats of blinds usually are slightly curved. We assume the curvature would negligibly impact indoor illuminance distribution.

Daylight factor will be used to compute the diffuse light. It is defined as

'the ratio of the daylight illumination at a point on a given plane due to the light received directly or indirectly from a sky of assumed or known luminance distribution, to the illumination on a horizontal plane due to an unobstructed hemisphere of this sky (Hopkinson *et al*., 1966). Previously, many researchers used the daylight factor under overcast sky to represent all sky types. As the ratio of interior to exterior illuminance varies greatly under real skies (Tregenza and Waters, 1983), large errors may be introduced by this approach (Li *et al*., 2004). This problem can be solved by separately calculating the daylight factors under different sky conditions. For example, DOE2 calculates one daylight factor under overcast sky and 20 daylight factors under clear sky to account for different solar conditions. A similar method is used in the model.

Diffuse and beam light can reach an indoor place in three ways. The horizontal illuminance IL_{in} at any point in a room may be expressed by

$$IL_{in} = IL_b \, T_v(\theta_{sol}) \, S_b + IL_{dif} (DF_d + DF_r + DF_{sr}) \quad (5.1)$$

where IL_b and IL_{dif} are outdoor beam and diffure illuminance on unobstructed horizontal plane (Lux), respectively; S_b is a factor equal to 0 when beam sunlight cannot directly reach the reference point, and otherwise to 1. It can be evaluated by the geometric optics and will be described in Section 5.2. $T_v(\theta_{sol})$ is the window transmittance at the solar incident angle θ_{sol}. Different window types can be considered in the model by inputting their $T_v(\theta_{sol})$. For single glazing windows, it can be calculated by Equation (5.2) (Bryan and Clear, 1981). DF_d, DF_r and DF_{sr} are daylight factors separately due to diffuse light passing through

gaps between the slats of blinds and then directly reaching the reference point, due to multi-reflections among the different interior surfaces of walls, ceiling and floor, and due to reflection directly from slats of the blinds. DF_d can be calculated by integration, which will be described in Section 5.4. DF_r is calculated by either radiosity method or regression equations obtained by more detailed computer tools such as Radiance. Regression technique is adopted in Chapter 6. The calculation of DF_r and DF_{sr} needs luminous exitances on corresponding surfaces, which are computed by radiosity method described in Sections 5.5 and 5.6. View factors among different surfaces or between surfaces and reference point are also needed, which will be presented in Chapter 6.

$$T_v(\theta_{sol}) = 1.018 T_v(0) \cos\theta_{sol} \left(1 + \sin^3 \theta_{sol}\right) \tag{5.2}$$

with

$$\cos\theta_{sol} = \cos\alpha_{sol} \cos\gamma'_{sol} \tag{5.3}$$

where γ'_{sol} is the difference between solar azimuth, γ_{sol}, and window azimuth, γ_{win}, i.e. $\gamma'_{sol} = \gamma_{sol} - \gamma_{win}$.

Normally, the window consists of both glazing and window bars. The window transmittance is then calculated by

$$T_v = \frac{(A_{win} - A_{bar}) T_{v,gl}}{A_{win}} \tag{5.4}$$

where A_{win} and A_{bar} are the areas of window and bar (m^2); $T_{v,gl}$ is the transmittance of glazing.

5.2 Direct illuminance from beam sunlight seen from reference point

Figure 5.1 shows a schematic diagram of venetian blinds. H_{ss} is the distance between two adjacent slats (m) and L is the width of the slat (m). β is the slat tilt angle, which is zero on horizontal, anti-clockwise positive and clockwise negative. *IB* and *EB* are internal and external surfaces of blinds, respectively. The light passing through *IB* can enter the room. To reduce the number of variables and simplify the model, we used the normalized form of dimension variables in the analysis.

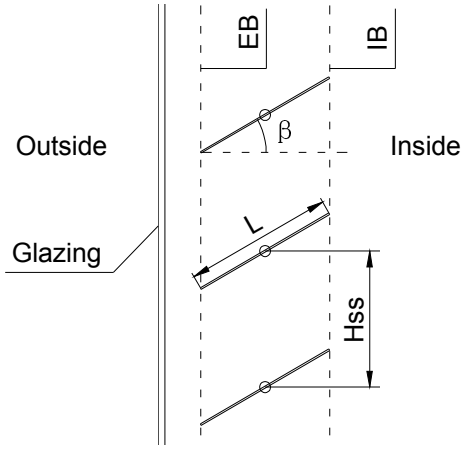

Figure 5.1 Schematic of venetian blinds.

If beam sunlight can penetrate the gaps between any two adjacent slats and directly reach the indoor reference points (S_b=1), the solar altitude α_{sol} must lie in the range between high solar altitude $\alpha_{tp,min}$ and low solar altitude $\alpha_{bt,max}$, which are determined by the dimension of the blinds and the position of indoor reference point. Let γ'_{sol} be the difference between solar azimuth, γ_{sol}, and window azimuth, γ_{win}. γ'_{sol} must lie in the range between maximum azimuth γ_{max} and minimum azimuth γ_{min}, which are determined by the width of window or blinds and the position of indoor reference point.

Figure 5.2 shows an altitude range in which the sky can be seen from reference point *R*, when γ'_{sol} is equal to zero. Let $\alpha_{tp,min}$ be the smaller one between two altitudes $\alpha_{tp,min,2}$ and $\alpha_{tp,min,1,}$ which are determined by the right and left edges of slats, as shown in Figure 5.2. $\alpha_{tp,min,2}$ and $\alpha_{tp,min,1}$ can be calculated by

$$\alpha_{tp,\min,2} = \arctan\left(\frac{H'_{slat} + 0.5L'\sin\beta}{D'_{slat} - 0.5L'\cos\beta}\right) \tag{5.5}$$

$$\alpha_{tp,\min,1} = \arctan\left(\frac{H'_{slat} - 0.5L'\sin\beta}{D'_{slat} + 0.5L'\cos\beta}\right) \tag{5.6}$$

where L' is the normalized slat width, $L' = L/H_{ss}$; H'_{slat} is the normalized height of the center of the slat under consideration, $H'_{slat} = H_{slat}/H_{ss}$; D'_{slat} is the normalized depth of indoor reference point from the blinds, $D'_{slat} = D_{slat}/H_{ss}$.

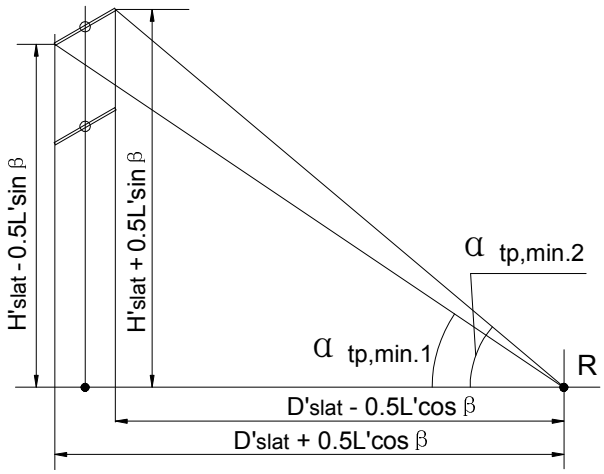

Figure 5.2 Altitude range in which the sky can be seen from the indoor reference point, $\gamma'_{sol} = 0°$.

When $\gamma'_{sol} \neq 0°$, $\alpha_{tp,min,2}$ and $\alpha_{tp,min,1}$ can be obtained as shown in Figure 5.3.

$$\alpha_{tp,\min,2} = \arctan\left(\frac{H'_{slat} + 0.5L'\sin\beta}{D'_{slat} - 0.5L'\cos\beta}\cos\gamma'_{sol}\right) \tag{5.7}$$

$$\alpha_{tp,\min,1} = \arctan\left(\frac{H'_{slat} - 0.5L'\sin\beta}{D'_{slat} + 0.5L'\cos\beta}\cos\gamma'_{sol}\right) \tag{5.8}$$

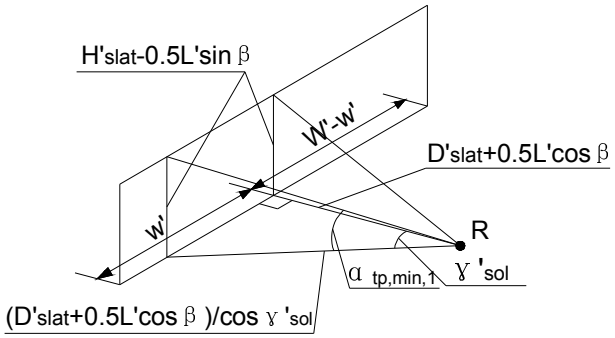

Figure 5.3 Limits to the solar altitude when $\gamma'_{sol} \neq 0°$.

Similarly, $\alpha_{bt,maz}$ is the larger one between $\alpha_{bt,max,1}$ and $\alpha_{bt,max,2}$, which can be calculated by

$$\alpha_{\mathrm{bt,max,2}} = \arctan\left(\frac{H'_{slat} - 1 + 0.5L'\sin\beta}{D'_{slat} - 0.5L'\cos\beta} \cos\gamma'_{sol} \right) \tag{5.9}$$

$$\alpha_{\mathrm{bt,max,1}} = \arctan\left(\frac{H'_{slat} - 1 - 0.5L'\sin\beta}{D'_{slat} + 0.5L'\cos\beta} \cos\gamma'_{sol} \right) \tag{5.10}$$

The values of γ_{max} and γ_{min} can be determined by (Figure 5.3)

$$\gamma_{\max} = \arctan\left(\frac{w'}{D'_{slat}} \right) \tag{5.11}$$

$$\gamma_{\min} = -\arctan\left(\frac{W' - w'}{D'_{slat}} \right) \tag{5.12}$$

where W' is the normalized width of the window or blinds, $W' = W/H_{ss}$; $w' = w/H_{ss}$

5.3 Diffuse daylight factor

The diffuse daylight factor DF_d indicates skylight passing through all gaps between the slats. It may be calculated by

$$DF_d = \sum_{i=0}^{n-1} DF_{dif,s,i}$$

where $DF_{dif,s,i}$ is the daylight factor caused by skylight directly passing through a

gap between two adjacent slats. $DF_{dif,s,i}$ may be calculated by (Eicker, 2003)

$$DF_{dif,s,i} = \frac{\int_{\gamma_{\min}}^{\gamma_{\max}} \int_{\alpha_{bt,\max}}^{\alpha_{tp,\min}} T_v(\theta_{sky}) SL \sin\alpha_{sky} \cos\alpha_{sky} \, d\alpha_{sky} d\gamma'_{sky}}{\int_0^{2\pi} \int_0^{\pi/2} SL \sin\alpha_{sky} \cos\alpha_{sky} \, d\alpha_{sky} d\gamma_{sky}}$$

where γ_{max} and γ_{min} are the maximum and minimum limits of γ'_{sky}, which is the difference between sky azimuth γ_{sky} and window azimuth γ_{win}. γ_{max} and γ_{min} can be calculated by Equations (5.11) and (5.12). $\alpha_{tp,min}$ and $\alpha_{bt,max}$ are the maximum and minimum limits of sky altitude α_{sky}. They can be determined by Equations (5.7)-(5.10). *SL* is sky luminance distribution model. There are many models available today (Moon and Spencer, 1942; CIE, 1973; Perez et al., 1993; Littlefair, 1994). One suitable for local daylight condition may be used in the integration.

5.4 Initial distribution of beam light intensities and daylight factors without reflection

The radiosity method is used to calculate light multi-reflections among slats, glazing and indoor room surfaces. This method requires the initial beam light intensities and daylight factors without reflection as inputs. The methods for calculating them are presented in this section.

Diffuse daylight that is initially on the external surface of blinds directly from both sky ground have three ways to go. The first part passes through the blinds and then reaches the internal surface of the blinds without any reflection; the second and third parts fall on the bottom and top slat surfaces, respectively. Therefore, we have the following light balance.

$$VDF_{o,dif} A_{gl,g} = VDF_{i,dif} A_{gl,g} + DF_{bt,dif} A_{slat} + DF_{tp,dif} A_{slat} \quad (5.13)$$

$$VDF_{o,gr} A_{gl,g} = VDF_{i,gr} A_{gl,g} + DF_{bt,gr} A_{slat} + DF_{tp,gr} A_{slat} \quad (5.14)$$

where A_{slat} is slat area; $A_{gl,g}$ is glazing area between adjacent slats; $VDF_{o,dif}$ and $VDF_{o,gr}$ are the vertical daylight factor on the external surface of the blinds due to diffuse skylight and ground reflection, respectively; $VDF_{i,dif}$ and $VDF_{i,gr}$ are the vertical daylight factor on the internal surface of the blinds due to diffuse skylight and ground reflection; $DF_{bt,dif}$ and $DF_{bt,gr}$ are the daylight factor on the bottom slat due to diffuse skylight and ground reflection; $DF_{tp,dif}$ and $DF_{tp,gr}$ are the daylight factor on the top slat due to diffuse skylight and ground reflection.

The width of the window and blinds generally is approximately the same, L' can represent the ratio of A_{slat} to $A_{gl,g}$. Rearranging Equations (5.13) and (5.14) yields

$$VDF_{o,dif} = VDF_{i,dif} + DF_{bt,dif} L' + DF_{tp,dif} L' \quad (5.15)$$

$$VDF_{o,gr} = VDF_{i,gr} + DF_{bt,gr} L' + DF_{tp,gr} L' \quad (5.16)$$

5.4.1 Vertical daylight factor on the external and internal surfaces of the blinds

Figure 5.4 shows an altitude range in which the sky can be seen from a point on the internal surface of the blinds R_T, when γ'_{sol} is equal to zero. In the figure, h' is the normalized height of the point R_T from the right edge of slats. $VDF_{o,dif}$, $VDF_{i,dif}$, $VDF_{o,gr}$ and $VDF_{i,gr}$ can be computed by integration. Unlike $VDF_{o,dif}$ and $VDF_{o,gr}$, $VDF_{i,dif}$ and $VDF_{i,gr}$ are not uniformly distributed because the points on the internal surface of blinds are obstructed by slats. We should first calculate the vertical daylight factor, $VDF_{p,dif}$ and $VDF_{p,gr}$, at any point in the gap.

Then $VDF_{i,dif}$ and $VDF_{i,gr}$ can be calculated by integrating $VDF_{p,dif}$ and $VDF_{p,gr}$ over the whole area of the internal surface of the blinds system as follows

$$VDF_{i,dif} = \frac{\int_0^{W'}\int_0^1 VDF_{p,dif}\,dh'\,dw'}{W'} \tag{5.17}$$

$$VDF_{i,gr} = \frac{\int_0^{W'}\int_0^1 VDF_{p,gr}\,dh'\,dw'}{W'} \tag{5.18}$$

If slat tilt angle $\beta>0$, a point on the internal surface of the blinds R_T can only receive light from the maximum altitude α_{dif2} and 0° (Figure 5.4a). If $h' \geq (1-L'\cdot\sin\beta)$, the high altitude limit α_{dif2} equals 0° because it is higher or equal to its maximum limit. If $h' \leq (1-L'\cdot\sin\beta)$, α_{dif2} can be calculated by (Figure 5.4a)

$$\alpha_{dif\,2} = \arctan\left(\frac{1-L'\sin\beta-h'}{L'\cos\beta}\cos\gamma'_{sky}\right)$$

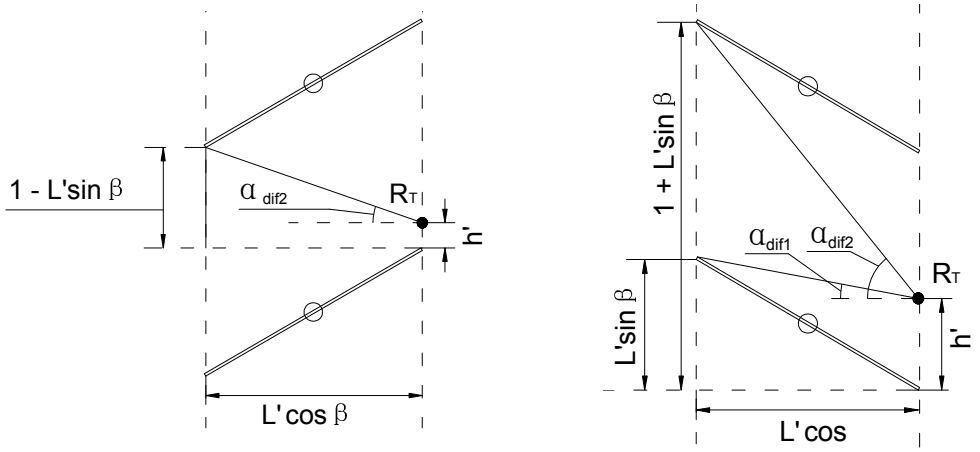

(a) $\beta\geq 0$. (b) $\beta<0$.

Figure 5.4 Altitude range in which the sky can be seen from a point on the internal surface of the blinds, $\gamma'_{sky} = 0°$.

If $\beta\leq 0$, α_{dif2} and α_{dif1} can be calculated by (Figure 5.5b)

$$\alpha_{dif\,2} = \arctan\left(\frac{1+L'\sin\beta-h'}{L'\cos\beta}\cos\gamma'_{sky}\right)$$

$$\alpha_{dif1} = \arctan\left(\frac{L'\sin\beta - h'}{L'\cos\beta}\cos\gamma'_{sky}\right)$$

Figure 5.5 shows reference point R_T can only receive light within the azimuth range between the maximum azimuth γ_{dif2} and the minimum azimuth γ_{dif1}. The two azimuth angles can be determined by

$$\gamma_{dif2} = \arctan\left(\frac{W'-w'}{L'\cos\beta}\right)$$

$$\gamma_{dif1} = -\arctan\left(\frac{w'}{L'\cos\beta}\right)$$

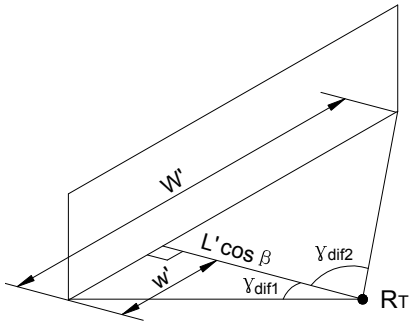

Figure 5.5 Azimuth range in which the sky can be seen from a point on the internal surface of the blinds

$VDF_{p,dif}$ in Equation (5.17) may be calculated by (Eicker, 2003)

$$VDF_{pi} = \frac{\int_{\gamma_{dif1}}^{\gamma_{dif2}}\int_{\alpha_{dif1}}^{\alpha_{dif2}} T_v(\theta_{sky})\, SL\, \cos\gamma'_{sky}\, \cos^2\alpha_{sky}\, d\alpha_{sky}\, d\gamma'_{sky}}{\int_0^{2\pi}\int_0^{\pi/2} SL\, \sin\alpha_{sky}\, \cos\alpha_{sky}\, d\alpha_{sky}\, d\gamma_{sky}}$$

where $T_v(\theta_{sky})$ is the window transmittance at the incident angle of sky element θ_{sky}, which can be calculated by Equation (5.19). Then Equation (5.2) can be used to calculate $T_v(\theta_{sky})$ by replacing θ_{sol} with θ_{sky}. α_{dif2} and α_{dif1} are the integration limits of α_{sky}; γ_{dif2} and γ_{dif1} are the integration limits of γ'_{sky}.

$$\cos\theta_{sky} = \cos\alpha_{sky}\cos\gamma'_{sky} \tag{5.19}$$

Equation (5.17) can also be used for the calculation of external vertical daylight factor due to diffuse light $VDF_{o,dif}$. As the external surface of the blinds is not obstructed by the slats, it can receive light from the whole 1/2 hemisphere facing the window. Hence, integration limits α_{dif2} and α_{dif1} should be $\pi/2$ and 0; and γ_{dif2} and γ_{dif1} should be $\pi/2$ and $-\pi/2$.

The outdoor ground is assumed as perfect diffuser. Therefore, the reflection from the outdoor ground obeys the law of cosine (Yang, 1980). If the outdoor ground is unobstructed horizontal plane, $VDF_{p,gr}$ in Equation (5.18) may be calculated by

$$VDF_{p,gr} = \frac{R_{global}\rho_{gr}}{\pi}\int_{-\gamma_{gr1}}^{\gamma_{gr2}}\int_{\alpha_{gr1}}^{\alpha_{gr2}} T_v(\theta_{gr})\cos\gamma'_{gr}\sin\alpha_{gr}\cos^2\alpha_{gr}\,d\alpha_{gr}\,d\gamma'_{gr}$$

where R_{global} is the ratio of outdoor global illuminance, which is the sum of diffuse IL_{dif} and beam illuminance IL_b on unobstructed horizontal plane, to IL_{dif}; ρ_{gr} is the reflectance of outdoor ground; α_{gr} is the altitude of ground element, whose integration limits are α_{gr2} and α_{gr1}; γ'_{gr} is the difference between the azimuth of the ground element γ_{gr} and window azimuth γ_{win}; γ_{gr2} and γ_{gr1} are the integration limits of γ'_{gr}; $T_v(\theta_{gr})$ is the window transmittance at the incident angle of ground element θ_{gr}. θ_{gr} can be calculated by

$$\cos\theta_{gr} = \cos\alpha_{gr}\cos\gamma'_{gr}$$

If $\beta \geq 0°$, α_{gr2} and α_{gr1} can be calculated by

$$\alpha_{gr2} = \arctan\left(\frac{L'\sin\beta + h' - 1}{L'\cos\beta}\cos\gamma'_{gr}\right) \tag{5.20}$$

$$\alpha_{gr1} = \arctan\left(\frac{L'\sin\beta + h'}{L'\cos\beta}\cos\gamma'_{gr}\right) \tag{5.21}$$

If $\beta < 0°$, α_{gr2} always equals 0. α_{gr2} equals 0 if $h' \leq L'\sin\beta$, as it is lower than

its minimum limit. If $h' > L'\sin\beta$, α_{gr1} can be calculated by

$$\alpha_{gr1} = \arctan\left(\frac{h' - L'\sin\beta}{L'\cos\beta}\cos\gamma'_{gr}\right) \tag{5.22}$$

Equation (5.19) can also be used for the calculation of external vertical daylight factor due to ground reflection $VDF_{o,gr}$. Because the ground-reflected light received by the external surface of the blinds is not obstructed by the slats, integration limits α_{gr2} and α_{gr1} should be *0* and $-\pi/2$; and γ_{gr2} and γ_{gr1} should be $\pi/2$ and $-\pi/2$.

5.4.2 Daylight factor on top and bottom slats

Figure 5.6 shows the maximum altitude at which the sky can be seen from a point on the imagined horizontal plane, when γ'_{sky} is equal to zero. In the figure, *l'* is the normalized distance between the point on imagined plane to the external surface of blinds. As all diffuse sky light is downward, the top slat cannot receive diffuse sky light when the tilt angle β is positive. When the tilt angle is negative, only the light comes from the part of the widow area higher than the right edge of the top slat can contribute to $DF_{tp,dif}$, as shown in Figure 5.6.

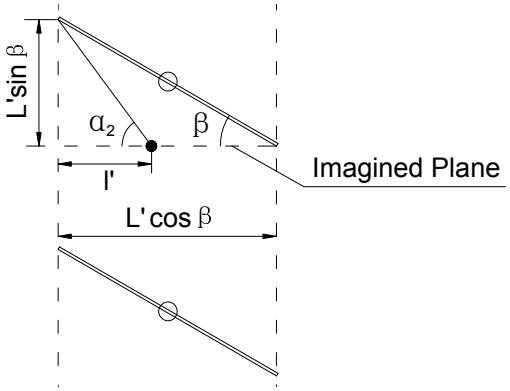

Figure 5.6 Maximum altitude at which the sky can be seen from a point on the imagined horizontal plane, $\gamma'_{sky} = 0°$.

The calculation of daylight factor on tilt surface is more difficult than that on horizontal or vertical surfaces. Hence, the calculation of daylight factor on slats will be simplified based on the balance of light incident on the external surface of the blinds. An imagined horizontal plane is created, as shown in Figure 5.6. Normally, the window width *W'* is much larger than the width of slat *L'*. Therefore, the areas of the vertical planes between two ends of the slats are ignorable compared with the areas of slats and the internal surfaces of the blinds between adjacent slats. The external surface of the blinds, the top slat and the imagined plane constitute an enclosed space. The light received by the external surface of the blinds should equal the sum of the light received by the top slat and the imagined horizontal plane, which can be expressed by

$$VDF_{o,dif} L' \sin\beta = DF_{h,dif} L' \cos\beta + DF_{tp,dif} L'$$

where $DF_{h,dif}$ is the daylight factor on the imagined horizontal plane.

Rearranging the about equation yields

$$DF_{tp,dif} = VDF_{o,dif} \sin\beta - DF_{h,dif} \cos\beta$$

Substituting the above equation into Equation (5.15) results in

$$DF_{bt,dif} = \frac{1}{L'}\left(VDF_{o,dif} - VDF_{i,dif}\right) - DF_{tp,dif}$$

Figure 5.7 shows the maximum altitude at which the light reflected from the ground can be received from a point on the imagined horizontal plane, when γ'_{sky} is equal to zero. As all ground-reflected light are upward, the bottom slat

cannot receive ground-reflected light when the tilt angle β is negative. When the tilt angle is positive, only the light that comes from the lower part of the widow area between slats can contribute to $DF_{bt,gr}$, as shown in Figure 5.7.

Similarly, based on the balance of light incident on the external surface of the blinds, the light received by the external surface of the blinds should equal the sum of the light received by the bottom slat and the imagined horizontal plane, which can be expressed by

$$DF_{bt,gr} = VDF_{o,gr} \sin\beta - DF_{h,gr} \cos\beta$$

where $DF_{h,p,gr}$ is the daylight factor on the imagined horizontal plane.

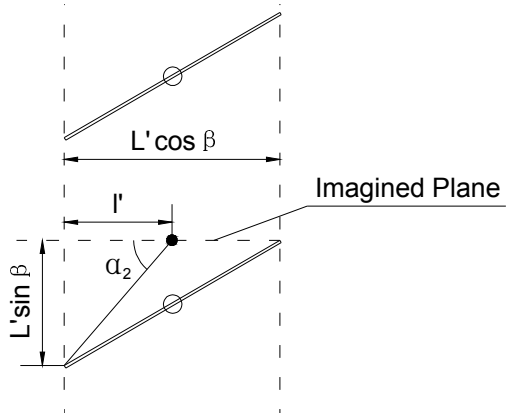

Figure 5.7 Maximum altitude at which the light reflected from the ground can be received from a point on the imagined horizontal plane, $\gamma'_{sky} = 0°$.

Substituting the above equation into Equation (5.16) results in

$$DF_{tp,gr} = \frac{1}{L'}\left(VDF_{o,gr} - VDF_{i,gr}\right) - DF_{bt,gr}$$

where $DF_{h,gr}$ is the daylight factor of the imagined plane due to the ground-reflected light.

$DF_{h,dif}$ and $DF_{h,gr}$ are not uniformly distributed on the imagined plane. We need to derive the equation of the daylight factor at a point on the imagined plane, $DF_{h,p,dif}$ and $DF_{h,p,gr}$. Then $DF_{h,dif}$ and $DF_{h,gr}$ can be obtained by averaging $DF_{h,p,dif}$ and $DF_{h,p,gr}$ over the imagined plane.

For simplicity, the sky luminance is assumed to be uniformly distributed over the sky hemisphere. Therefore, $DF_{h,p,dif}$ can be calculated by

$$DF_{h,p,dif} = \frac{T_{v,d}\int_{\gamma_1}^{\gamma_2}\int_0^{\alpha_2}\sin\alpha_{sky}\cos\alpha_{sky}\,d\alpha_{sky}\,d\gamma'_{sky}}{\int_0^{2\pi}\int_0^{\pi/2}\sin\alpha_{sky}\cos\alpha_{sky}\,d\alpha_{sky}\,d\gamma'_{sky}} \tag{5.23}$$

where $T_{v,d}$ is the diffuse transmittance of window, which approximately equals $0.8T_v(0)$ (ASHRAE Handbook, 2005).

The limits of the integration may be calculated by (Figure 5.7)

$$\alpha_2 = \arctan\frac{L'\sin\beta}{l'/\cos\gamma'_{sky}}$$

$$\gamma_2 = \arctan\frac{W'-w'}{l'}$$

$$\gamma_1 = -\arctan\frac{w'}{l'}$$

Normally, W' is much larger than l'. To simplify the equation, we assume there is not limit on the azimuth. Thus, $\gamma_2 = \pi/2$ and $\gamma_1 = -\pi/2$. Our calculation results show that the error introduced by this assumption is less than 0.2%.

Denominator of Equation (5.23) represents the illuminance on outdoor

unobstructed plate, which can be calculated by

$$\int_0^{2\pi}\int_0^{\pi/2}\sin\alpha_{sky}\cos\alpha_{sky}\,d\alpha_{sky}\,d\gamma_{sky}=\int_0^{2\pi}\int_0^{\pi/2}\sin\alpha_{sky}\,d(\sin\alpha_{sky})\,d\gamma_{sky}=\pi$$

$$\int_0^{2\pi}\int_0^{\frac{\pi}{2}}\sin\alpha_{sky}\cos\alpha_{sky}\,d\alpha_{sky}\,d\gamma_{sky}\int_0^{2\pi}\int_0^{\pi/2}\sin\alpha_{sky}\,d(\sin\alpha_{sky})\,d\gamma_{sky}=\pi$$

Numerator of Equation (5.23) represents the illuminance on the imagined plane. It can be calculated by

$$T_{v,d}\int_{-\pi/2}^{\pi/2}\int_0^{\alpha_2}\sin\alpha_{sky}\cos\alpha_{sky}\,d\alpha_{sky}\,d\gamma_{sky}=\frac{T_{v,d}}{2}\int_{-\pi/2}^{\pi/2}\sin^2\alpha_2\,d\gamma_{sky} \tag{5.24}$$

where the sine of upper limit altitude α_2 may be calculated by (Figure 5.6)

$$\sin\alpha_2=\frac{L'\sin\beta}{\sqrt{(L'\sin\beta)^2+(l'/\cos\gamma_{sky})^2}} \tag{5.25}$$

Substituting Equation (5.24) and (5.25) into Equation (5.23) yields (Gui et al., 1993)

$$DF_{h,p,dif}=\frac{T_{v,d}}{2}-\frac{T_{v,d}}{\pi}\sqrt{\frac{l'^2}{L'^2\sin^2\beta+l'^2}}\cdot\left[\arctan\frac{\sqrt{L'^2\sin^2\beta+l'^2}-L'\sin\beta}{l'}+\arctan\frac{\sqrt{L'^2\sin^2\beta+l'^2}+L'\sin\beta}{l'}\right]$$

We assumed all points on the imagined plane have the same integration limits of γ'_{sky}. Therefore, the value of $DF_{h,p,dif}$ is independent of the slat width. The average daylight factor over the depth of the imagined plane equals that over the whole area of the imagined plane. Hence, $DF_{h,dif}$ may be calculated by

$$DF_{h,dif}=\frac{\int_0^{L'\cos\beta}DF_{h,p,dif}\,dl'}{L'\cos\beta}$$

There is no analytic solution to the above integration. The Simpson's rule (Gao, 1979) is used to simplify the calculation. $DF_{h,dif}$ may be calculated by

$$DF_{h,dif} \approx \frac{1}{6}\left[DF_{h,p,dif}\left(l'=0\right)+4DF_{h,p,dif}\left(l'=0.5L'\cos\beta\right)+DF_{h,p,dif}\left(l'=L'\cos\beta\right)\right]$$

As the light reflected from ground obeys the law of cosine, $DF_{h,p,gr}$ may be calculated by

$$DF_{h,p,gr}=\frac{R_{global}\rho_{gr}T_{v,d}}{\pi}\int_{\gamma_1}^{\gamma_2}\int_{0}^{\alpha_2}\sin^2\alpha_{gr}\cos\alpha_{gr}d\alpha_{gr}d\gamma'_{gr}=\frac{R_{global}\rho_{gr}T_{v,d}}{3\pi}\int_{\gamma_1}^{\gamma_2}\sin^3\alpha_2 d\gamma_{gr}$$

with

$$\alpha_2=\arctan\frac{L'\sin\beta}{l'/\cos\gamma_{gr}}$$

$$\gamma_2=\pi/2$$

$$\gamma_1=-\pi/2$$

The remaining process is similar to that of $DF_{h,dif}$. Finally, $DF_{h,gr}$ may be calculated by

$$DF_{h,gr} \approx \frac{1}{6}\left[DF_{h,p,gr}\left(l'=0\right)+4DF_{h,p,gr}\left(l'=0.5L'\cos\beta\right)+DF_{h,p,gr}\left(l'=L'\cos\beta\right)\right]$$

with

$$DF_{h,p,gr}=\frac{2R_{global}\rho_{gr}T_{v,d}\left(L'\sin\beta\right)^3}{9\pi\cdot\sqrt[3]{\left(L'\sin\beta\right)^2+\left(l'/\cos\gamma_{sky}\right)^2}}$$

5.4.3 Ratio of the slat area receiving beam light to entire slat area

If the top slat faces the sun, the whole area can receive beam light as the top slat almost cannot be obstructed by the bottom slat for commonly used blinds systems with *L'* value between 1.0 and 1.2. However, if the bottom slat faces the sun, only a certain area of the slat may receive beam sunlight while other area may be obstructed by the top slats. This can be seen from Figure 5.8, which

shows the critical or deepest inside point R_{sol} at which the beam sunlight can reach.

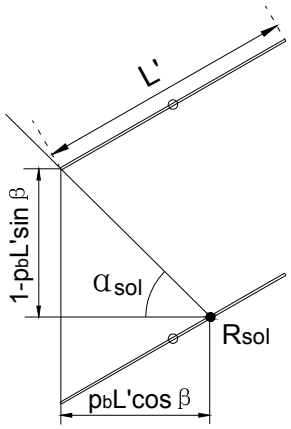

Figure 5.8 Critical point R_{sol} that can receive beam sunlight.

The ratio of the slat area receiving beam light to the entire slat area p_b may be computed through analysis of the geometrical optics. The position of R_{sol} should satisfy the following relationship (Figure 5.8)

$$\tan \alpha_{sol} = \frac{1 - p_b L' \sin \beta}{p_b L' \cos \beta / \cos \gamma'_{sol}}$$

Solving the above equation, we have

$$p_b = \frac{\cos \gamma'_{sol}}{L' \left(\tan \alpha_{sol} \cos \beta + \sin \beta \cos \gamma'_{sol} \right)} \tag{5.26}$$

Beam sunlight on the slats is uniformly distributed. Let R_b be the ratio of beam light incident on the bottom and top slats to IL_{dif}. It may be computed by

$$R_b = \frac{IL_b T_v (\theta_{sol}) \cos \theta_{slat}}{\sin \alpha_{sol} IL_{dif}} \tag{5.27}$$

where θ_{slat} is the solar incident angles on slats. θ_{slat} on bottom and top slats, $\theta_{slat,bt}$ and $\theta_{slat,tp}$, can be calculated by (ASHRAE 2005)

$$\cos \theta_{slat,bt} = \cos \alpha_{sol} \cos \gamma'_{sol} \sin \beta + \sin \alpha_{sol} \cos \beta$$
$$\cos \theta_{slat,tp} = -\cos \alpha_{sol} \cos \gamma'_{sol} \sin \beta - \sin \alpha_{sol} \cos \beta$$

If $p_b \leq 1.0$, all beam light is obstructed by the slats. Therefore, the partial beam transmittance of blinds $TV_{b,g}$ equals 0. If $p_b > 1.0$, the entire area of the slat can receive the beam light and a portion of the beam light can penetrate the blinds without reflection, as shown in Figure 5.9. Then $TV_{b,g}$ can be calculated by

$$TV_{b,g} = \frac{p_b - 1}{p_b} = 1 - \frac{L'\left(\tan\alpha_{sol}\cos\beta + \sin\beta\cos\gamma'_{sol}\right)}{\cos\gamma'_{sol}} \tag{5.28}$$

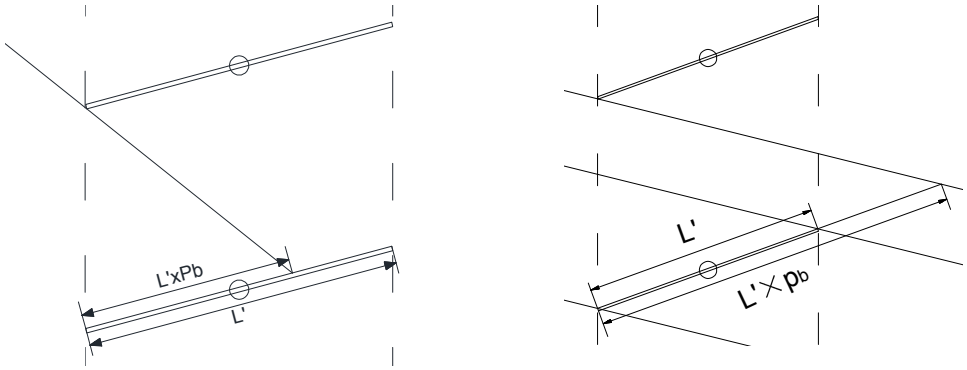

(a) (b)

Figure 5.9 Beam sunlight can penetrate the blinds when (a) $p_b \leq 1.0$ and (b) $p_b > 1.0$.

5.5 Final luminous exitances of top and bottom slats, and internal surface of the blinds

Beside the diffuse light directly reach the internal surface of the blinds without reflections, the internal vertical daylight factor should also include the light reflected from glazing, slats and indoor room surfaces. The glazing can only receive light reflected from slats and indoor room surfaces, which is very diffuse because these surfaces are assumed to be perfect diffusers. Therefore, the light reflected from glazing must also be diffuse. Hence the radiosity method can be used to obtain the final luminous exitances of slats, glazing and internal surface of a room.

For diffuse incident light that includes diffuse skylight and ground-reflected light, the blinds and the room can be modeled by four surfaces: the internal surface of the glazing, bottom and top slats; and the internal surfaces of the room. Then the final luminous exitances of these surfaces can be determined by the following radiosity equation (Sillion and Puech, 1994):

$$\begin{pmatrix} 1-\rho_{rm}VF_{rm-rm} & -\rho_{rm}VF_{rm-gl} & -\rho_{rm}VF_{rm-bt} & -\rho_{rm}VF_{rm-tp} \\ -\rho_{gl}VF_{gl-rm} & 1-\rho_{gl}VF_{gl-gl} & -\rho_{gl}VF_{gl-bt} & -\rho_{gl}VF_{gl-tp} \\ -\rho_{slat}VF_{bt-rm} & -\rho_{slat}VF_{bt-gl} & 1-\rho_{slat}VF_{bt-bt} & -\rho_{slat}VF_{ss} \\ -\rho_{slat}VF_{tp-rm} & -\rho_{slat}VF_{tp-gl} & -\rho_{slat}VF_{ss} & 1-\rho_{slat}VF_{tp-tp} \end{pmatrix} \begin{pmatrix} B_{rm,dg} \\ B_{gl,dg} \\ B_{bt,dg} \\ B_{tp,dg} \end{pmatrix} = \begin{pmatrix} E_{rm,dg} \\ E_{gl,dg} \\ E_{bt,dg} \\ E_{tp,dg} \end{pmatrix} \quad (5.29)$$

where B is final luminous exitance (Lux); E is self-emissive light intensity (Lux); ρ is surface reflectance; VF is view factor between two surfaces. Subscripts *bt*, *tp*, *gl* and *rm* represent bottom and top slats, the internal surface of the glazing, the internal surface of a room, respectively; VF_{ss} is the view factor between the whole areas of two adjacent slats.

The view factors $VF_{gl\text{-}gl}$, $VF_{bt\text{-}bt}$ and $VF_{tp\text{-}tp}$ equal zero because convex and flat planes cannot directly receive the light emitted from themselves. We only need to derive the formulas for the calculation of VF_{ss}, $VF_{bt\text{-}rm}$ and $VF_{tp\text{-}rm}$. Other view factors in Equation (5.29) can be obtained by using the summation rule and reciprocity relation (Frank and David, 2002), as described below.

The glazing, bottom and top slat, and the internal surfaces of the room constitute an enclosed space. Therefore, we have the following relationships

according to the summation rule.

$$VF_{bt-gl} = 1 - VF_{bt-rm} - VF_{ss}$$

$$VF_{tp-gl} = 1 - VF_{tp-rm} - VF_{ss}$$

$$VF_{gl-rm} = 1 - VF_{gl-bt} - VF_{gl-tp}$$

$$VF_{rm-rm} = 1 - VF_{rm-gl} - VF_{rm-bt} - VF_{rm-tp}$$

Using the reciprocity relation, we can calculate the view factors from the internal surfaces of the room to the bottom and top slats; and the glazing area between two slats by

$$VF_{rm-gl} = \frac{A_{slat} / L'}{A_i} VF_{gl-rm}$$

$$VF_{rm-bt} = \frac{A_{slat}}{A_i} VF_{bt-rm}$$

$$VF_{rm-tp} = \frac{A_{slat}}{A_i} VF_{tp-rm}$$

$$VF_{gl-bt} = VF_{bt-gl} L'$$

$$VF_{gl-tp} = VF_{tp-gl} L'$$

where A_i is the internal surface area of the room (m^2), excluding the wall with window. *L'* in above equations represents the ratio of the slat area to the glazing area between adjacent slats.

The self-emissive light intensities of the bottom and top slats and the internal surface of the room are due to the reflection of the light received from the external surface of the blinds. They may be determined by Equations (5.30)-(5.32). The self-emissive light intensity of the internal surface of the

glazing equal zero as it cannot directly receive the light that comes from the external surface of the blinds. Thus

$$E_{rm,dg} = \left(VDF_{i,dif} + VDF_{i,gr}\right)\rho_{rm}\frac{A_{win}}{A_{rm}} \tag{5.30}$$

$$E_{bt,dg} = \left(DF_{bt,dif} + DF_{bt,gr}\right)\rho_{slat} \tag{5.31}$$

$$E_{tp,dg} = \left(DF_{tp,dif} + DF_{tp,gr}\right)\rho_{slat} \tag{5.32}$$

If the top slat faces the sun, the whole slat can be regarded as a surface in the modeling because the top slat almost cannot be obstructed by the bottom slat. Therefore, four surfaces are needed in the radiosity equation, which can be obtained from equation (5.29) by replacing the subscript *dg* with *b*.

The self-emissive light intensity of the top slat can be calculated by Equations (5.33) and (5.34). All other self-emissive light intensities equal zero as they cannot directly receive beam sun light.

$$E_{rm,b} = R_{vb-hd}TV_{b,g}\rho_{rm}\frac{A_{win}}{A_{rm}} \tag{5.33}$$

$$E_{tp,b} = R_{tp,b}\rho_{slat} \tag{5.34}$$

Substituting Equations (5.30)-(5.34) into Equation (5.29) and solving it, we can obtain the final luminous exitances of glazing, bottom and top slats. Then the vertical daylight factor of the internal surface of the blinds after multi-reflection of beam and diffuse light may be calculated by Equation (5.35).

$$VDF_{i,dg}+VDF_{i,b}=\left(B_{gl,dg}+B_{gl,b}\right)VF_{gl-i}+\left(B_{bt,dg}+B_{bt,b}\right)L'\cdot VF_{bt-i}+\left(B_{tp,dg}+B_{tp,b}\right)L'\cdot VF_{tp-i}$$
$$+VDF_{i,dif}+VDF_{i,gr}-\left(B_{rm,dg}+B_{rm,b}\right)\frac{A_{slat}}{A_{wc}}VF_{rm-bt}-\left(B_{rm,dg}+B_{rm,b}\right)\frac{A_{slat}}{A_{wc}}VF_{rm-tp} \quad (5.35)$$
$$-\left(B_{rm,dg}+B_{rm,b}\right)\frac{A_{slat}/L'}{A_{wc}}VF_{rm-gl}$$

where A_{wc} is the area of the vertical walls and ceiling (m^2), excluding the wall containing window.

In Equation (5.35), the light directly reflected back to the window and blinds system from indoor walls and ceiling is excluded from the total amount of light passing through the internal surface of the blinds. That is because this part of light does not contribute to the illuminance on indoor horizontal plane, which designers often care about in daylighting design.

If the bottom slat faces the sun, there may be only part of the slat area can receive beam sunlight due to the obstruction from the top slat. Then the areas of the slat that can and cannot receive beam light have to be treated separately. Therefore, blinds and the room need to be modeled by five surfaces: the internal surface of the glazing, the top slat; the internal surfaces of the room; and the two parts of the bottom slat that can and cannot receive beam sunlight, separately. The final luminous exitances of these surfaces are determined by the following radiosity equation:

$$\begin{pmatrix} 1-\rho_{rm}VF_{rm-rm} & -\rho_{rm}VF_{rm-gl} & -\rho_{rm}VF_{rm-bt,1} & -\rho_{rm}VF_{rm-bt,0} & -\rho_{rm}VF_{rm-tp} \\ -\rho_{gl}VF_{g-rm} & 1-\rho_{gl}VF_{gl-gl} & -\rho_{gl}VF_{gl-bt,1} & -\rho_{gl}VF_{gl-bt,0} & -\rho_{gl}VF_{gl-tp} \\ -\rho_{slat}VF_{bt1-rm} & -\rho_{slat}VF_{bt1-gl} & 1-\rho_{slat}VF_{bt1-bt1} & -\rho_{slat}VF_{bt1-bt0} & -\rho_{slat}VF_{bt1-tp} \\ -\rho_{slat}VF_{bt0-rm} & -\rho_{slat}VF_{bt0-gl} & -\rho_{slat}VF_{bt0-bt1} & 1-\rho_{slat}VF_{bt0-bt0} & -\rho_{slat}VF_{bt0-tp} \\ -\rho_{slat}VF_{tp-rm} & -\rho_{slat}VF_{tp-g} & -\rho_{slat}VF_{tp-bt1} & -\rho_{slat}VF_{tp-bt0} & 1-\rho_{slat}VF_{tp-tp} \end{pmatrix} \begin{pmatrix} B_{rm,b} \\ B_{gl,b} \\ B_{bt1,b} \\ B_{bt0,b} \\ B_{tp,b} \end{pmatrix} = \begin{pmatrix} E_{rm,b} \\ E_{gl,b} \\ E_{bt1,b} \\ E_{bt0,b} \\ E_{tp,b} \end{pmatrix} \quad (5.36)$$

where the subscripts *bt1* and *bt0* represent the parts of the bottom slat that can and cannot receive beam sun light.

The self-emissive light intensities from the internal surfaces of the room and the bottom slat area receiving beam light can be calculated by Equations (5.37) and (5.38). All the other self-emissive light intensities equal zero as they cannot receive beam sun light.

$$E_{i,b} = R_{vb-hd} TV_{b,g} \rho_{rm} \frac{A_{win}}{A_{rm}} \quad (5.37)$$

$$E_{bt1,b} = R_{bt,b} \rho_{slat} \quad (5.38)$$

The view factors $VF_{bt1\text{-}bt1}$, $VF_{bt0\text{-}bt0}$, $VF_{bt1\text{-}bt0}$ and $VF_{bt0\text{-}bt1}$ equal zero as the two surfaces that emit and receive light are on the same flat plane. We only need to derive the formulas for the calculation of $VF_{bt1\text{-}tp}$ and $VF_{gl\text{-}bt1}$. Other view factors in Equation (5.36) can be obtained by using the summation rule and reciprocity relation.

$$VF_{tp-bt1} = p_b VF_{bt1-tp}$$

$$VF_{tp-bt0} = VF_{ss} - VF_{tp-bt1}$$

$$VF_{bt0-tp} = \frac{VF_{tp-bt0}}{1-p_b}$$

$$VF_{gl-bt0} = VF_{gl-bt} - VF_{gl-bt1}$$

Substituting above equations into Equation (5.39) and solving it, we can obtain the final luminous exitances of the glazing, top and bottom slats due to beam sunlight on the bottom slat. Then the vertical daylight factor of the internal surface of the blinds after multi-reflection of beam light can be calculated by

$$VDF_{i,b} = B_{gl,b}VF_{gl-i} + B_{bt1,b}\,p_b L'VF_{bt1-i} + B_{bt0,b}(1-p_b)L'VF_{bt0-i} + B_{tp,b}L'VF_{tp-i} - B_{rm,b}\frac{A_{slat}}{A_{wc}}VF_{rm-bt} - B_{rm,b}\frac{A_{slat}}{A_{wc}}VF_{rm-tp} - B_{rm,b}\frac{A_{slat}/L'}{A_{wc}}VF_{rm-gl} \quad (5.39)$$

5.6 Daylight factor due to multi-reflections among interior surfaces

Radiosity method can be used for the calculation of DF_r. However, the self-emissive light intensity and final luminous exitance are not uniformly distributed on the internal surfaces of the room. To accurately predict the indoor illuminance due to the multi-reflections, the room surfaces should be divided into lots of patches. This will result in very complex radiosity equation, which may be difficult and time-consuming to solve. To enhance the computational efficiency, fitting equations were obtained from the simulation results of Radiance. Room dimension, surface reflectance, slat tilt angle and solar incident angle have great influence on the multi-reflections among interior surfaces. Hence, they are included in the fitting equations. Details about the fitting equations are presented in Chapter 6.

DF_r is affected by both outdoor diffuse and beam light. Hence the ratio,

$R_{vb\text{-}hd}$, of beam illuminance on the outside vertical surface of the blinds VIL_b to diffuse illuminance on the outside horizontal surface IL_{dif} should be considered. It is defined by

$$R_{vb-hd} = VIL_b / IL_{dif} \tag{5.40}$$

DF_r may be expressed by

$$DF_r = \left(VDF_{i,dg} + VDF_{i,b}\right)DF_{r,d} + R_{vb-hd}TV_{b,g}DF_{r,b} \tag{5.41}$$

where $DF_{r,d}$ is the indoor internal reflection daylight factor due to diffuse light, which actually shows indoor illuminance distribution only due to the multi-reflections of diffuse light. The components in the bracket represent the total diffuse light received by the internal surface of the blinds. It is not only from the diffuse skylight and the ground reflected light, but also from a part of original beam sunlight that enters the space in the form of diffuse light. $DF_{r,b}$ is daylight factor due to the internal multi-reflections of the incoming beam light among the interior surfaces of the room. The fitting equations of $DF_{r,d}$ and $DF_{r,b}$ are presented in Chapter 6.

5.7 Daylight factor due to light directly from the blinds slats

The top or bottom slats may be partly obstructed from the reference point by the adjacent slat. This means that daylight reflected only by the unobstructed part of the slat can directly reach the indoor reference point. If the lower side of the top slat that can be seen by the indoor reference point, the daylight factor due to reflection directly from the slats of the blinds DF_{sr} may be calculated by

$$DF_{sr} = \left(B_{tp,dg} + B_{tp,b}\right)A_{slat}\sum_{i=1}^{n-1} pp_i PVF_{tp-r,i} \tag{5.42}$$

where pp_i is the fraction of the slat area i that can be seen by the indoor reference point; n is the number of slats in the blinds; $PVF_{tp\text{-}r,i}$ is the view factor from the unobstructed part of the top slat i to the indoor reference point.

The beam sunlight incident on the bottom slat may have a clear boundary, and cannot be assumed to be uniform, the slat areas can and cannot receive beam light should be treated separately. Thus, if the upper side of the bottom slat can be seen by the indoor reference point, DF_{sr} may be calculated by

$$\begin{aligned} DF_{sr} = {} & B_{bt,dg} A_{slat} \sum_{i=1}^{n\text{-}1} pp_i PVF_{bt-r,i} + B_{bt0,b}\left(1-p_b\right) A_{slat} \sum_{i=1}^{n\text{-}1} pp_{0,i} PVF_{bt0-r,i} \\ & + B_{bt1,b} p_b A_{slat} \sum_{i=1}^{n\text{-}1} pp_{1,i} PVF_{bt1-r,i} \end{aligned} \tag{5.43}$$

where $PVF_{bt\text{-}r,i}$ is the view factor from the unobstructed part of the bottom slat i to the indoor reference point; $pp_{0,i}$ is the ratio of the slat area not receiving beam light that can be seen by the indoor reference point to the entire slat area not receiving beam light; $pp_{1,i}$ is the ratio of the slat area receiving beam light that can be seen by the indoor reference point to the entire slat area receiving beam light; $PVF_{bt0\text{-}r,i}$ is the view factor from the unobstructed part of the slat area that cannot receive beam light to the indoor reference point; $PVF_{bt1\text{-}r,i}$ is the view factor from the unobstructed part of the slat area receiving beam light to the indoor reference point.

5.8 Summary

A model is developed for the simulation of indoor daylighting when

windows are shaded by venetian blinds. Algebraic equations have been derived for computing different daylight factors and optical transmittances through the blinds, based on the geometric optics and radiosity method. The equations contain all the primary design variables that impact the efficiency and effectiveness of daylighting, and significantly enhance the computational efficiency of daylighting modeling. Different types of window can be simulated by this model by inputing their optical transmittance at different incident angles. Hence, the model is particularly suitable for long-term daylighting simulation, optimal building design, and parametric analysis.

CHAPTER 6

IMPLEMENTATION AND VALIDATION OF THE MODEL FOR DAYLIGHTING SIMULATION WITH VENETIAN BLINDS

Vertical daylight factors on the external and internal surfaces of blinds, and view factors among different surfaces and reference points can be obtained by tedious numerical double integrations in the theoretical model in Chapter 5. To further enhance the computational efficiency of the model, several algebraic equations will be derived in this chapter for determining the above-mentioned daylight factors and view factors. The model then was validated by experimental data and simulated illuminance by Radiance.

6.1 Determination of VDF_{dif} and VDF_{gr}

In Chapter 5, equations have been given to calculate VDF_{dif} and VDF_{gr} by double integrations. To enhance the computational efficiency, fitting equations were obtained from numerical integration results. CIE standard clear and overcast sky models (Moon and Spencer, 1942; CIE, 1973) were used in the theoretical model. Under overcast sky, the vertical daylight factor at the external surface of the blinds due to diffuse skylight $VDF_{o,dif,ov}$ is impendent of blinds and solar position, and can be calculated by

$$VDF_{o,dif,ov} = 0.34T_v(0)$$

The vertical daylight factor at the internal surface of the blinds due to diffuse skylight $VDF_{i,dif,ov}$ is affected by both tilt angle β and the normalized dimension L'. The considered ranges of β and L' are from 75° to -75° with the interval of 15°, and from 1.0 to 1.2 with the interval of 0.5, respectively. The fitting equation for $VDF_{i,dif,ov}$ is expressed by ($R^2 = 0.984$)

$$VDF_{i,dif,ov} = \frac{T_v(0)}{L'}\exp\left(-2.09 - 1.91\sin\beta - 1.81\sin^2\beta\right)$$

For clear sky, the solar altitude α_{sol}, and the difference between window azimuth and solar azimuth γ'_{sol} should be taken into consideration. The considered ranges of α_{sol} and γ'_{sol} are from 15° to 90° with the interval of 15°, and from 0° to 180° with the interval of 15°, respectively. The vertical daylight factor at the external and internal surfaces of the blinds due to diffuse sky light, $VDF_{i,dif,cl}$ and $VDF_{o,dif,cl}$, may be calculated by

$$VDF_{o,dif,cl} = T_v(0)\left(0.44 - 0.47\cos\alpha_{sol} - 0.07\cos\gamma'_{sol} + 0.80\cos^2\alpha_{sol} + 0.17\cos^2\gamma'_{sol} + 0.57\cos\alpha_{sol}\cos\gamma'_{sol}\right) \quad (R^2 = 0.972)$$

$$VDF_{i,dif,cl} = \frac{T_v(0)}{L'}\left(a_1 + a_2\cos\alpha_{sol} + a_3\sin\beta + a_4\cos^2\alpha_{sol} + a_5\sin^2\beta + a_6\cos\alpha_{sol}\sin\beta\right) \quad (R^2 = 0.966)$$

where

$$a_1 = 0.233 + 0.077\cos\gamma'_{sol} + 0.072\cos^2\gamma'_{sol}$$
$$a_2 = -0.1 + 0.006\cos\gamma'_{sol} + 0.017\cos^2\gamma'_{sol}$$
$$a_3 = -0.146 - 0.084\cos\gamma'_{sol} - 0.142\cos^2\gamma'_{sol}$$
$$a_4 = -0.166 - 0.11\cos\gamma'_{sol} - 0.114\cos^2\gamma'_{sol}$$
$$a_5 = 0.206 + 0.258\cos\gamma'_{sol} + 0.274\cos^2\gamma'_{sol}$$
$$a_6 = -0.077 - 0.149\cos\gamma'_{sol} - 0.094\cos^2\gamma'_{sol}$$

The vertical daylight factor at the external surface of the blinds due to

ground-reflected light $VDF_{o,gr}$ is independent of blinds, and can be calculated by

$$VDF_{o,gr} = 0.49T_v(0)\frac{R_{global}\rho_{gr}}{\pi}$$

The vertical daylight factor at the internal surface of the blinds due to ground-reflected light $VDF_{i,gr}$ is affected by both tilt angle β and the normalized dimension L'. The considered ranges of β and L' are the same as those for diffuse sky light. The fitting equation for $VDF_{i,gr}$ is shown as follows ($R^2 = 0.974$).

$$VDF_{i,gr} = \frac{T_v(0)R_{global}\rho_{gr}}{\pi L'}\exp\left(0.174 - 0.312\sin\beta + 0.162\sin^2\beta - 0.02\sin^3\beta\right)$$

6.2 View factor between adjacent slats

In this section, two types of view factors need to be derived, which are the view factor from the portion of the bottom slat that can receive beam sunlight to the entire top slat, $VF_{bt1\text{-}tp}$; and the view factor between adjacent slats VF_{ss}. The only difference between these two view factors is that the portion of slat area is involved in the calculation of the former view factor, while the entire area is considered in the latter one. Therefore, we only need to derive a more general equation for the calculation of view factor when any slat area is involved.

Traditionally, the view factors between surfaces are calculated by forth-integration (Yang, 1980), which are tedious and time-consuming to calculate. Hence, new method is developed to convert the view factors under different tilt angles to those for parallel and perpendicular planes. As the

equations of view factors for parallel and perpendicular planes are available in many literatures, the tedious forth-integration can be replaced by algebraic equations. Hence the calculation can be greatly simplified.

According to Incropera et al. (2007), the view factor for infinite parallel planes with midlines connected by perpendicular (as shown in Figure 6.1) may be calculated by Equation (6.1). In Figure 6.1, w_i and w_j are the widths of parallel planes; and d_{ss} is the distance between them.

$$VF_{i,j} = \frac{\sqrt{\left(W_i + W_j\right)^2 + 4} - \sqrt{\left(W_i - W_j\right)^2 + 4}}{2W_i} \tag{6.1}$$

where $W_i = w_i/d_{ss}$, $W_j = w_j/d_{ss}$.

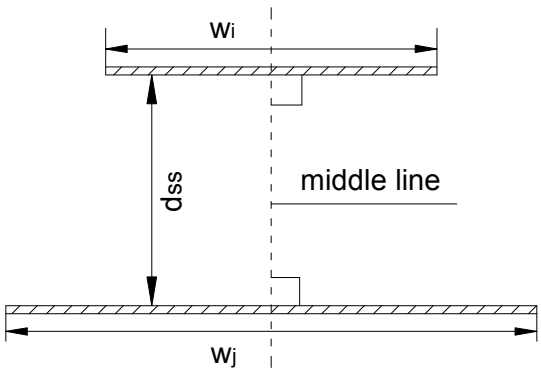

Figure 6.1 Infinite parallel planes with midlines connected by perpendicular.

As shown in Figure 6.2, the normalized perpendicular distance between adjacent slats is cosβ at the tilt angle β. If the ratio of the bottom slat area receiving beam light to the entire bottom slat area is p_b, the relative positions of bottom and top slats is shown in Figure 6.3. In the figure, the portion of the bottom slat area not receiving beam light is represent by dashed line.

Examination of Figure 6.3 shows that the middle line of the bottom slat area receiving beam light divides the top slat into two parts. The view factor from the bottom slat area receiving beam light to the top slat areas at left and right sides of the middle line can be separately calculated by Equation (6.1). Then $VF_{bt1,tp}$ may be calculated by summing up these two view factors, as shown below.

$$VF_{bt1-tp} = \frac{\sqrt{(\sin\beta + L')^2 + \cos^2\beta} - \sqrt{(p_b L' - \sin\beta - L')^2 + \cos^2\beta}}{2p_b L'} + \frac{\sqrt{(p_b L' - \sin\beta)^2 + \cos^2\beta} - 1}{2p_b L'}$$

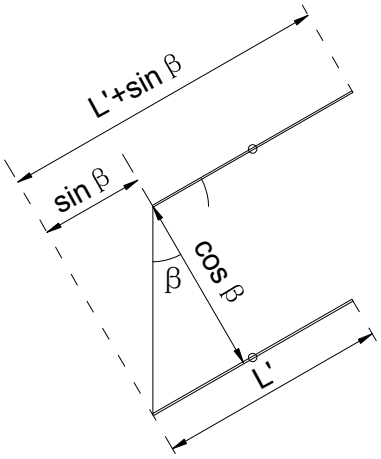

Figure 6.2 Distance between adjacent slats.

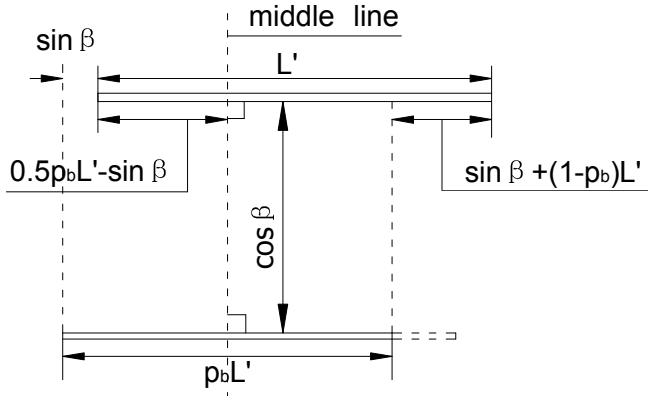

Figure 6.3 Relative positions of bottom and top slats when a portion of bottom slat area can receive beam light.

6.3 View factor from slat surface to internal&external surface of blinds

In this section, two types of view factors need to be derived, which are view factor from the portion of the bottom slat that can receive beam sunlight to the internal surface of the blinds $VF_{bt1\text{-}i}$; and the view factor from the entire bottom slat to the internal surface of the blinds $VF_{bt\text{-}i}$. The only difference between these two view factors is that the former view factor only involves the portion of bottom slat area receiving beam light, while the entire bottom slat area is considered in the latter one. Therefore, we only need to derive a more general equation for the calculation of view factor when any slat area is involved.

The view factor for infinite perpendicular planes with a common edge (as shown in Figure 6.4) may be calculated by (Incropera et al., 2007)

$$VF_{i,j} = \frac{1 + w_j / w_i - \sqrt{1 + \left(w_j / w_i\right)^2}}{2} \tag{6.2}$$

where w_i and w_j are the widths of perpendicular planes.

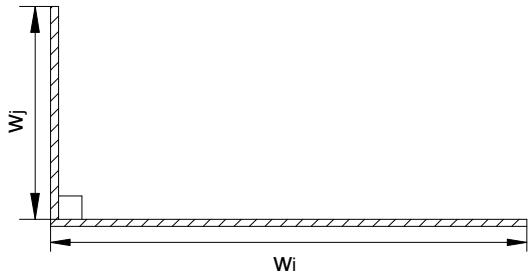

Figure 6.4 Infinite perpendicular planes with a common edge.

Figure 6.5 show the sections of blinds with positive and negative tilt angles. Normally, the window width *W'* is much larger than the width of slat *L'*.

Therefore, the areas of the vertical planes between two ends of the slats are ignorable compared with the areas of slats and the internal surfaces of the blinds between adjacent slats. Hence, plane r3r4, plane r3r5, the internal surface of blinds r1r5, and the imagined plane r1r4 constitute an enclosed space, as shown in Figure 6.5a. Then we have the following relationship based on the summation rule (Frank and David, 2002).

$$VF_{bt1-i} + VF_{bt1-14} = 1 \tag{6.3}$$

where $VF_{bt1\text{-}14}$ is the view factor from the slat area receiving beam light to the imagined plane r1r4.

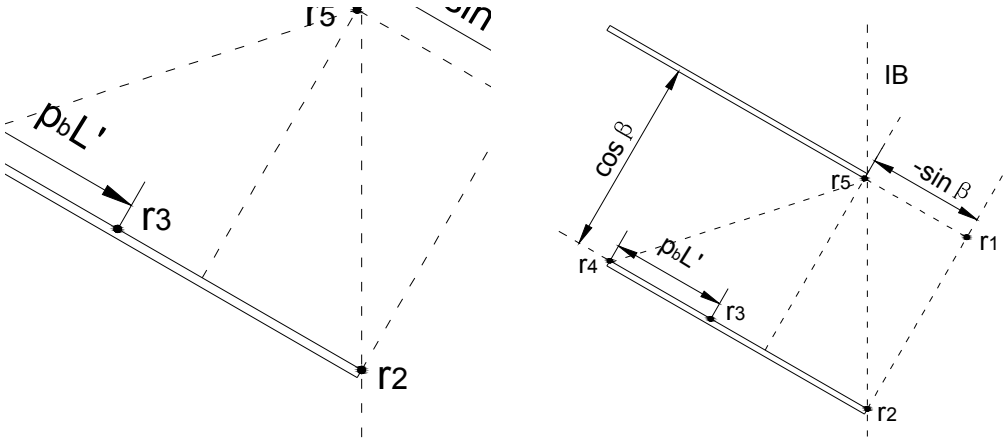

(a) (b)

Figure 6.5 Enclosed space created by the slat, internal surfaces of blinds and the imagined plane; (a) $\beta \geq 0°$, (b) $\beta < 0°$.

From Figure 6.5a we can find that plane r3r4, plane r2r3, plane r1r2, and the imagined plane r1r4 also constitute an enclosed space, which can be expressed by

$$VF_{bt1-12} + VF_{bt1-14} = 1 \tag{6.4}$$

where $VF_{bt1\text{-}12}$ is the view factor from the slat area receiving beam light to the

imagined plane r1r2.

Combining Equations (6.3) and (6.4) yields

$$VF_{bt1-i} = VF_{bt1-12} \tag{6.5}$$

Therefore, the view factor from the slat to the internal surface of blinds can be approximately converted to the view factor from slat to an imagined plane perpendicular to the slat surface. Then Equation (6.2) can be used to calculate the view factor. If the tilt angle $\beta \geq 0°$, we need to derive the equations for the view factor from plane r_2r_4 to r_1r_2 ($VF_{24\text{-}12}$) and the view factor from plane r_2r_3 to r_1r_2 ($VF_{23\text{-}12}$). Then $VF_{bt1\text{-}i}$ may be calculated by

$$VF_{bt1-i} = \frac{VF_{24-12}\left(L'+\sin\beta\right) - VF_{23-12}\left[\left(1-p_b\right)L'+\sin\beta\right]}{p_b L'}$$

$VF_{24\text{-}12}$ and $VF_{23\text{-}12}$ may be calculated by Equation (6.2) as follows

$$VF_{24-12} = \frac{1+\dfrac{\cos\beta}{L'+\sin\beta} - \sqrt{1+\left(\dfrac{\cos\beta}{L'+\sin\beta}\right)^2}}{2}$$

$$VF_{23-12} = \frac{1+\dfrac{\cos\beta}{\left(1-p_b\right)L'+\sin\beta} - \sqrt{1+\left[\dfrac{\cos\beta}{\left(1-p_b\right)L'+\sin\beta}\right]^2}}{2}$$

If the tilt angle $\beta < 0°$, $VF_{bt1\text{-}i}$ can be approximately converted to the sum of the view factor from plane r_3r_4 to r_1r_2 ($VF_{34\text{-}12}$) and the view factor from plane r_3r_4 to r_1r_5 ($VF_{34\text{-}12}$), as shown in Figure6.5b. That is

$$VF_{bt1-i} = VF_{34-12} + VF_{34-15} \tag{6.6}$$

$VF_{34\text{-}12}$ and $VF_{34\text{-}12}$ may be calculated by Equations (6.1) and (6.2) as follows.

$$VF_{34-12} = \frac{p_b L' - \sqrt{L'^2 + \cos^2\beta} + \sqrt{(L' - p_b L')^2 + \cos^2\beta}}{2 p_b L'} \tag{6.7}$$

$$VF_{34-15} = \frac{\sqrt{L'^2 + \cos^2\beta} - \sqrt{(L' - p_b L')^2 + \cos^2\beta}}{2 p_b L'} - \frac{\sqrt{(L' + \sin\beta)^2 + \cos^2\beta} - \sqrt{(\sin\beta + (1 - p_b)L')^2 + \cos^2\beta}}{2 p_b L'} \tag{6.8}$$

Using the same method, we derived the equation for the calculation of the view factor from the entire top slat to the internal surface of the blinds $VF_{tp\text{-}i}$, which is shown below.

$$VF_{tp-i} = \frac{L' + 1 - \sqrt{(L' - \sin\beta)^2 + \cos^2\beta}}{2L'} \tag{6.9}$$

6.4 View factor from slat surface to reference point

6.4.1 Ratio of slat area seen from reference point

Figure 6.6 shows how much slat can be seen from an indoor reference point. Let the plane A_s be the slat plane under consideration and the line L_1 be the upper edge of the slat that just below plane A_s. At any azimuth angle γ'_{sky}, the critical point R_C on the slat that can be seen by the indoor reference point R is limited by the line L_1. Therefore, all critical points on the slat can be determined by the line L_1 and the point R (plane RL_1). It can be seen that the line (L_2) formed by all critical points is the intersected line of the two planes RL_1 and A_s. The line L_1 is parallel to the plane A_s, then L_2 must be parallel to L_1 (Jiten, 1984). This means L_2 is perpendicular to the axes Y and Z, and all the critical points have the same height and depth. Accordingly, we can simplify the question by only studying the simplest case, in which the line linking the reference point R and the critical

point on the slat R_C is perpendicular to the X axis, as shown in Figure 6.6.

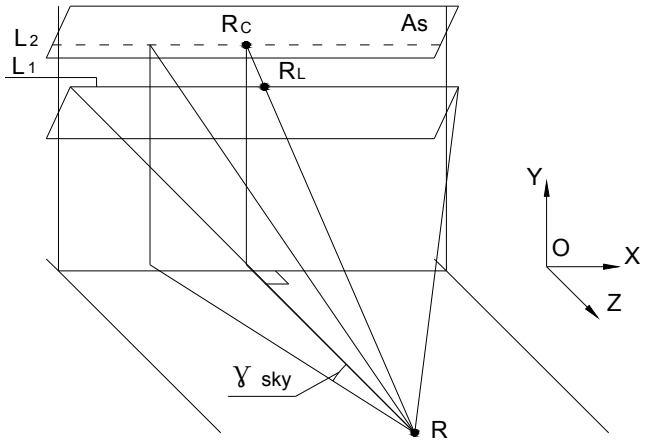

Figure 6.6 Critical points on slats that can be seen by indoor reference point.

Figure 6.7 shows the relative positions of the critical point on slat and the indoor reference point. Let the Cartesian coordinate of the indoor reference point R be $(0, 0, 0)$ and the Cartesian coordinate of the point R_L be (x_L, y_L, z_L). Let x'_L,= x_L/H_{ss}, y'_L,= y_L/H_{ss} and $z'_L = z_L/H_{ss}$. They can be calculated by following equation, as shown in Figure 6.7.

$$x'_L = 0 \tag{6.10}$$

$$y'_L = H'_{slat} - 1 + 0.5L' \sin\beta \tag{6.11}$$

$$z'_L = D'_{slat} - 0.5L' \cos\beta \tag{6.12}$$

where L' is the normalized slat width, $L' = L/H_{ss}$; H'_{slat} is the normalized height of the center of the slat under consideration, $H'_{slat} = H_{slat}/H_{ss}$

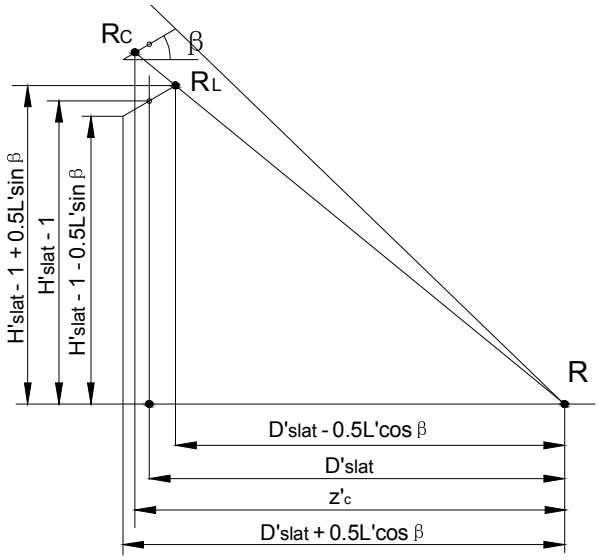

Figure 6.7 Relative positions of the critical point on slat and the indoor reference point.

Then the line RR_C can be mathematically expressed by

$$y' = \left(\frac{y'_L}{z'_L} \right) z' = \left(\frac{H'_{slat} - 1 + 0.5L' \sin\beta}{D'_{slat} - 0.5L' \cos\beta} \right) z' \tag{6.13}$$

The vertical coordinate y' the plane A_s can be expressed by

$$y' = (D'_{slat} - z') \tan\beta + H'_{slat} \tag{6.14}$$

The critical point R_C must satisfy Equations (6.13) and (6.14) simultaneously. Let the Cartesian coordinate of the critical point R_C be $(0, y_c, z_c)$. Using the normalized form of $y'_c = y_c/H_{ss}$ and $z'_c = z_c/H_{ss}$, we can determine y'_c and z'_c by solving Equations (6.13) and (6.14) as follows.

$$z'_c = \frac{D'^{\,2}_{slat} \tan\beta + H'_{slat} D'_{slat} - 0.5 D'_{slat} L' \sin\beta - 0.5 L' H'_{slat} \cos\beta}{H'_{slat} - 1 + D'_{slat} \tan\beta} \tag{6.15}$$

$$y'_c = \left(\frac{H'_{slat} - 1 + 0.5L' \sin\beta}{D'_{slat} - 0.5L' \cos\beta} \cdot \right) z'_c \tag{6.16}$$

From Figure 6.7, we can determine the ratio of slat area that can be seen by the reference point to the entire slat area pp_i by

$$pp_i = \frac{z'_c - (D'_{slat} - 0.5L' \cos\beta)}{L' \cos\beta} \tag{6.17}$$

6.4.2 View factor from unobstructed slat surface to reference point

Traditionally, the view factors from flat plane to a reference point are calculated by double-integration (Yang, 1980). In this section, new method is presented to simplify the calculation by using the equation for view factors from a reference point to half wall.

6.4.2.1 Positive tilt angle

If the inward side of the top slat can be seen by the indoor reference point, the projection of the unobstructed part of the slat on the central surface of the blinds may be illustrated by Figure 6.8. In the figure, $H'_{p2,i}$ and $H'_{p1,i}$ are the normalized upper and lower heights of the projection, $H'_{p2,i}= H_{p2,i}/H_{ss}$ and $H'_{p1,i}= H_{p1,i}/H_{ss}$. Examination of Figure 6.8 shows that the view factor from the unobstructed part of the lower side of the top slat to the indoor reference point $PVF_{tp\text{-}r,i}$ can be equivalently converted to the view factor from the projection of the unobstructed slat on the central surface of the blinds to the indoor reference point $VF_{c\text{-}r,i}$ by the following equation.

$$PVF_{tp-r,i}\, pp_i A'_{slat} = VF_{c-r,i} A'_{p,i} \tag{6.18}$$

where $A'_{p,i}$ is the normalized area of the projection.

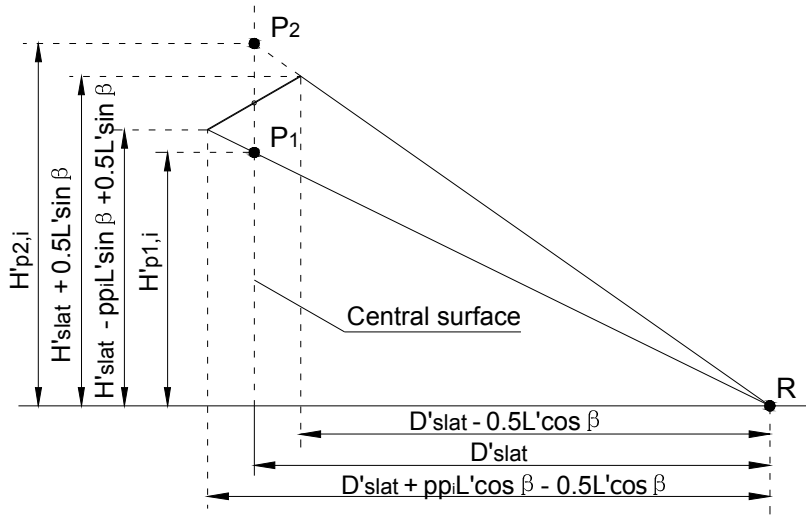

Figure 6.8 Projection of the top slat on the central surface of the blinds

Strictly speaking, the projection of the slat on the central surface of the blinds is a trapezoid. However, it can be regarded as a rectangle without introducing noticeable error if the window width *W'* is much larger than the width of slat *L'*. Therefore, $A'_{p,i}$ may be computed by

$$A'_{p,i} = W'\left(H'_{p2,i} - H'_{p1,i}\right) \tag{6.19}$$

$H'_{p2,i}$ and $H'_{p1,i}$ may be calculated by (Figure 6.8)

$$H'_{p2,i} = D'_{slat}\frac{H'_{slat} + 0.5L'\sin\beta}{D'_{slat} - 0.5L'\cos\beta} \tag{6.20}$$

$$H'_{p1,i} = D'_{slat}\frac{H'_{slat} - pp_i L'\sin\beta + 0.5L'\sin\beta}{D'_{slat} + pp_i L'\cos\beta - 0.5L'\cos\beta} \tag{6.21}$$

Yang (1980) provides an equation for the calculation of view factor from the reference point to half wall $VF_{i\text{-}hw}$, as shown in Figure 6.9.

$$VF_{i-hw} = \frac{1}{2\pi}\left[\arctan\left(\frac{X}{Z}\right) - \frac{Z}{\sqrt{Y^2+Z^2}}\arctan\left(\frac{X}{\sqrt{Y^2+Z^2}}\right)\right] \tag{6.22}$$

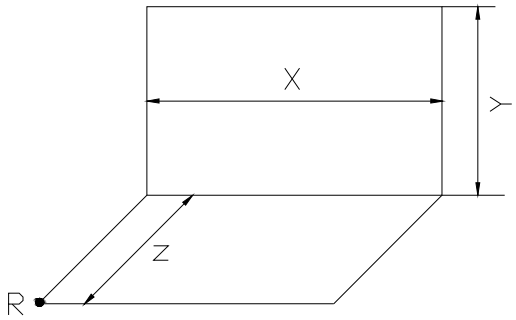

Figure 6.9 Sketch of the reference point and half wall

The view factor from the reference point to the projection area is determined by the upper and lower edges of a slat, and the projection areas to the left and right sides of the reference point. Therefore, Equation (6.22) needs to be used four times, and the equation of $VF_{c\text{-}r,i}$ may be obtained by using the reciprocity relation and the summation rule as follows.

$$
\begin{aligned}
VF_{c-r,i} = \frac{1}{2\pi W\left(H'_{p2,i}-H'_{p1,i}\right)}\Bigg[& \arctan\left(\frac{w'}{D'_{slat}}\right)-\frac{D'_{slat}}{\sqrt{H'^{\,2}_{p2,i}+D'^{\,2}_{slat}}}\arctan\left(\frac{w'}{\sqrt{H'^{\,2}_{p2,i}+D'^{\,2}_{slat}}}\right) \\
& +\arctan\left(\frac{W'-w'}{D'_{slat}}\right)-\frac{D'_{slat}}{\sqrt{H'^{\,2}_{p2,i}+D'^{\,2}_{slat}}}\arctan\left(\frac{W'-w'}{\sqrt{H'^{\,2}_{p2,i}+D'^{\,2}_{slat}}}\right) \\
& -\arctan\left(\frac{w'}{D'_{slat}}\right)+\frac{D'_{slat}}{\sqrt{H'^{\,2}_{p1,i}+D'^{\,2}_{slat}}}\arctan\left(\frac{w'}{\sqrt{H'^{\,2}_{p1,i}+D'^{\,2}_{slat}}}\right) \\
& -\arctan\left(\frac{W'-w'}{D'_{slat}}\right)+\frac{D'_{slat}}{\sqrt{H'^{\,2}_{p1,i}+D'^{\,2}_{slat}}}\arctan\left(\frac{W'-w'}{\sqrt{H'^{\,2}_{p1,i}+D'^{\,2}_{slat}}}\right)\Bigg]
\end{aligned}
\tag{6.23}
$$

6.4.2.2 Negative tilt angle

The final luminous exitance on the bottom slat may have a clear boundary as only a portion of bottom slat area may receive beam light. Therefore, the bottom slat area receiving and not receiving beam light need to be treated

separately in the calculation of the view factor from the unobstructed part of the upper side of the bottom slat to the indoor reference point $PVF_{bt\text{-}r,i}$. Figure 6.10 shows the ratio of area receiving beam light that can be seen by the indoor reference point p_s , which may be calculated by Equation (6.24). In the figure, R_{sol} is the critical points that the slat can receive beam light, and R_C is the critical point that the slat can be seen by the indoor reference point.

$$p_s = p_b + pp_i - 1 \tag{6.24}$$

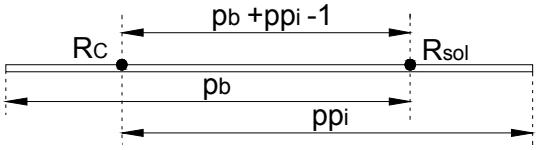

Figure 6.10 Ratio of area receiving beam light that can be seen by the indoor reference point

If value of p_s is positive, the ratio of the slat area not receiving beam light that can be seen by the indoor reference point to the entire slat area not receiving beam light $pp_{0,i}$; and the ratio of the slat area receiving beam light that can be seen by the indoor reference point to the entire slat area receiving beam light $pp_{1,i}$, can be determined by

$$pp_{0,i} = 1$$

$$pp_{1,i} = \frac{pp_i}{p_b}$$

Figure 6.11 show the projection of the bottom slat on the central surface of the blinds. Similar to the calculation of $PVF_{tp\text{-}r,i}$, the view factor from the unobstructed part of the bottom slat receiving beam light to the indoor reference point $PVF_{bt1\text{-}r,i}$ may be calculated by

$$PVF_{bt1-r,i}\,p_s\,A'_{slat} = VF_{c-r,i}W'\left(H'_{p2,i} - H'_{p1,i}\right) \tag{6.25}$$

with

$$H'_{p2,i} = D'_{slat}\,\frac{H'_{slat} + pp_i L'\sin\beta - 0.5L'\sin\beta}{D'_{slat} + pp_i L'\cos\beta - 0.5L'\cos\beta}$$

$$H'_{p1,i} = D'_{slat}\,\frac{H'_{slat} - p_b L'\sin\beta + 0.5L'\sin\beta}{D'_{slat} - p_b L'\cos\beta + 0.5L'\cos\beta}$$

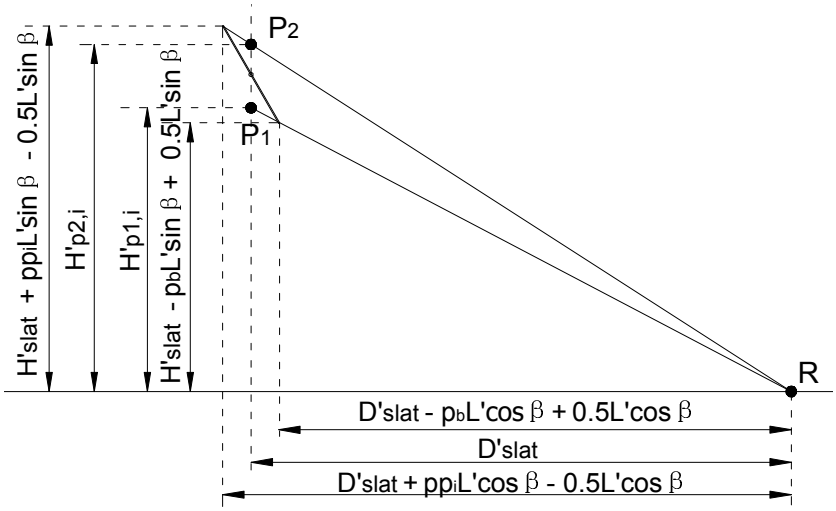

Figure 6.11 Projection of the bottom slat on the central surface of the blinds

The view factor from the unobstructed part of the bottom slat not receiving beam light to the indoor reference point $PVF_{bt0\text{-}r,i}$ may be calculated by

$$PVF_{bt0-r,i}\left(1-p_b\right)A'_{slat} = VF_{c-r,i}W'\left(H'_{p2,i} - H'_{p1,i}\right) \tag{6.26}$$

with

$$H'_{p2,i} = D'_{slat}\,\frac{H'_{slat} + \left(1-p_b\right)L'\sin\beta - 0.5L'\sin\beta}{D'_{slat} + \left(1-p_b\right)L'\cos\beta - 0.5L'\cos\beta}$$

$$H'_{p1,i} = D'_{slat}\,\frac{H'_{slat} - L'\sin\beta + 0.5L'\sin\beta}{D'_{slat} - L'\cos\beta + 0.5L'\cos\beta}$$

If the value of p_s is negative, it means there is no beam light can be directly reflected to the indoor reference point from the bottom slat. Then $pp_{0,i}$ and $pp_{1,i}$

can be calculated by

$$pp_{0,i} = \frac{pp_i}{1 - p_b}$$

$$pp_{1,i} = 0$$

$PVF_{bt0\text{-}r,i}$ may be calculated by

$$PVF_{bt0-r,i}\, pp_i\, A'_{slat} = VF_{c-r,i} W' \left(H'_{p2,i} - H'_{p1,i} \right) \tag{6.27}$$

with

$$H'_{p2,i} = D'_{slat} \frac{H'_{slat} + pp_i L' \sin\beta - 0.5 L' \sin\beta}{D'_{slat} + pp_i L' \cos\beta - 0.5 L' \cos\beta}$$

$$H'_{p1,i} = D'_{slat} \frac{H'_{slat} - L' \sin\beta + 0.5 L' \sin\beta}{D'_{slat} - L' \cos\beta + 0.5 L' \cos\beta}$$

6.5 Daylight factor caused by indoor multi-reflections in room with blinds

The split-flux method was used in DOE2 to calculate the daylight factor due to the multi-reflections of light among the interior surfaces when the blinds are not used. This method assumes the internally reflected illuminance is evenly distributed throughout the room. It could overestimate the illuminance at the rear part of the room and underestimate the illuminance at the area near window. Radiance was used to generate indoor illuminance distribution due to the internal multi-reflections of incoming diffuse and beam daylight in the wide range of room and window configurations, sky conditions and slat tilt angles.

Radiance cannot directly show the indoor illuminance purely caused by multi-reflection among the interior surfaces of a room. Hence, two Radiance

models were used in the simulation of each case. The real interior reflectance was adopted in the first model, while it was set to zero in the second one. The difference between two simulated indoor illuminance results is the illuminance purely caused by multi-reflection among the interior surfaces. Then fitting technique was applied to the computed illuminances to obtain daylight factors caused by the internal reflection of diffuse and beam light. CIE standard clear and overcast sky models were used in the simulations. Examination of the Radiance results shows that $DF_{r,d}$ and $DF_{r,b}$ are affected by several key parameters, which are shown in Table 6.1. Their ranges and intervals considered in the fitting equations are also shown in the table.

Table 6.1 Key parameters considered in the fitting equations for $DF_{r,d}$ and $DF_{r,b}$

Parameter	Range	Interval
$H'_{win,c}$	From 0.15 to 0.5	0.05
D'_{ref}	From 0.1 to 0.9	0.1
W'_{rm}	From 0.3 to 1.5	0.1
ρ_{rm}	From 0.0 to 0.7	0.1
α_{sol}	From 15º to 90º	15º
γ'_{sol}	From 0º to 180º	15º

where $H'_{win,c}$ is the normalized height of the central line of window, $H_{win,c}/D_{rm}$; D_{rm} is the depth of a room (m); D'_{ref} is the normalized depth of reference point, D_{ref}/D_{rm}; W'_{rm} is the normalized width of a room, W_{rm}/D_{rm}; ρ_{rm} is the reflectance of indoor room surfaces.

The fitting equations for $DF_{r,d}$ and $DF_{r,b}$ are (R^2 = 0.968 and 0.962)

$$DF_{r,d} = \frac{A_{win}\rho_{rm}}{A_{rm}(1-\rho_{rm})} SDF_{r,d}^{\,f_\rho f_d f_W f_{slat}} \tag{6.28}$$

$$DF_{r,b} = \frac{A_{win}\rho_{rm}}{A_{rm}(1-\rho_{rm})} SDF_{r,b}^{\ f_\rho f_b f_W} \tag{6.29}$$

where A_{rm}, A_{win} and ρ_{rm} are the interior surface area (m^2), window area (m^2) and the reflectance of room, respectively; $SDF_{r,d}$ and $SDF_{r,b}$ are factors that describe the distribution of internally reflected daylight at different depth of the room; f_ρ, f_W, f_{slat}, f_d and f_b are correction coefficients for reflectance of indoor room surface, normalized room width, slat tilt angle and solar position, respectively.

$SDF_{r,d}$ and $SDF_{r,b}$ can be calculated by

$$\begin{aligned} SDF_{r.b} &= 4.90 - 23.84\, H'_{win,c} - 3.67\, D'_{ref} + 40.79\, H'^{2}_{win,c} - 4.76\, D'^{2}_{ref} + 26.54\, H'_{win,c} D'_{ref} \\ &\quad - 23.67\, H'^{3}_{win,c} + 3.91\, D'^{3}_{ref} - 2.84\, H'_{win,c} D'^{2}_{ref} - 23.60\, H'^{2}_{win,c} D'_{ref} \\ SDF_{r.d} &= 3.43 - 15.18\, H'_{win,c} - 2.56\, D'_{ref} + 25.48\, H'^{2}_{win,c} - 4.48\, D'^{2}_{ref} + 20.43\, H'_{win,c} D'_{ref} \\ &\quad - 14.95\, H'^{3}_{win,c} + 3.52\, D'^{3}_{ref} - 2.16\, H'_{win,c} D'^{2}_{ref} - 17.25\, H'^{2}_{win,c} D'_{ref} \end{aligned}$$

Coefficients in Equations (6.28) and (6.29) can be calculated by

$$f_\rho = -\rho_{rm} + 1.4$$

$$f_W = 0.77\, W'^{2}_{rm} - 2.07\, W'_{rm} + 2.19$$

$$f_{slat} = 0.82\cos^2\beta - 1.95\cos\beta + 2.33$$

$$f_d(\alpha_{sol}, \gamma'_{sol}) = \frac{1.06 - 0.71\cos\alpha_{sol} - 0.34\cos\gamma'_{sol}}{1 - 0.54\cos\alpha_{sol} - 0.60\cos\gamma'_{sol} + 0.28\cos^2\gamma'_{sol}}$$

$$f_b(\alpha_{sol}, \gamma'_{sol}) = -3.48 + 6.2\cos\alpha_{sol} + 4.61\cos\gamma'_{sol} - 2.31\cos^2\alpha_{sol} - 1.23\cos^2\gamma'_{sol} - 3.66\cos\alpha_{sol}\cos\gamma'_{sol}$$

6.6 Comparison of measured and simulated illuminance

The same measured and simulated data with Radiance used in Chapter 4 are utilized here to validate the new daylighting simulation model. Clear glazing was used in the simulation. The optical transmittance and internal reflectance are 78% and 6%, respectively. Totally over 500 sets of data were used in the validation. Simulation results of EnergyPlus, an hourly simulation program with

more advanced technique in blinds simulation, are also presented for comparison.

Figure 6.12 shows simulated indoor illuminance and averaged measured data represented by the solid lines. We can see that the new model has comparable accuracy with Radiance and better accuracy than EnergyPlus. All the three methods have acceptable performance in general cases. Figure 6.13 presents measured and simulated indoor illuminances at different reference points under overcast sky. Table 6.2 summaries the MBEs and RMSEs of the new model and Radiance in the simulation of windows with the blinds at different tilt angles under overcast sky. The tilt angle -60° is seldom used under overcast sky and hence is not considered here. Radiance slightly overestimates the indoor illuminance in most of the cases. EnergyPlus underestimates the indoor illuminance at most reference points. The reason may be that EnergyPlus ignores the internally reflection between blinds and glazing (EnergyPlus Engineering Reference, 2010), which may underestimate the daylight passing through the blinds system, especially when window with high internal reflectance is used. For example, our comparison is based on clear glass with internal reflectance of 6% (Radiance Material Library, 2000). If high internal reflectance of 20% is input to EnergyPlus, Radiance and the new model while other simulation parameters remain unchanged, MBE and RMSE error of EnergyPlus may increase to -23% and 40%, compared to Radiance results. While the MBE and RMSE error of the new model is only 4% and 19%. Another

disadvantage of EnergyPlus is the speed of calculation. As EnergyPlus uses radiosity method for the calculation of indoor illuminance due to internal reflections among internal surfaces (EnergyPlus Engineering Reference, 2010), a lot of room patches have to be used to get an accurate result. Our calculation shows the average time consumption of EnergyPlus is 2.8 seconds, which is almost 2 times longer than the new model's time consumption of 1.02 seconds.

Figure 6.13 presents the distributions of indoor measured and simulated illuminance throughout the room by new model, Radiance and EnergyPlus at 4 different slat tilt angles under overcast sky, while Figure 6.14 gives those under clear sky. Tables 6.2 and 6.3 summarize the MBEs and RMSEs between these measured and simulated data. It can be seen from these results that the slat tilt angle strongly impact the distribution of indoor illuminance. In the overall result, EnergyPlus generally underestimates indoor illuminance under both overcast and clear sky and gives higher errors as compared to those produced by Radiance and the new model.

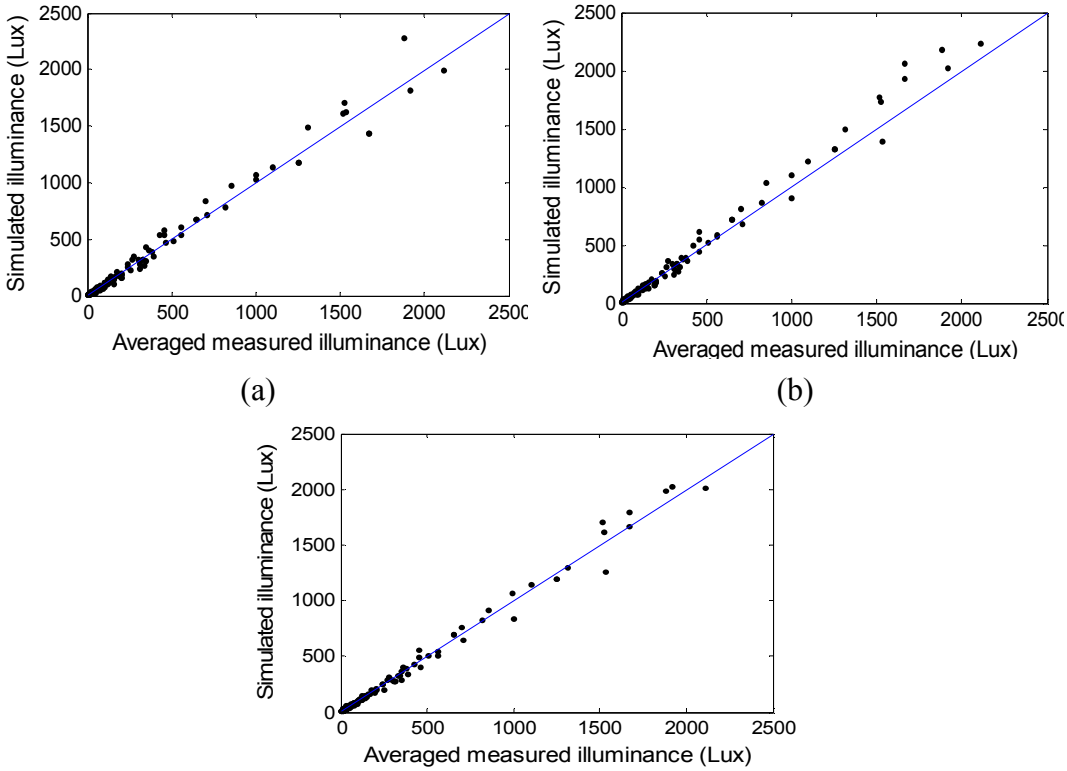

(a) (b)

(c)

Figure 6.12 Simulated indoor illuminances vs. measured illuminance, (a) Radiance, (b) New model, (c) EnergyPlus.

Table 6.2 MBE and RMSE for windows with blinds under overcast sky (%).

	Tilt angle	Radiance	EnergyPlus	New model
MBE	-30°	16	-12	15
	0°	1	-15	-5
	30°	12	-17	-8
	60°	10	3	9
	Overall	10	-9	4
RMSE	-30°	16	15	21
	0°	20	25	16
	30°	12	30	13
	60°	18	13	18
	Overall	17	21	17

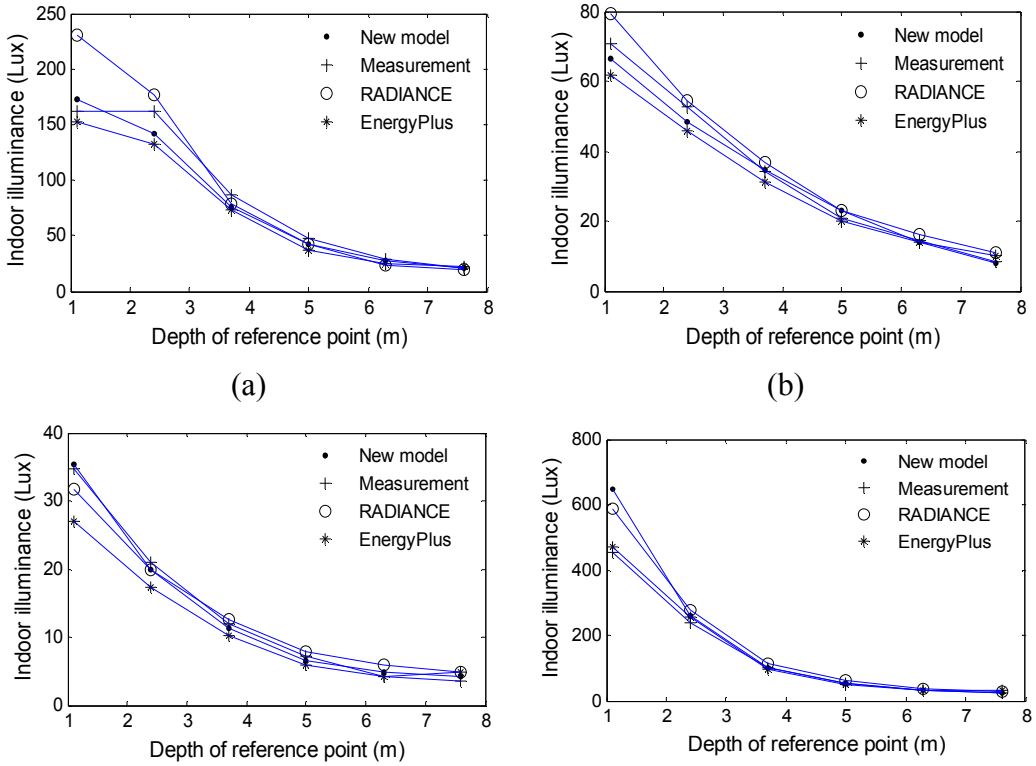

Figure 6.13 Comparison of measured and simulated indoor daylight illuminance under overcast sky, (a) $\beta = 0°$; (b) $\beta = 30°$; (c) $\beta = 60°$; (d) $\beta = -30°$. Outdoor diffuse illuminance is 6100 Lux.

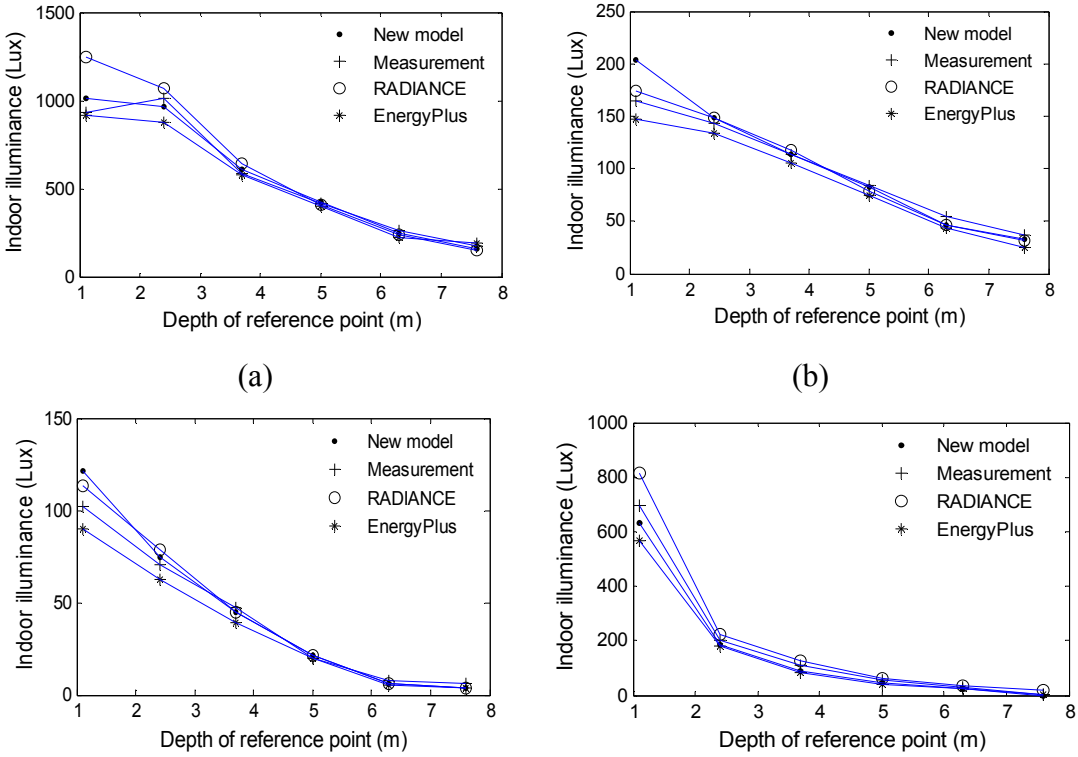

Figure 6.14 Comparison of measured and simulated indoor daylight illuminance under clear sky, solar altitude = 40°, solar azimuth = 50° west of south, (a) $\beta = 0°$; (b) $\beta = 30°$; (c) $\beta = 60°$; (d) $\beta = -60°$, Outdoor diffuse and beam illuminance are 13800 Lux and 26300 Lux, respectively.

Table 6.3 MBE and RMSE for windows with blinds under clear sky (%).

	Tilt angle	Radiance	EnergyPlus	New model
MBE	-60°	-8	-17	12
	0°	-3	-5	-3
	30°	-7	-7	10
	60°	-11	-3	-13
	Overall	-7	-8	2
RMSE	-60°	16	25	21
	0°	16	22	18
	30°	16	27	19
	60°	29	34	25
	Overall	19	27	21

The new model separately calculates the indoor illuminance caused by diffuse

skylight passing through gaps between blind slats and direct reaching the reference point (IL_{dif}), due to multi-reflections on different interior surfaces (IL_r) and due to reflection directly from the blinds (IL_{sr}). Radiance and EnergyPlus cannot directly generate these three illuminance components separately. We can obtain them separately by the following procedure:

1) IL_{dif} produced by Radiance and EnergyPlus could be obtained by excluding all reflections from the indoor illuminance due to diffuse daylight by setting the reflectance of blinds slat and internal walls as zero;
2) To obtain IL_r generated by Radiance and EnergyPlus, the first model considers all three components of indoor illuminance, while the second model excludes multi-reflections on different interior surfaces by setting the reflectance of internal walls as zero. Difference of the two simulation results with the two models is illuminance IL_r given by Radiance and EnergyPlus, which was used to validate that of the new model;
3) Similar to IL_r, to obtain IL_{sr} given by Radiance and EnergyPlus, the first model considers all three components of indoor illuminance, while the second model exclude multi-reflections between blinds slats by setting slat reflectance as zero. Difference of the simulation results of two models is IL_{sr} simulated by Radiance and EnergyPlus, which were used to validate this component of the new model.

Validation results show results of new model are in good agreement with

Radiance, while EnergyPlus greatly underestimate IL_{sr} under all conditions. Figures 6.15 and 6.16 present simulation results at different reference points under overcast and clear skies. Table 6.4 summaries the MBEs and RMSEs of new model and EnergyPlus against Radiance.

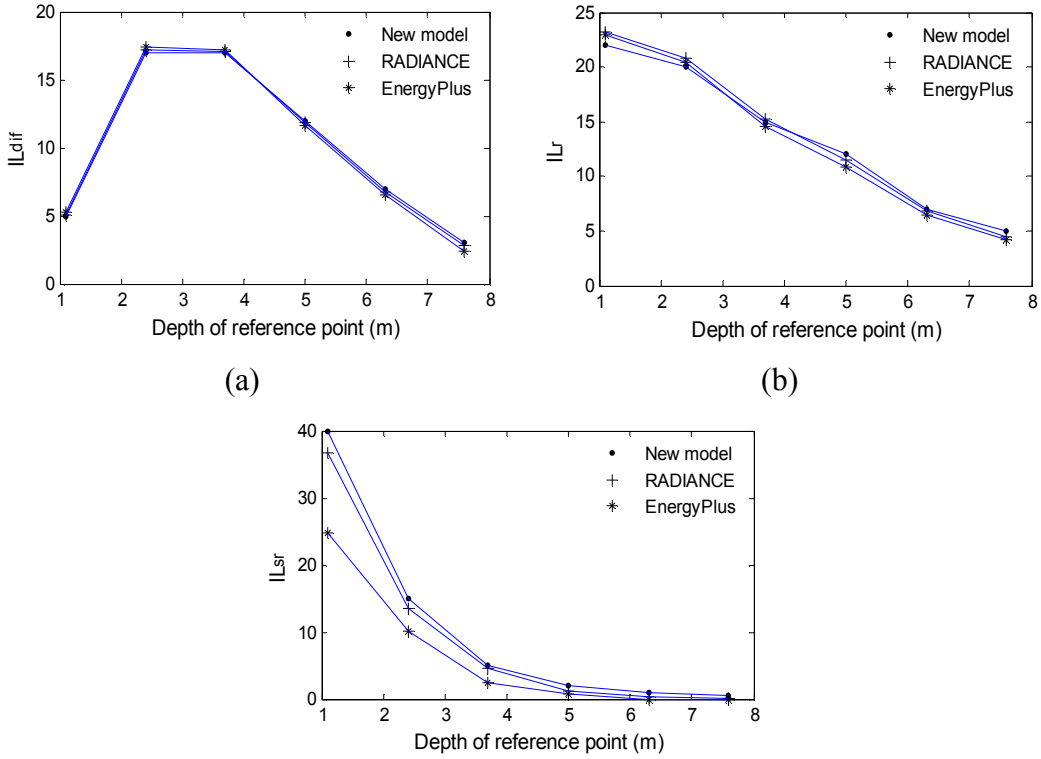

Figure 6.15 Comparison of different daylight components under overcast sky, $\beta = 30°$, Outdoor diffuse illuminance is 6100 Lux.

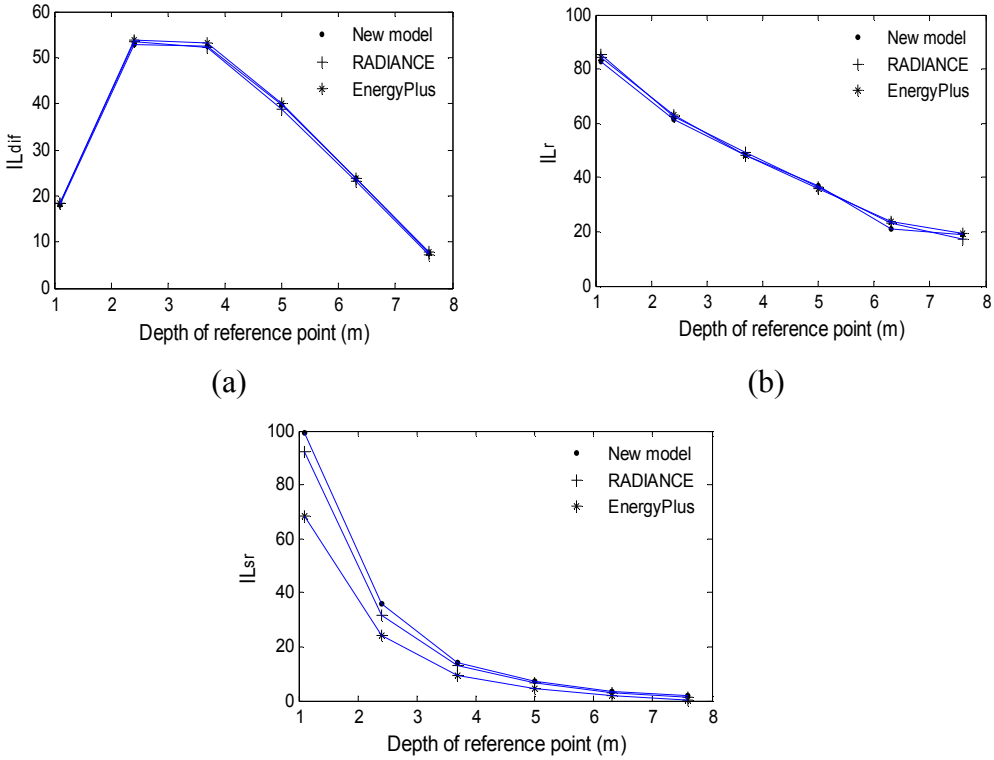

Figure 6.16 Comparison of different daylight components under clear sky, $\beta = 30°$, Outdoor diffuse and beam illuminance are 13800 Lux and 26300 Lux, respectively.

Table 6.4 MBE and RMSE for three daylight components (%).

	Component	New Model		EnergyPlus	
		Clear sky	Overcast sky	Clear sky	Overcast sky
MBE	IL_{dif}	0.1	0.1	0.1	0.1
	IL_r	4.7	4.2	4.4	4.0
	IL_{sr}	-9.4	-8.9	-28.4	-28.9
RMSE	IL_{dif}	0.3	0.2	0.4	0.2
	IL_r	7.7	6.9	7.4	6.3
	IL_{sr}	12.7	11.8	35.2	35.9

From Figures 6.15 and 6.16 and Table 6.4, we can see that the IL_{dif} values simulated by three models are almost equal. This is because all these models use the same method for the calculation of this component. The model and Radiance also have very similar IL_r results because the IL_r fitting equation used by the new

model is derived from simulation results of Radiance. EnergyPlus can also provide accurate result as it adopts detailed radiosity method. The value of IL_{sr} simulated by the new model have relatively poorer accuracy as compared with other two components. This may be because IL_{sr} decreases rapidly with depth of room, and most of room areas have very small IL_{sr} value. A small error at the deep area could leads to a large relative error duet to the small true illuminance. If only the reference points 1.1m and 2.4m from window are considered, MRE values under overcast and clear skies decreases to 6.7% and 6.4%, respectively. And RMSE values under overcast and clear skies are 10.3% and 9.7%. EnergyPlus greatly underestimate IL_{sr} under all conditions. This further proves that much of the error of EnergyPlus comes from ignoring the internal reflections between blinds and glazing plates.

6.7 Analysis of indoor illuminance components

Many researches on blinds concentrate on the calculation of total amount of light that passes through the blinds and enters a room (Pfrommer et al., 1996; Breitenbach et al., 2001; Tzempelikos, 2008). The new model separately calculates the indoor illuminance due to reflection directly from the blinds IL_{sr}, which may account for a large part of total indoor illuminance, as demonstrated by Figures 6.17 and 6.18. From Figures 6.15 we can see that IL_{sr} has great influence at reference points near the window when tilt angle is positive. For example, at the reference point 1.1 meters from the window, IL_{sr} may account for 55% and 66% of total indoor illuminance when the tilt angle is 30° and 60°.

However, IL_{sr} decreases rapidly with the depth of reference point. At the reference point 7.6 meters from the window, IL_{sr} only accounts for 9% and 27% of total indoor illuminance at these two angles.

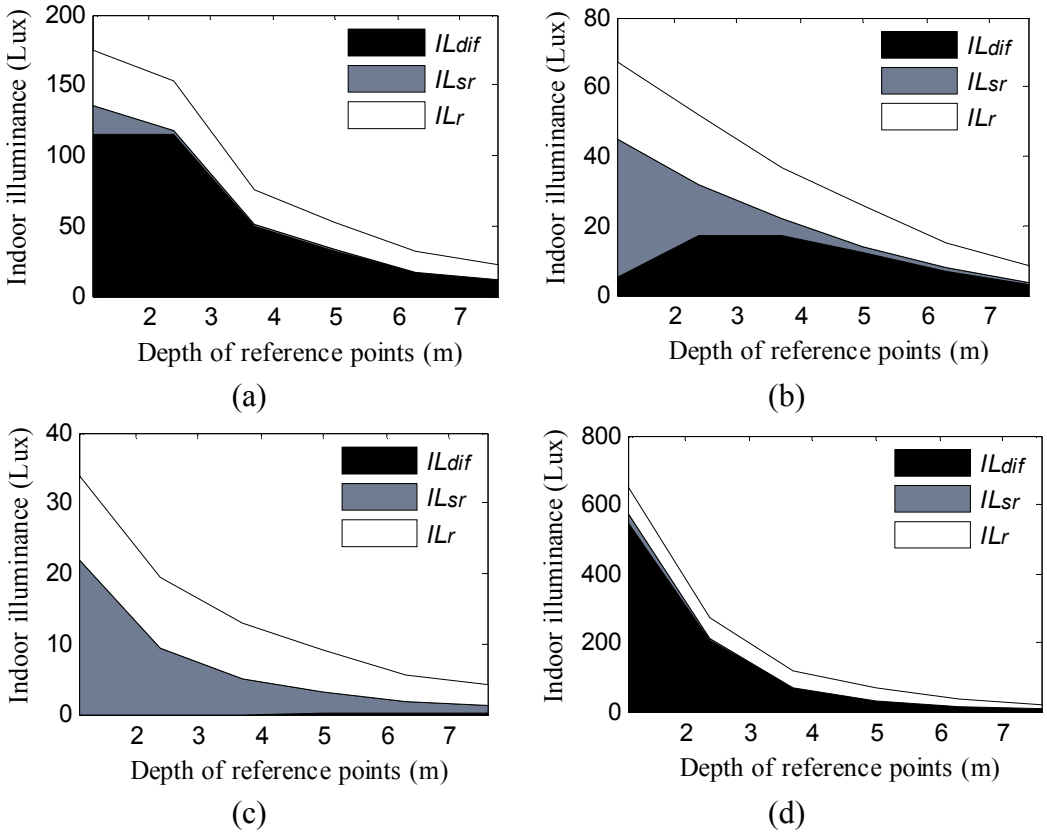

Figure 6.17 Breakdown of indoor illuminance under overcast sky,
(a) $\beta = 0°$; (b) $\beta = 30°$; (c) $\beta = 60°$; (d) $\beta = -30°$.

Figure 6.18 presents indoor illuminance caused by IL_{dif}, IL_r and IL_{sr} under clear sky. The results are similar to those under overcast sky. The introduction of beam sunlight increases both IL_r and IL_{sr}, making them more important in the total indoor illuminance.

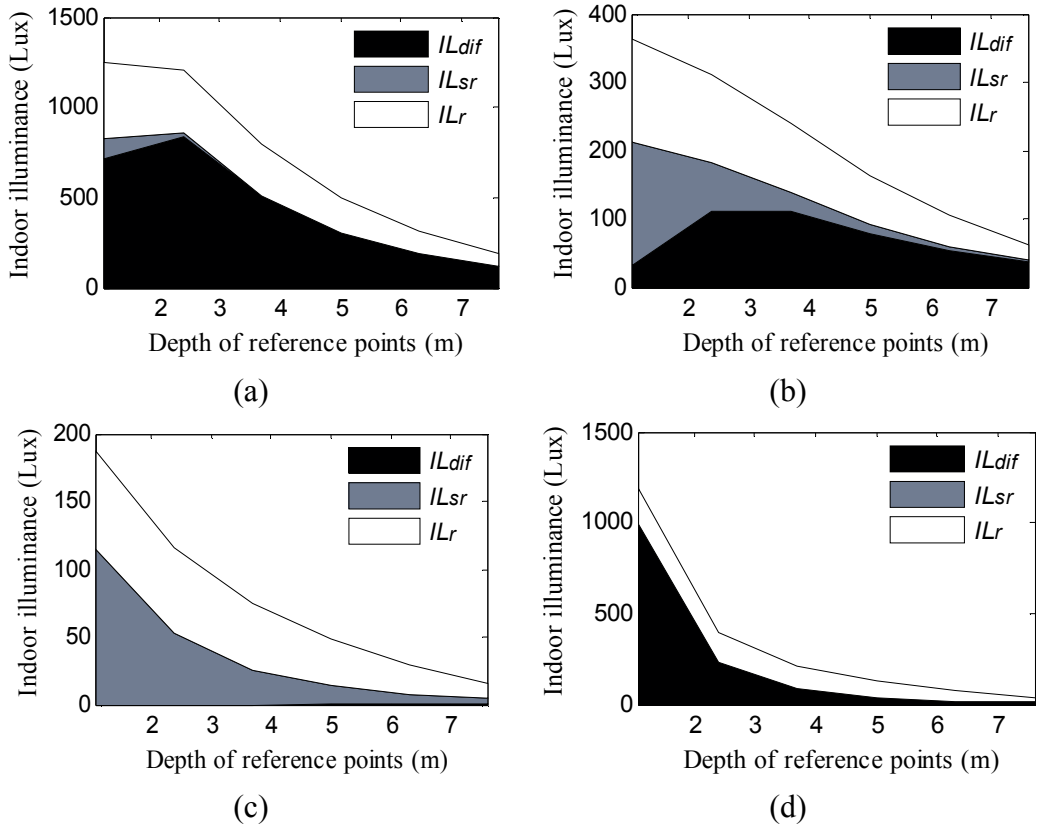

Figure 6.18 Breakdown of indoor illuminance under clear sky, solar altitude = 60° and the solar azimuth equals the window azimuth, (a) β = 0°; (b) β = 30°; (c) β = 60°; (d) β = -60°.

The percentage of IL_{sr} in the total indoor illuminance (IL_{in}) may vary significantly with slat tilt angle. Figure 6.19 presents the ratio of IL_{sr} to total indoor illuminance IL_{in} under different slat tilt angles. The reference point at 1.1 meter from the window was considered. The percentage of IL_{sr} roughly increases with the slat tilt angle. The minimum percentage occurs at β = -30°. The reason is that most slats are nearly parallel to the reference point, resulting in very small areas that can be seen by the reference point.

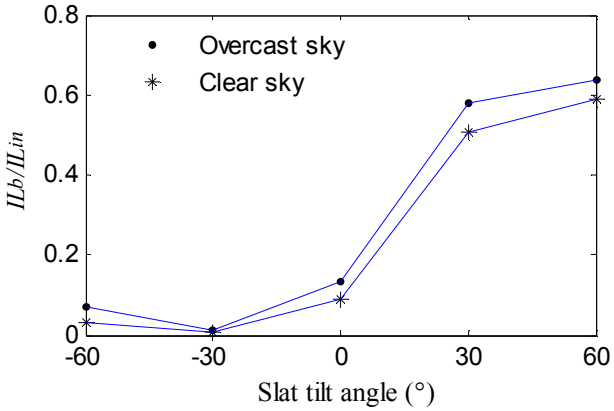

Figure 6.19 Ratio of IL_{sr} to IL_{in} vs. slat tilt angles at t 1.1 meter from the window. Under clear sky, solar altitude = 60° and the solar azimuth equals the window azimuth.

6.8 Summary

To enhance the computational efficiency, fitting equations for the calculation of daylight factors at the external and internal surfaces of blinds, and the distribution of internally reflected daylight at different depth of the room, have been provided based on the simulation results of Radiance. Traditionally, the view factors from slat to the internal surface of blinds and those from slat to indoor reference point need to be calculated by fourth- and double-integration, which are tedious and time-consuming to calculate. Therefore, new methods have been provided to simplify the calculation. The new method is primarily based on the reciprocity relation and the assumption that the areas at the two ends of slat can be ignored in the calculation. The assumption is feasible because these areas are quite small compared with the areas of slats and the internal surface of blinds between adjacent slats. As the tedious fourth- and double-integration equations for computing the view factors can be replaced by algebraic equations, the calculation of view factors can be greatly simplified, and the computational

efficiency can be greatly enhanced.

The measured illuminance data have been compared with the simulated data generated by the newly developed model, Radiance and EnergyPlus. Results show that indoor illuminances simulated by the new model agree well with the experimental data under both overcast and clear skies, and its MBE and RMSE are equivalent to those of Radiance. Large errors normally occur at two special conditions. The first is the places close to the window when the tilt angle is -30°. However, the errors at these may have small effect on the artificial lighting energy saving because these areas normally already have adequate daylight illuminance. The MBEs and RMSEs for new method, Radiance and EnergyPlus decrease if the reference point 1.1 meter from the window is excluded from the analysis when the tilt angle is -30°. The second one is the places far away from the window, especially when the tilt angle is 30°, 60° and -60°. Three daylight components simulated by the new model and EnergyPlus were separately validated with the results of Radiance. Validation results show the new model can provide more accurate results than EnergyPlus because EnergyPlus ignores the inter-reflection between blinds slats and glazing surface. Another advantage of the new model over EnergyPlus is calculation speed. EnergyPlus consumes much more time in calculation because it uses radiosity method for the calculation of illuminance due to internal reflection among indoor room surfaces. More room patches has to be used in order to get more accurate results.

Unlike many researches that concentrate on the total transmittance of blinds, the newly developed model separately calculates the illuminance due to light directly reflected from the slats. This part of illuminance may account for a large percentage of the total indoor illuminance at reference points near the window when tilt angle is positive. The percentage decreases with the depth of reference points and roughly increases with the slat tilt angle.

CHAPTER 7

RIGOROUS CALCULATION OF RESPONSE FACTORS OF MULTI-LAYERED WALLS

A direct numerical method is developed for calculation of response factors and z-transfer coefficients of multilayered slabs. It can avoid a tedious, sometimes uncertain root-finding procedure in Laplace inverse transformation based on Haviside's theorem, and approximations in many numerical methods. It does not have an instability problem with numerical calculations. The method is based on a principle that different transfer functions should be equivalently transformable. The response factors of multilayered slabs can be easily computed by the discrete Fourier transform. The time consumption of the calculation can be greatly reduced by the utilization of fast Fourier transform (FFT). The whole calculation can be finished in less than 1 second, even for very high mass slabs. The calculated response factors can then be equivalently transformed to z-transfer coefficients. Validation results indicate that the accuracy of response transfer factors computed by the new developed method is the same as that of the theoretical results. The method can also generate more accurate and reliable z-transfer coefficients as compared to other available methods.

7.1 Transfer functions of multilayered slabs

A multilayered slab consists of a number of slabs with homogeneous and constant physical properties, which can be considered as one-dimensional heat

conduction through them. For modeling heat conduction through a multilayered slab, it is convenient to represent the temperatures and heat flows at its both sides in the form of matrix (Pipes, 1957)

$$\begin{bmatrix} T_i(s) \\ q_i(s) \end{bmatrix} = \mathbf{M}(s) \begin{bmatrix} T_o(s) \\ q_o(s) \end{bmatrix} \tag{7.1}$$

where $\mathbf{M}(s)$ is the overall transmission matrix of the slab, T_i and T_o are temperatures at the inside and outside surfaces of the slab (ºC), q_i and q_o are heat fluxes at the inside and outside surfaces of the slab (W/m^2), and s is the Laplace transform variable. The overall transmission matrix of the multilayered slab may be expressed by the multiplication of the transmission matrixes of all the n homogeneous slabs, i.e.

$$\mathbf{M}(s) = \begin{bmatrix} A(s) & B(s) \\ C(s) & D(s) \end{bmatrix} = \mathbf{M}_1(s) \cdot \mathbf{M}_2(s) \cdots \mathbf{M}_{n-1}(s) \cdot \mathbf{M}_n(s) \tag{7.2}$$

where $\mathbf{M}_i(s)$ is the transmission matrix for each slab and can be expressed by

$$\mathbf{M}_i(s) = \begin{bmatrix} A_i(s) & B_i(s) \\ C_i(s) & D_i(s) \end{bmatrix} \tag{7.3}$$

The four entries in the matrix for single slab are given by hyperbolic functions

$$A_i(s) = D_i(s) = \cosh\left(\sqrt{\frac{s}{\alpha_i}} \cdot l_i\right) \tag{7.4}$$

$$B_i(s) = \frac{\sinh\left(\sqrt{\frac{s}{\alpha_i}}\, l_i\right)}{k_i \sqrt{\frac{s}{\alpha_i}}} \tag{7.5}$$

$$C_i(s) = k_i \sqrt{\frac{s}{\alpha_i}} \sinh\left(\sqrt{\frac{s}{\alpha_i}}\, l_i\right) \tag{7.6}$$

where l_i, k_i and a_i are the thickness (m), thermal conductivity (W/m/ºC) and

thermal diffusivity (m^2/hr) of the *i*th layer, respectively, and $a_i = k_i/(\rho_i\, c_{pi})$ where ρ_i and c_{pi} are the density (kg/m^3) and specific heat (J/kg/ ºC) of the *i*th layer. When the heat capacity of a slab or layer is negligible, its transmission matrix becomes

$$\mathbf{M} = \begin{bmatrix} 1 & R \\ 0 & 1 \end{bmatrix} \tag{7.7}$$

where R is the thermal resistance (m^2/ºC/W). Air films at the inside and outside surfaces of the multilayered slab can be considered as homogeneous layers. Their transmission matrix can be expressed by Equation (7.7) because the specific heat of air is very small.

Equation (7.1) may be rearranged to obtain the overall transmission matrix relating the temperatures to the heat flows at the two sides of the slab. It can be expressed by

$$\begin{bmatrix} q_o(s) \\ q_i(s) \end{bmatrix} = \begin{bmatrix} -H_x(s) & H_y(s) \\ -H_y(s) & H_z(s) \end{bmatrix} \begin{bmatrix} T_o(s) \\ T_i(s) \end{bmatrix} \tag{7.8}$$

Since $A(s)D(s) - B(s)C(s) = 1$, the entries in the above transmission matrix are given by

$$H_x(s) = \frac{A(s)}{B(s)} \tag{7.9}$$

$$H_y(s) = \frac{1}{B(s)} \tag{7.10}$$

$$H_z(s) = \frac{D(s)}{B(s)} \tag{7.11}$$

where $H_x(s)$, $H_y(s)$ and $H_z(s)$ are the transfer functions of external, cross and internal heat conduction through the multilayered slab. The inverse Laplace

transform of the above three transfer functions will results in response factors $X(i)$, $Y(i)$ and $Z(i)$, respectively. As commented earlier, however, the use of the conventional inverse method may lead to incorrect response factors.

A simple new method for inverse Laplace transform is to use the fast Fourier transform (FFT). Fourier transfer functions can be easily obtained by replacing Laplace transform variable s in the Laplace transfer functions with Fourier transform variable $j\omega$, where j is the imaginary operator, defined by $j^2 = -1$, and ω is the frequency in rad/hr. Fourier transfer functions will be used to generate the response factors and z-transfer coefficients.

7.2 Discrete Fourier transform (DFT) method

A triangular impulse is usually used to describe an exciting function in building energy simulations (Stephenson and Mitalas, 1967). This is because generally the triangular impulse can more accurately simulate an arbitrary exciting function in the same time interval than the rectangular impulse. The response of a linear and invariant equation system to this unit triangular impulse is called as the unit response function (URF). The time-series representations of this URF are the response factors (Clarke, 2001).

The triangular impulse $f(t)$ can be expressed by

$$f(t)=\begin{cases}0 & \frac{T}{2} < t \le -\Delta t \\ \frac{1}{\Delta t}(t+\Delta t) & -\Delta t \le t \le 0 \\ \frac{1}{\Delta t}(\Delta t - t) & 0 \le t \le \Delta t \\ 0 & \Delta t \le t < \frac{T}{2}\end{cases} \tag{7.12}$$

where t is time, Δt is a time interval (conventionally Δt = 1 h), and T is periodic time period. If T is long enough, the unit triangular impulse can only impact the system response within the periodic time period of this impulse. Therefore, the solution should be the same as that in non-periodic conditions.

The unit triangular impulse may be expressed in the exponential form of discrete Fourier series

$$f(k\Delta t) = \sum_{n=-(N-1)}^{N-1} c_n \exp(j\,\omega_n k\Delta t) \tag{7.13}$$

where n represents a harmonic number. If the periodic time period, T, is equal to $K\Delta t$, then frequency, ω_n, is equal to

$$\omega_n = \frac{2\pi n}{T} = \frac{2\pi n}{K\Delta t} = n\,\omega_1 \tag{7.14}$$

Substituting Equation (7.14) into Equation (7.13) yields

$$f(k\Delta t) = \sum_{n=-(N-1)}^{N-1} c_n \exp(2\pi\, j\, n\, k / K) \tag{7.15}$$

The complex coefficients c_n can be determined by

$$c_n = \frac{1}{T}\int_{-T/2}^{T/2} f(t)\exp(-jn\omega_1 t)dt \tag{7.16}$$

Substituting Equation (7.12) into Equation (7.16), we have

$$c_n = \frac{1}{T}\left[\int_{-\Delta t}^{0} \frac{1}{\Delta t}(t+\Delta t)\exp(-jn\omega_1 t)dt + \int_{0}^{\Delta t} \frac{1}{\Delta t}(\Delta t - t)\exp(-jn\omega_1 t)dt\right] \tag{7.17}$$

Integrating Equation (7.13) results in

$$c_n = \frac{-K}{(2\pi n)^2}\left[\exp(jn\omega_1\Delta t) + \exp(-jn\omega_1\Delta t) - 2\right] \tag{7.18}$$

Substituting Equation (7.18) into Equation (7.13) yields the discrete Fourier series of the unit triangular impulse. The overall system response to this impulse may be expressed by superposition of all the products of the transfer function and the exciting input in each harmonic as follows

$$Y(k\Delta t) = \sum_{n=-(N-1)}^{N-1} H(j\omega_n) c_n exp(j\omega_n k\Delta t) \tag{7.19}$$

where $H(j\omega_n)$ is the discrete frequency transfer function of interest, and $Y(k\Delta t)$ are response factors, where $k = 0, 1, 2, \ldots$.

DFT inherently contain the computational redundancy. A fast Fourier transform (FFT) is much more efficient for computing DFT and discrete Fourier inverse. This efficient method will be presented in the next section.

7.3 Fast Fourier transform (FFT)

Combination of Equations(7.18) into (7.19) yields

$$Y(k\Delta t) = Y_+(k\Delta t) + Y_-(k\Delta t) \tag{7.20}$$

with

$$Y_+(k\Delta t) = \frac{-K}{(2\pi)^2}\sum_{n=0}^{N-1}\frac{H(j\omega_n)}{n^2}\left[\exp(j\omega_n\Delta t) + \exp(-j\omega_n\Delta t) - 2\right]\exp(j\omega_n k\Delta t) \tag{7.21}$$

$$Y_-(k\Delta t) = \frac{-K}{(2\pi)^2}\sum_{n=-1}^{-(N-1)}\frac{H(j\omega_n)}{n^2}\left[\exp(j\omega_n\Delta t) + \exp(-j\omega_n\Delta t) - 2\right]\exp(j\omega_n k\Delta t) \tag{7.22}$$

Note that the term at frequency number $n = 0$ has an indeterminate fraction function as follows

$$f(n) = \frac{\exp(jn\omega_1\Delta t) + \exp(-jn\omega_1\Delta t) - 2}{n^2}$$

The limit of the above indeterminate function is $-(2\pi/K)^2$, according to l'Hôpital's rule.

In Fourier transform, a non-periodic triangular impulse becomes a periodic exciting input. Therefore, the time period used, $T = K\Delta t$, should be long enough to eliminate the effect of the periodic inputs. The long time period requires a large number of harmonics, N, for the accurate simulation of unit triangular impulse. Our simulation results show that the value of N should be 2 to 5 times that of K. For convenient calculations and programming, the magnitude of N taken should be the integer times that of K, i.e. $n_k = N/K$.

The principle of FFT is to utilize the symmetry and periodicity of the complex exponential function in DFT to avoid the unnecessarily redundant calculations (Phillips and Parr, 1999). The periodicity can be expressed by

$$\exp\left(j\frac{2\pi}{K}kn\right) = \exp\left[j\frac{2\pi}{K}k(n+K)\right] = \exp\left[j\frac{2\pi}{K}(k+K)n\right] \tag{7.23}$$

The symmetry can be expressed by

$$\exp\left(j\frac{2\pi}{K}kn\right) = \exp\left[j\frac{2\pi}{K}k(n-K)\right] \tag{7.24}$$

Examination of Equations (7.18) and (7.19) indicates that many redundant calculations when the number of harmonics, N, is greater than the periodic time length, K. Hence, the common factors periodically repeated in calculations may be sorted out first. Thus, the number of harmonics, N, can be reduced to K,

according to the periodicity in Equation (7.23). Equations (7.21) and (7.22) may be reorganized by

$$Y_{+}(k\Delta t)=\frac{-K}{(2\pi)^2}\sum_{n=0}^{K-1}\left[\exp(j\omega_n k\Delta t)[\exp(j\omega_n\Delta t)+\exp(-j\omega_n\Delta t)-2]\sum_{m=0}^{n_k-1}\frac{H(j\omega_{n+m\cdot K})}{(n+m\cdot K)^2}\right] \tag{7.25}$$

and

$$Y_{-}(k\Delta t)=\frac{-K}{(2\pi)^2}\sum_{n=1}^{K-1}\left[\exp(j\omega_{-n} k\Delta t)[\exp(j\omega_n\Delta t)+\exp(-j\omega_n\Delta t)-2]\sum_{m=0}^{n_k-1}\frac{H(j\omega_{-n-m\cdot K})}{(-n-m\cdot K)^2}\right] \tag{7.26}$$

According to the symmetry in Equation (7.19), the values of the exponential function at ω_{-n} and ω_{K-n} are equal and at ω_n and ω_{n-K} should be equal. Thus, Equation (7.26) may be reorganized by

$$Y_{-}(k\Delta t)=\frac{-K}{(2\pi)^2}\sum_{n=1}^{K-1}\left[\exp(j\omega_n k\Delta t)[\exp(j\omega_n\Delta t)+\exp(-j\omega_n\Delta t)-2]\sum_{m=0}^{n_k-1}\frac{H(j\omega_{n-K-m\cdot K})}{(n-K-m\cdot K)^2}\right] \tag{7.27}$$

For the convenient implementation of FFT algorithm, K should be generally assigned by a power of 2, which means $K = 2^m$ where m is a positive integer.

To simplify the mathematic expression, let

$$y(n)=\begin{cases}\displaystyle\sum_{m=0}^{n_k-1}\left[\frac{H(j\omega_{n+m\cdot K})}{(n+m\cdot K)^2}+\frac{H(j\omega_{n-K-m\cdot K})}{(n-K-m\cdot K)^2}\right] & n\neq 0\\ \displaystyle\sum_{m=0}^{n_k-1}\frac{H(j\omega_{n+m\cdot K})}{(n+m\cdot K)^2} & n=0\end{cases} \tag{7.28}$$

and

$$W_K^{nk}=\exp(j\omega_1 n\,k\,\Delta t) \tag{7.29}$$

where subscript K is the original periodic time length. Combination of Equations. (7.20), (7.25), (7.27), (7.28) and (7.29) yield

$$Y(k\Delta t) = \frac{-K}{(2\pi)^2}\sum_{n=0}^{K-1} y(n)\left(W_K^{n(k+1)} - 2W_K^{nk} + W_K^{n(k-1)}\right) \tag{7.30}$$

It can be seen from Equation (7.30) that only one Fourier transform needs to be determined and the overall response factors can be derived from the results from the this Fourier transform. Thus, the problem becomes to calculate the following Fourier transform

$$Y'(k) = \sum_{n=0}^{K-1} y(n) W_K^{nk} \qquad k = -1, 0, 1, \cdots, K \tag{7.31}$$

The summation in the above equation contains a great number of redundant calculations, which significantly deteriorates the computational efficiency. The DFT generally requires K^2 complex multiplications (Phillips and Parr, 1999). The FFT utilizes the periodicity and symmetry of the basic exponential function in the DFT to successively divide the point-number, K, of DFT into $K/2$ two-point DFT until there are only two points left in each DFT. The amount of complex multiplications in FFT is only $(K/2)\log_2(K)$.

A simple four-point DFT, i.e. $K = 4$, is used here to illustrate the principle of decomposition-in-time, radix-2 FFT without losing the generality. When $K = 4$, we have

$$Y_{K=4} = \sum_{n=0}^{3} y(n) W_4^{nk} = y(0) + y(1)W_4^k + y(2)W_4^{2k} + y(3)W_4^{3k} \tag{7.32}$$

The above equation may be rewritten by

$$Y_{K=4} = [y(0) + y(2)(-1)^k] + [y(1) + y(3)(-1)^k]W_4^k \tag{7.33}$$

It can be seen that each sample y is only calculated once and each two-point DFT contains a pair of samples in the equation. The two-point DFT with even numbers does not have a multiplier of W_4^k while the corresponding two-point DFT with odd numbers is multiplied by a common factor W_4^k.

A general formula with any period $K \geq 4$ may be expressed by

$$Y(k) = \sum_{l=0}^{K/4-1} \left\{ \left[y(l) + y(l+K/2)(-1)^k \right] + \left[y(l+K/4) + y(l+3K/4)(-1)^k \right] W_4^k \right\} W_K^{lk} \tag{7.34}$$

7.4 Generation of z -transfer coefficients

Z-transfer coefficients decay much faster than the response factors. This is because the calculation with z-transfer function involves historic outputs, which contain a great amount of information on the product of historic inputs and the system transfer coefficients. The primary aim of adopting z-transfer is to enhance the computational efficiency, i.e. using much less number of transfer coefficients to obtain the system outputs.

There is always a truncation error when a limited number of z-transfer coefficients are used in numerical calculations. A new method to be presented for calculating the z-transfer coefficients aims at minimizing the truncation error.

No matter which transfer functions are used, their transfer factor series for the same system should be the same. Hence, the relationship between response factors and z-transfer coefficients may be expressed by

$$Y(0)+Y(1)z^{-1}+Y(2)z^{-2}+\ldots=\frac{\sum_{i=0}^{n}b_i z^{-i}}{\sum_{i=0}^{n}d_j z^{-i}} \tag{7.35}$$

where z^{-1} is the backward operator, Y(i) are response factors, and b_i and d_i are z-transfer function coefficients. Fraction function (7.35) allows one coefficient to be arbitrarily determined. Generally, d_0 is equal to 1.

Equation (7.35) may be rewritten as

$$b_0+b_1z^{-1}+b_2z^{-2}+\ldots=Y(0)d_0+[Y(1)+Y(0)d_1]z^{-1}+[Y(2)+Y(1)d_1+Y(0)d_2]z^{-2}+\ldots \tag{7.36}$$

Sorting Equation (7.36) for z with different orders yields

$$\begin{aligned} &b_0=Y(0)\\ &b_j-\sum_{i=0}^{j-1}Y(i)d_{j-i}=Y(j) \qquad j\geq 1 \end{aligned} \tag{7.37}$$

The value of b_j and d_j decays rapidly with index j. Assuming that b_j is negligible when $j = n$, Equation (7.37) becomes

$$-\sum_{i=0}^{j-1}Y(i)d_{j-i}=Y(j) \qquad j\geq n \tag{7.38}$$

The number of equations, m, in linear equation system (7.38) should not be less than n, otherwise there is no unique solution to the problem. Generally, the large value of m should be used as compared to n in order to fully take into account the effect of truncated series. Thus, a set of Equation (7.38) may be

rewritten in the form of matrix

$$\mathbf{M}_z \boldsymbol{\theta} = \mathbf{g} \tag{7.39}$$

with

$$\boldsymbol{\theta}^T = \begin{bmatrix} d_1 & d_2 & \dots & d_n \end{bmatrix} \tag{7.40}$$

$$\mathbf{g}^T = \begin{bmatrix} Y(n) & Y(n+1) & Y(n+2) & \dots & Y(n+m-1) \end{bmatrix} \tag{7.41}$$

$$\mathbf{M}_z = -\begin{bmatrix} Y(n-1) & Y(n-2) & \cdots & Y(0) \\ Y(n) & Y(n-1) & \cdots & Y(1) \\ \vdots & \vdots & \ddots & \vdots \\ Y(n+m-2) & Y(n+m-3) & \cdots & Y(m-1) \end{bmatrix} \tag{7.42}$$

When m > n, a least-square algorithm should be used. The solution to the above problem is given by (Anton, 2005)

$$\boldsymbol{\theta} = (\mathbf{M}_z^T \mathbf{M}_z)^{-1} \mathbf{M}_z^T \mathbf{g} \tag{7.43}$$

The accuracy of the solution largely depends on the relative values of *m* and *n*. The simulation results show that the high accuracy of z-transfer coefficients can be obtained when *n* is equal to 4, 5 and 6 respectively for low, median and high mass slabs. The value of *m* should be about four times larger than that of *n*.

7.5 Validation of method for computing response factors

7.5.1 Homogeneous slab

Homogeneous slab is use in the validation because the response factors of a homogeneous slab can be accurately calculated because all roots of $B(s)$ can be analytically obtained (Clarke J.A., 2001). Then a comparison between the numerical and analytical solutions will show the true accuracy of response factors computed by the FFT method.

A 300 mm concrete slab was utilized in the study. The periodic time duration was 80 hours and the number of harmonics was 400. The results show that the numerically and analytically computed response factors are exactly the same in eleven-digits after fixed decimal point. This means that the FFT method can provide the same accurate response factors as those given by the analytical method. Figure 7.1 shows the heat flux at one side of the concrete slab after the unit triangular pulse of temperature acts at the other side of the slab.

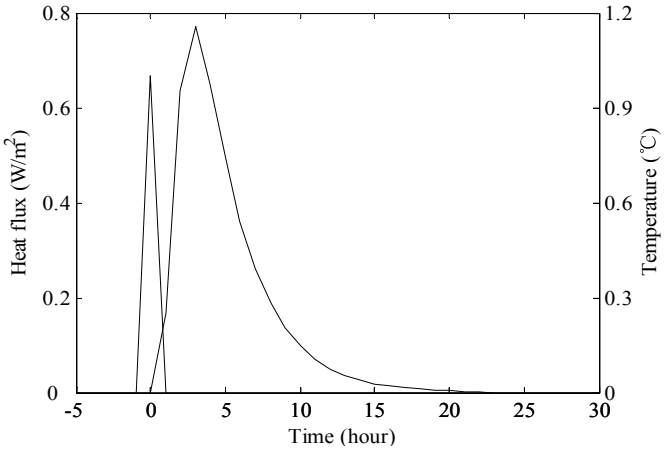

Figure 7.1 Heat flux due to a unit triangular impulse of temperature.

7.5.2 Multilayered slab

Spitler and Fisher (1999) published the periodic response factors of 41 representative wall groups and 42 representative roof groups for design cooling load calculations. The wall group 38 and roof group 38 were selected to examine the accuracy of response factors calculated by the new method.

Response factors to the unit triangular impulse contain all the information on the heat conduction characteristics of a slab, including the periodic response coefficients and the overall heat transfer coefficient in steady-state heat conduction. Hence, the periodic response factors, $Y_{RTS}(i)$, in a 24-hour period, also called as radiant time series, may be formed by the normal response factors, $Y(i)$, as follows

$$Y_{RTS}(i) = Y(i) + Y(i+24) + Y(i+48) + \ldots, \qquad i = 0,1,2,\ldots 23 \tag{7.44}$$

Temperature difference at the two side surfaces of the slab is constant under steady-state heat transfer. Correspondingly, the overall heat transfer coefficient, U, through the slab should be equal to the summation of all the response factors, i.e.

$$U = \sum_{i=0}^{\infty} Y(i) = \sum_{i=0}^{23} Y_{RTS}(i) \tag{7.45}$$

Table 7.1 shows the periodic response factors computed by the FFT method and the conventional method. Examination of Table 7.1 indicates that the overall heat transfer coefficient calculated by the periodic response factors given by the FFT method is exactly the same as the theoretic value. Actually, this should be

expected because influence factors on the accuracy of the FFT method are the number of frequencies, N, and periodic duration, T, rather than the number of layers. As long as N and T are large enough, the FFT method can generate the response factors as accurate as those in a homogeneous slab because all the theoretic calculation procedure and principle are the same. It has been proved that the response factors of single slab are the same as those analytical values. Table 7.1 also clearly indicates that the conventional method may produce inaccurate response factors for massive multilayered slabs due to missing roots. Difference between the overall heat transfer coefficient given by the conventional method and the theoretic value is 30.8% for wall 38 and 7.07 for roof 38, respectively.

The calculation results show that the FFT method can generate response factors as accurate as the analytical solutions when the periodic time period K is 64 for light walls and 256 for very heavy walls. Generally, the number of harmonics N should be 2 to 4 times the periodic time period K. FFT greatly enhance the computational efficiency. It only takes 0.67% of the total computation time used by the DFT for light walls and 0.25% of that for heavy walls.

Table 7.1 Comparison of the radiant time series for Wall 38 and Roof 38, W/(m^2℃).

k	Wall 38		Roof 38	
	$Y_{RTS}(k)^a$	$Y_{RTS}(k)^b$	$Y_{RTS}(k)^a$	$Y_{RTS}(k)^b$
0	0.008311	0.005342	0.007135	0.006529
1	0.007918	0.004934	0.006895	0.006304
2	0.007539	0.004541	0.006663	0.006088
3	0.007207	0.004196	0.006481	0.005925
4	0.007066	0.004046	0.006485	0.005973
5	0.007311	0.004285	0.006785	0.006347
6	0.007966	0.004939	0.007327	0.006960
7	0.008875	0.005839	0.007964	0.007621
8	0.009834	0.006779	0.008562	0.008192
9	0.010685	0.007608	0.009043	0.008612
10	0.011344	0.008251	0.009377	0.008874
11	0.011787	0.008687	0.009568	0.008998
12	0.012022	0.008929	0.009635	0.009010
13	0.012080	0.009003	0.009604	0.008939
14	0.011993	0.008941	0.009496	0.008806
15	0.011795	0.008771	0.009333	0.008630
16	0.011513	0.008519	0.009130	0.008425
17	0.011173	0.008205	0.008902	0.008201
18	0.010794	0.007845	0.008657	0.007965
19	0.010390	0.007453	0.008404	0.007723
20	0.009972	0.007040	0.008146	0.007479
21	0.009550	0.006616	0.007888	0.007236
22	0.009130	0.006187	0.007632	0.006996
23	0.008715	0.005761	0.007381	0.006760
$\sum Y_{RTS}(k)$	0.234970	0.162717	0.196491	0.182593
U	0.234970		0.196491	
Relative error	0.00%	30.75％	0.00％	7.07％

[a]Fourier transform method.

[b]Spilter and Fisher.

7.6 Validation of z-transfer coefficients

The overall heat transfer coefficient, U, can also be deducted by z transfer coefficients as follows

$$U = \frac{\sum_{n=0} b_n}{1 + \sum_{n=1} d_n} \tag{7.46}$$

Harris and McQuiston (1988) calculated the z-transfer coefficients of 41 representative wall groups and 42 representative roof groups. The walls groups 6 and 38 were used to validate the accuracy of z-transfer coefficients given by the new method. Tables 7.2 and 7.3 show the z-transfer coefficients computed by the new method and conventional method. It can be observed from the two tables that the two methods can give similar accuracy for wall group 6. However, the conventional method cannot generate correct z-transfer coefficients for wall group 38 while the new method can still provide relatively accurate coefficients.

Table 7.2 z-transfer coefficients of wall group 6.

	New method	Harris and McQuiston
b_0	0.002872	0.002868
b_1	0.053303	0.053248
b_2	0.059914	0.060036
b_3	0.007030	0.007236
b_4	-0.000002	0.000051
b_5	0.000000	0.000000
b_6	0.000000	0.000000
d_0	1.0	1.0
d_1	-1.178747	-1.175710
d_2	0.303875	0.300710
d_3	-0.016168	-0.015605
d_4	0.000000	0.000006
d_5	0.000000	0.000000
U	1.129870	
$\frac{\sum_{n=0} b_n}{1 + \sum_{n=1} d_n}$	1.129857	1.128327

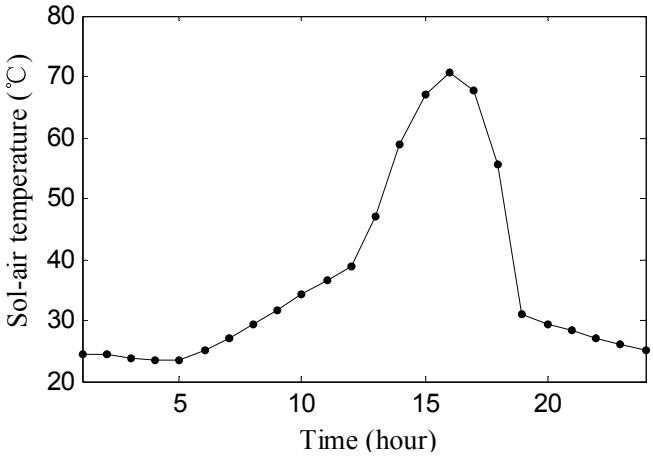

Figure 7.2 Hourly sol-air temperature data.

The overall heat transfer coefficient cannot be sued to test the dynamic characteristics of z-transfer coefficients. As mentioned earlier, there are always truncated series when heat fluxes are calculated by z-transfer coefficients. In order to take into account the effect of truncated series, the resultant heat fluxes were computed in periodic hourly sol-air temperatures, which are given in Figure 7.2 (ASHRAE Handbook of Fundamentals 1997). It was assumed that the daily sol-air temperature cycle is repeated for several consecutive days and the room temperature is 24℃. Then heat fluxes through the unit area of wall group 6 were calculated using z transfer coefficients from both methods. Response factors computed by the FFT method were also used to generate reference heat fluxes because the method can provide solutions as accurate as the analytical results.

Figure 7.2 shows heat fluxes through wall group 6 computed by response factor method, the new method, and the conventional method. It can be seen that all the heat fluxes are almost overlapped. Using the heat flux calculated by the

response factor method as the reference, the results from the proposed method are better than those given by the coefficients from Harris and McQuishton (1988). The relative maximum errors and average errors are 0.056‰ and0.021‰ for the newly proposed method and 0.63‰ and 0.453‰ for the conventional method, respectively. For massive wall group 38, the conventional method cannot give correct heat fluxes because its overall heat transfer coefficient is negative. The proposed method can generate very accurate heat fluxes, and the relative maximum and average errors are 0.068‰ and 0.04‰, respectively.

Table 7.3 z-transfer coefficients of wall group 38.

	New method	Harris and McQuiston
b_0	1.01316E-08	-2.4331E-14
b_1	-2.212613E-08	1.9748E-09
b_2	1.212280E-06	1.1873E-06
b_3	3.013402E-05	3.0290E-05
b_4	0.000136	0.000142
b_5	0.000162	0.000187
b_6	0.000050	0.000085
d_0	1.0	1.0
d_1	-3.328638	-3.149900
d_2	4.519145	3.951200
d_3	-3.252701	-2.537900
d_4	1.344613	0.894380
d_5	-0.315216	-0.17209
d_6	0.034415	0.017057
U	0.234970	
$\frac{\sum_{n=0} b_n}{1+\sum_{n=1} d_n}$	0.234717	-0.002481

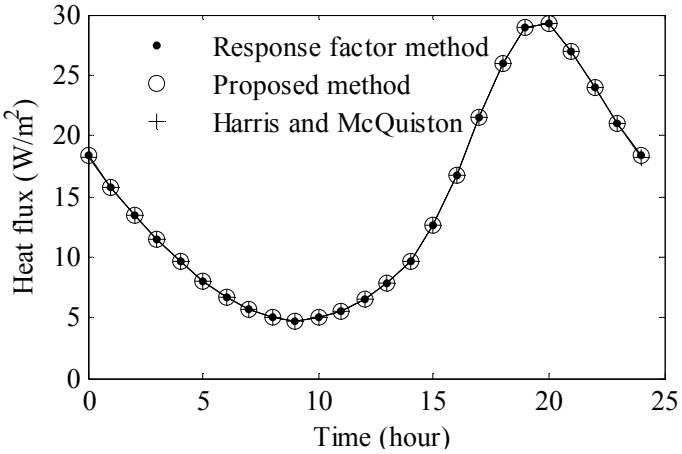

Figure 7.3 Hourly heat fluxes through wall group 6.

7.7 Summary

The conventional methods commonly used for inverse Laplace transform, such as Heaviside's expansion, need to determine all the poles of the image function of solutions of partial differential equations. Some poles may be missed in any approaches for finding them, which results in incorrect response factors. Many methods have been developed to avoid the root-searching process so as to overcome the weakness of the conventional method. Some of these methods still have other numerical calculation problems while the others can only generate approximate solutions.

A new method has been developed for the direct and rigorous calculation of response factors of multilayered slabs. This method uses FFT, and hence does not need to numerically search for the poles of the image function of solutions to heat conduction through multilayered slabs. Through the calculation of analytical response factors in each harmonics, the FFT method can generate response factors as accurate as the analytical solutions when the periodic time period K is

64 for light walls and 256 for very heavy walls. Generally, the number of harmonics N should be 2 to 4 times the periodic time period K. FFT is of high efficiency. It takes 0.67% of the total computation time used by the DFT for light walls and 0.25% of that for heavy walls. It can be concluded from the validation results that the new method can provide the 'benchmark results' because no other currently available methods can guarantee such accurate solutions.

The new method can provide symbolic transfer functions that keep design variables as symbols because the inverse Laplace transform by the FFT does not need change the format of the original Laplace transfer function. Therefore, the method is particularly useful for the optimal design, sensitivity analysis and control study of buildings.

Explicit FFT formulae have been derived for the first time for efficient calculating the DFT of heat conduction through multilayered slabs. They significantly facilitate the implementation of FFT in computer programming. It can be easily applied to inverse Laplace transfer in the other topics or areas.

Z-transfer coefficients have been generated by the least square method from accurate response factors. Validation results show that z-transfer coefficients obtained by this method are much more accurate than those from the conventional method.

CHAPTER 8

DIRECT EVALUATION OF DYNAMIC LONG-TERM COOLING LOADS WITHOUT HOURLY THERMAL SIMULATON

Currently, hourly heat transfer simulations are widely used for long-term energy analysis and optimal design. However, many cases, such as building optimal design, only need the annual cooling load in the comparison of different options. The unnecessary hourly calculations could greatly reduce its computational efficiency, and lead to long time consumption in the optimization. Therefore, primarily based on the principle of superposition and symbolic transfer function, an accurate and efficient building thermal simulation method is developed for computing the total long-term cooling load of buildings. With this model, the long-term cooling load can be directly calculated and the tedious hourly calculations can be avoided. Combined with the Fourier transform method developed in Chapter 7, this new method can generate symbolic response factors. The approach is illustrated by an example in Hong Kong. The new thermal simulation method was validated by DOE2 and the results show the method has high accuracy.

8.1 Method for direct and efficient estimating long-term cooling load

8.1.1 Total cooling load in steady and continuous operation

It is assumed that all the heat transfer processes in a building can be approximately treated as linear and time-independent ones. If there is any non-linear element in the system, it may be isolated from the system by a special treatment (Athienitis et al., 1987). The time-independent elements may be treated in two ways. First, averaged value over the period time may be used in the system. Second, the time-dependent element may be isolated from the system and regarded as a part of the heat source. Both of these two methods are used in the method to be given in this chapter.

As the life cycle of a building may be longer than 80 years, it is preferable to evaluate the long-term energy performance of a building based on the weather data of several years. Although the new model can use the weather data of any number of years as input, a yearly period is used in the following derivations as examples. The equations for any periodic heat sources in any long time period can be derived in the same way.

Consider first the simplest operation of air-conditioning, steady and continuous operation, which means the indoor air temperature is kept as constant. The results derived from this operation strategy will also provide a basis for the calculation of total cooling loads in any complicated dynamic operation.

In steady and continuous operation, an hourly cooling load, $Q_{c,h}(k)$, may be computed by

$$Q_{c,h}(k) = \sum_{j=1}^{J} Q_{c,h,j}(k) = \sum_{j=1}^{J} \sum_{i=0}^{\infty} Y_j(i) S_j(k-i) \tag{8.1}$$

where Y means the symbolic response factor relating a heat source as input to hourly cooling load as output; S means a heat source; and J is the number of heat sources that impact the cooling load. Notice that temperature difference between outdoor air and indoor air is used for the heat source of ambient air temperature.

No matter how many independent heat sources impact the cooling load, equations for computing the total cooling load due to different heat sources should be similar. Hence, one heat source S is considered in deriving equations for estimating the total cooling load. The annual cooling load $Q_{c,y}$ caused by a heat source S should be equal to the summation of hourly cooling loads. Thus,

$$Q_{c,y} = \sum_{j=0}^{\infty} Y(j) S(1-j) + \sum_{j=0}^{\infty} Y(j) S(2-j) + \cdots + \sum_{j=0}^{\infty} Y(j) S(8760-j) = \sum_{i=1}^{8760} \sum_{j=0}^{\infty} Y(j) S(i-j) \tag{8.2}$$

A heat source in the typical year, such as ambient air temperature and solar radiation, may be assumed approximately as a yearly periodic heat source, and hence we have

$$\sum_{i=1}^{8760} S(i) = \sum_{i=1}^{8760} S(i-1) = \sum_{i=1}^{8760} S(i-2) = \cdots$$

Combination of the above two equations yields

$$Q_{c,y} = \sum_{j=0}^{\infty} Y(j) \cdot \sum_{i=1}^{8760} S(i) = \left[\sum_{j=0}^{\infty} Y(j) \right] SUM_y \tag{8.3}$$

where SUM_y is the summation of hourly heat driving forces in the typical year,

which is expressed by

$$SUM_y = \sum_{i=1}^{8760} S(i) \tag{8.4}$$

Equation (8.3) shows that in steady and continuous operation with periodic heat sources, the total thermal load in long-term can be evaluated by steady state heat transfer. The summation of response factors, $Y(j)$, should be equal to the overall thermal conductance in the steady state heat transfer.

There is a pre-condition for Equation (8.3). All the hourly thermal loads in the equation should either cooling or heating loads. If the equation contains both heating and cooling loads, the direct summation of hourly thermal loads will result in cancellations between them. In the tropic and sub-tropic regions, however, there is almost no heating load. Our simulations show that the cancellation between heating and cooling loads could account for only less than 1% of the annual cooling load in Hong Kong. For the other regions where heating loads are not negligible, the total cooling load in the cooling season can be computed by Equation (8.3) in the optimal design of buildings. This is because all heat source inputs should be approximately equal at the two ends of the cooling season, and Equation (8.3) is still approximately held for the calculation of seasonal cooling loads.

8.1.2 Hourly cooling loads in intermittent operation

In general operation schedule, an air-conditioning system is assumed to be operated between hour n_1+1 to n_2 every day in a year, while not from n_2 +1 to n_1. Equations for calculating hourly cooling loads in intermittent operation have to be derived before the total cooling load can be directly computed. The hourly cooling loads previously computed in steady and continuous operation may be imagined as convectively supplied heat during unoccupied hours in intermittent operation. This imagined convective heat from hour n_2+1 to n_1 would cause additional cooling loads during occupied hours in two ways.

- It would directly lead to additional cooling loads, $Q_{c,1}(k)$, during occupied time period.
- It would also lead to indoor air temperature increases during unoccupied hours, which would result in more additional cooling loads, $Q_{c,2}(k)$, during occupied hours.

Thus, the hourly cooling load, $Q_{c,d}(k)$, in dynamic or intermittent operation may be calculated by

$$Q_{c,d}(k) = Q_{c,h}(k) + Q_{c,1}(k) + Q_{c,2}(k) \tag{8.5}$$

The first term in the Equation (8.5) can be directly computed, using Equation (8.1). It is difficult, if not impossible, to determine a transfer function relating the supplied convective heat to the cooling load in the condition of constant indoor air temperature. This is because the convective heat is directly added to the

cooling load, and is removed by AC system immediately to keep the air temperature constant. To calculate the second term in Equation (8.5), the effect of the supplied convective heat on indoor air temperature is first found when indoor air temperature is allowed to be freely floating. The amount of cooling load required for eliminating this indoor air temperature increase is then determined. This cooling load is equivalent to that when no cooling services are provided during unoccupied hours, and the indoor air temperature is kept constant during occupied hours. Thus, the second cooling load, $Q_{c,1}$, may be calculated by

$$Q_{c,1}(k) = Y_{c,a}(0)\Delta T_{a,on}(k) \tag{8.6}$$

where $Y_{c,a}$ is the response factor relating the indoor air temperature as input to the cooling load as output; and $\Delta T_{a,on}$ is the temperature increase during occupied hours.

Hourly indoor air temperature, $\Delta T_{a,on}$, during occupied hours from $n_1 + 1$ to n_2 is impacted by the imaginarily supplied convective heat during unoccupied hours. It may be expressed by

$$\Delta T_{a,on}(m) = \sum_{i_d=0}^{\infty} \sum_{i=1}^{24+n_1-n_2} Y_{a,c}(24i_d + i - n_1 + m - 1) Q_{c,h}(-24i_d - i + n_1 + 1) \tag{8.7}$$

where $m = n_1+1, n_1+2, \ldots, n_2$. The above equation is derived in Appendix A. Submitting Equation (8.7) into Equation (8.6) yields

$$Q_{c,1}(m) = Y_{c,a}(0) \sum_{i_d=0}^{\infty} \sum_{i=1}^{24+n_1-n_2} Y_{a,c}(24i_d + i + m - n_1 - 1) Q_{c,h}(-24i_d - i + n_1 + 1) \tag{8.8}$$

As mentioned previously, only one heat source needs to be treated in the derivation to simplify the expressions because the same resultant formulae can be used for the other heat sources. Assuming J equals 1, substituting Equation (8.1) into Equation (8.8) yields

$$Q_{c,1}(m) = Y_{c,a}(0)\sum_{i_d=0}^{\infty}\sum_{i=1}^{24+n_1-n_2}\left[Y_{a,c}(24i_d + i + m - n_1 - 1)\sum_{l=0}^{\infty}Y(l)S(-24i_d - i - l + n_1 + 1)\right] \quad (8.9)$$

The third term, $Q_{c,2}$, in Equation (8.5) is an additional cooling load caused by indoor air temperature increases due to the imaginarily supplied convective heat during unoccupied hours. Hence, it can be similarly derived as above. Let $\Delta T_{a,off}$ be the temperature increase during the unoccupied hours and $Y_{c,a}$ be the response factor relating the indoor temperature increase $\Delta T_{a,off}$ as input to the additional cooling load as output. Replacing $\Delta T_{a,on}$, $Y_{a,c}$ and $Q_{c,h}$ in Equation (8.7) respectively with $Q_{c,2}$, $Y_{c,a}$ and $\Delta T_{a,off}$ yields

$$Q_{c,2}(m) = \sum_{i_d=0}^{\infty}\sum_{i=1}^{24+n_1-n_2}Y_{c,a}(24i_d + i + m - n_1 - 1)\Delta T_{a,off}(-24i_d - i + n_1 + 1) \quad (8.10)$$

Using the same method in the derivation of Equation (8.7), we can obtain a formula for the calculation of $\Delta T_{a,off}$ as follows

$$\begin{aligned}\Delta T_{a,off}(n_1 + 1 - i) = &\sum_{k=1}^{n_1+1-i+24-n_2}Y_{a,c}(k-1)Q_{c,h}(n_1 - k + 2 - i) \\ &+ \sum_{l_d=0}^{\infty}\sum_{k=1}^{24+n_1-n_2}Y_{a,c}(24l_d + k + 24 - i)Q_{c,h}(-24l_d + n_1 - k - 23)\end{aligned} \quad (8.11)$$

where i = 1, 2, …, (n_1 + 24 - n_2). The first part in Equation (8.11) shows the effect of imaginarily supplied convective heat in the hours during the current

unoccupied period. The second one indicates the effect in the hours during all the past unoccupied periods.

Substituting Equation (8.11) into Equation (8.10) yields

$$Q_{c,2}(m)=\sum_{i_d=0}^{\infty}\sum_{i=1}^{24+n_1-n_2}Y_{c,a}(24i_d+i-n_1-1+m)\left[\sum_{k=0}^{n_1+24-n_2-i}Y_{a,c}(k)Q_{c,h}(-24i_d+n_1+1-k-i)\right.$$
$$\left.+\sum_{l_d=0}^{\infty}\sum_{k=1}^{24+n_1-n_2}Y_{a,c}(24l_d+24+k-i)Q_{c,h}(-24i_d-24l_d-24+n_1+1-k)\right] \quad (8.12)$$

Substituting Equations (8.1), (8.9) and (8.12) into Equation (8.5) results in a formula for computing hourly cooling loads in intermittent operation as follows

$$Q_{c,d}(m)=\sum_{j=0}^{\infty}Y(j)S(m-j)+Y_{c,a}(0)\sum_{i_d=0}^{\infty}\sum_{i=1}^{24+n_1-n_2}\left[Y_{a,c}(24i_d+m-n_1-1+i)\sum_{j=0}^{\infty}Y(j)S(-24i_d+n_1+1-i-j)\right]$$
$$+\sum_{i_d=0}^{\infty}\sum_{i=1}^{24+n_1-n_2}Y_{c,a}(24i_d+m-n_1-1+i)\left[\sum_{k=0}^{n_1+24-n_2-i}Y_{a,c}(k)\sum_{j=0}^{\infty}Y(j)S(-24i_d+n_1+1-k-i-j)\right. \quad (8.13)$$
$$\left.+\sum_{l_d=0}^{\infty}\sum_{k=1}^{24+n_1-n_2}Y_{a,c}(24l_d+24+k-i)\sum_{j=0}^{\infty}Y(j)S(-24i_d-24l_d-24+n_1+1-k-j)\right]$$

8.1.3 Total cooling load in intermittent operation

The summation of hourly cooling loads given in Equation (8.13) in all the operated hours of one day and then in 365 days leads to the total annual cooling load. Thus, the total annual cooling load, $Q_{cd,y}$, in intermittent operation may be computed by

$$
\begin{aligned}
Q_{cd,y} = & \sum_{j=0}^{\infty}\left[Y(j)\sum_{m_d=0}^{364}\sum_{m=n_1+1}^{n_2} S(24m_d+m-j)\right] \\
& + Y_{c,a}(0)\sum_{i_d=0}^{\infty}\sum_{i=1}^{24+n_1-n_2}\left[\sum_{m=n_1+1}^{n_2} Y_{a,c}(24i_d+m-n_1-1+i)\sum_{j=0}^{\infty}Y(j)\sum_{m_d=0}^{364}S(24m_d-24i_d+n_1+1-i-j)\right] \\
& + \sum_{i_d=0}^{\infty}\sum_{i=1}^{24+n_1-n_2}\sum_{m=n_1+1}^{n_2} Y_{c,a}(24i_d+m-n_1-1+i)\left[\sum_{k=0}^{24+n_1-n_2-i} Y_{a,c}(k)\sum_{j=0}^{\infty}Y(j)\sum_{m=0}^{364}S(24m_d-24i_d+n_1+1-k-i-j)\right. \\
& \left. + \sum_{l_d=0}^{\infty}\sum_{k=1}^{24+n_1-n_2} Y_{a,c}(24i_d+24+k-i)\sum_{j=0}^{\infty}Y(j)\sum_{m_d=0}^{364}S(24m_d-24l_d-24i_d+24+n_1+1-k-j)\right]
\end{aligned}
\tag{8.14}
$$

When a heat source, such as outdoor air temperature and solar radiation, varies periodically in one year, we have

$$
\sum_{m_d=0}^{364} S(24\,m_d\,+\,j) = \sum_{m_d=0}^{364} S(24\,m_d\,\pm 24\,n+\,j) \qquad j=0,1,2,\cdots,23 \tag{8.15}
$$

where n is integer. Examination of Equation (8.15) shows that number of previous day n can be eliminated from Equation (8.15) and then Equation (8.15) depends only on the number of daily hour j. Hence, a periodic yearly heat source in Equation (8.14) can be converted to a periodic daily heat source. This results in that the response factors of a room can also become the periodic daily response factors because there are only 24 different values in a heat source. Let subscript p represents periodic, and pm is periodic collective response factor. The expression of the periodic heat source may be simplified by

$$
SUM_{p,1}(-j) = \sum_{m_d=0}^{364}\sum_{m=n_1+1}^{n_2} S(24m_d+m-j) \qquad j=0,1,2,\cdots,23 \tag{8.16}
$$

$$
SUM_{p,2}(n_1+1-j) = \sum_{m_d=0}^{364} S(24m_d+n_1+1-j) \qquad j=0,1,2,\cdots,23 \tag{8.17}
$$

Utilizing the periodic property of response factors, let

$$Y_p(i)=\sum_{i=0}^{\infty}Y(i)=\sum_{i_d=0}^{\infty}Y(24i_d+i) \qquad i=0,\,1,\,2,\cdots,23 \tag{8.18}$$

$$Y_{pm\ ac}(-n_1-1+i)=\sum_{i_d=0}^{\infty}\sum_{m=n_1+1}^{n_2}Y_{a,c}(24i_d+m-n_1-1+i) \qquad i=0,1,2,\cdots;23 \tag{8.19}$$

$$Y_{pm\ ca}(-n_1-1+i)=\sum_{i_d=0}^{\infty}\sum_{m=n_1+1}^{n_2}Y_{c,a}(24i_d+m-n_1-1+i) \qquad i=0,1,2,\cdots;23 \tag{8.20}$$

$$Y_{p,ac}(i)=\sum_{i=0}^{\infty}Y_{a,c}(i)=\sum_{i_d=0}^{\infty}Y_{a,c}(24i_d+i) \qquad i=0,\,1,\,2,\cdots,23 \tag{8.21}$$

Substituting Equations (8.16) to (8.21) into Equation (8.14) yields

$$\begin{aligned}Q_{cd,y}=&\sum_{j=0}^{23}Y_p(j)\,SUM_{\ p,1}(-j)+Y_{c,a}(0)\sum_{i=1}^{24+n_1-n_2}Y_{pm,ac}(-n_1-1+i)\sum_{j=0}^{23}Y_p(j)\;SUM_{p,2}(n_1+1-i-j)\\&+\sum_{i=1}^{24+n_1-n_2}Y_{pm,\ ca}(-n_1-1+i)\left[\sum_{k=0}^{24+n_1-n_2-i}Y_{a,c}(k)\sum_{j=0}^{23}Y_p(j)\;SUM_{p,2}\,(n_1+1-k-i-j)\right.\\&\left.+\sum_{k=1}^{24+n_1-n_2}Y_{p,ac}(k-i)\sum_{j=0}^{23}Y_p(j)\;SUM_{p,2}(n_1+1-k-j)\right]\end{aligned} \tag{8.22}$$

Close examination of Equation (8.22) shows that the last three terms contain the common factor, periodic heat source $SUM_{p,2}$. This common factor can be taken out when the order of summations is reversed. Let $l_p = i + j$ in the discrete time of the first $SUM_{p,2}$, and $l_p = k + i + j$ and $l_p = k + j$ in that of the second and third $SUM_{p,2}$, respectively. Subscript p indicates periodic. Whenever the discrete time is negative, l_p should be either added or subtracted by the periodic time length, i.e. 24, to make the time positive. The limits of summation with respect to l_p can be determined by the above three relations defined for l_p in reversing the order of summations. However, the values of l_p should be limited

by the periodic time length because it is a discrete time that varies within the periodic time length. Thus, the two limits of l_p should be equal to 0 and 23 in the reversed order of summation. Equation (8.22) may be rearranged by

$$Q_{cd,y} = \sum_{j=0}^{23} Y_p(j)\, SUM_{\,p,1}(-j) + \sum_{l_p=0}^{23} SUM_{p,2}(n_1+1-l_p') \left\{ Y_{c,a}(0) \sum_{i=1}^{24+n_1-n_2} Y_{pm,ac}(-n_1-1+i)\, Y_p(l_p'-i) + \sum_{i=1}^{24+n_1-n_2} Y_{pm,\,ca}(-n_1-1+i) \left[\sum_{k=0}^{24+n_1-n_2-i} Y_{a,c}(k)\; Y_p(l_p'-k-i) + \sum_{k=1}^{24+n_1-n_2} Y_{p,ac}(k-i)\, Y_p(l_p'-k) \right] \right\} \tag{8.23}$$

where $l_p^{'}$ depends on $n_1 + 1 - l_p$ and is computed by

$$l_p^{'} = \begin{cases} l_p & n_1+1-l_p \geq 0 \\ l_p - 24 & n_1+1-l_p < 0 \end{cases} \tag{8.24}$$

It can be seen from the above derivation that the annual cooling load in the periodic daily dynamic operation consists of two parts. The first part can be considered as the cooling load during operated hours in the continuous operation. The second one is caused by intermittent operation in which cooling is not served during unoccupied hours. The response factors relating this part of cooling loads to a heat source is given in the braces in the second term of Equation (8.23).

8.2 Generation of fully-symbolic room transfer functions when all parameters are symbolic

Although some designers usually are only interested in some parameters in the design of buildings, fully symbolic transfer functions will be generated with all parameters are symbolic. Then different specific symbolic transfer functions

can be easily obtained by giving the selected values to several symbolic parameters. This is more efficient than solving a set of simultaneous equations every time.

Through thermal network analysis, two symbolic transfer functions will be derived as examples. The first transfer function is for the calculation of cooling load due to solar diffuse radiation; and the second one is for the calculation of indoor air temperature due to convective heat gain. The transfer functions to other heat sources can be obtained in the same way.

8.2.1 Room model

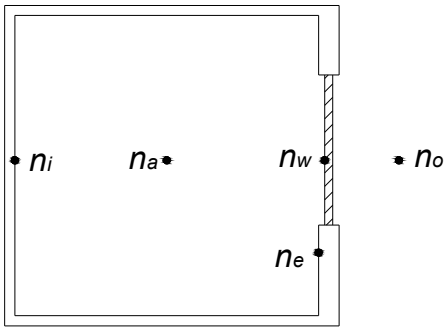

Figure 8.1 Room model.

A room model is shown in Figure 8.1. It has one external wall containing a window with interior venetian blinds. Nodes *e*, *i* and *w* represent the interior surfaces of the external wall, the internal wall and the window system, respectively. Nodes *a* and *o* represent indoor and outdoor air, respectively.

8.2.2 Symbolic transfer function of cooling load to solar diffuse radiation

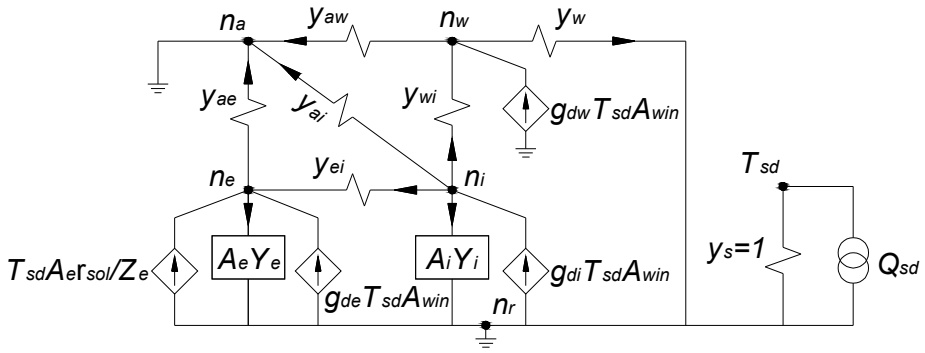

Figure 8.2. Thermal network of the room when solar diffuse radiation acts only.

Assuming that only solar diffuse radiation acts on the system and utilizing the method for describing a general thermal network of a space (Chen and Athienitis, 1993; Chen, 2003), a thermal network describing the room model (Figure 8.1) is presented by Figure 8.2. Q_{sd} is the total solar diffuse radiation incident on the unit area of the external surface of the room envelope. Nodes n_a, n_w, n_e, n_i and n_o have same meanings as the corresponding nodes in Figure 8.1. Node n_r indicates a reference. In the thermal network, the capital symbols Y_e, Y_i and Z_e contain the Laplace transform variable s in addition to other symbolic parameters. The symbolic parameters Y_e, Y_i and Z_e represent the Norton equivalent thermal admittances of the unit area of the external and internal. Y_e, Y_i and Z_e are symbolic transfer functions in the Laplace domain. A procedure to calculation of Y_e, Y_i and Z_e is presented in Appendix B. The thermal admittances y_{aw}, y_{ai} and y_{ae} represent the convective thermal conductances between the indoor air and the interior surfaces of window, internal and external walls, respectively. y_{ei} and y_{wi} are the radiative conductance among window, interior and exterior walls.

Thermal admittance y_w is the thermal conductance between the interior surface of the window and the outdoor air. The thermal admittance y_{inf} is the convective thermal conductance between the indoor and outdoor air. A_e and A_i are the area of the external and internal walls. In Figure 8.2, the node n_a is connected to the reference node. It is because the cooling load $Q_{c,sd}$ due to Q_{sd} is removed from the room to hold the indoor air temperature constant. $Q_{c,sd}$ does not have corresponding branch in the thermal network because the thermal network would be short-circuited if such a branch is connected to the node n_a. Under this condition, $Q_{c,sd}$ should be equal to the sum of the heat flows through the branches *aw*, *ai* and *ae*.

Node *sd* is the imaginary node denoting a diffuse radiation heat source. T_{sd} is imaginary solar diffuse temperature, whose value is equal to that of Q_{sd} when y_{sd} is set to one. Then the solar diffuse radiation is expressed as temperature-controlled heat flow source. This allows any complex heat transfer processes and derived thermal parameters to be explicitly and precisely modeled (Chen, 2003). The solar diffuse radiation absorbed by different surfaces is represented by temperature-controlled heat flow sources $T_{sd}A_e r_{sol}/Z_e$, $g_{dw}T_{sd}A_{win}$, $g_{de}T_{sd}A_{win}$ and $g_{di}T_{sd}A_{win}$. r_{sol} is the solar absorpance of the external wall. The values of r_{sol} for different walls can be found at Chinese Building Standard GB 50176-93. A_{win} is the window area. g_{dw} represents the fraction of the solar diffuse radiation absorbed by the window system, which may include both the window

and the blinds. g_{di} and g_{de} represent the fraction of solar diffuse radiation that passes through the window system and falls on the interior surfaces of the internal and external walls, respectively.

The convective thermal conductance between the indoor air and the interior surfaces may be calculated by

$$y_{aw} = y_i A_{win}, \quad y_{ai} = y_i A_i, \quad y_{ae} = y_i A_e$$

where y_i is interior convective coefficient; A_i and A_e are the area of the interior and external walls. A_e may be calculated by

$$A_e = A_{en} - A_{win}$$

where A_{en} is area of the room envelope, which includes both the window and the exterior wall.

The thermal conductance y_w may be calculated by

$$y_w = A_{win} y_o$$

where y_o is exterior convective coefficient.

The convective thermal conductance of air infiltration, y_{inf}, may be calculated by

$$y_{\inf} = \frac{N_{\inf} c_{air} \rho_{air} V_{rm}}{3600}$$

where N_{inf} is air change rate per hour; V_{rm} is room volume; c_{air} and ρ_{air} are the specific heat and density of air.

Following the method used in DOE2 (DOE-2 Engineers Manual, 1982), the radiant heat transfer coefficient between two interior surfaces enclosing a room may be calculated by

$$y_{ij} = 4\varepsilon_i \sigma T_{ir}^{\ 3} A_i VF_{ij} \tag{8.25}$$

where ε_i is the emissivity of surface i; σ is the Stefan-Boltzmann constant; T_{ir} is the reference room temperature (°C); A_i is the area of surface i emitting the radiant energy (m^2) and VF_{ij} is the view factor from surface i to surface j. The values of ε_i and T_{ir} used are 0.9 and 21°C, respectively. These values are also adopted in this research. Then the value of $4\varepsilon_i \sigma T_{ir}^{\ 3}$ equals 5.19 W/(m^2°C). The view factor may be approximated by (Kerrisk *et al.*, 1981; DOE-2 Engineers Manual, 1982)

$$VF_{ij} = A_j / A_t \tag{8.26}$$

where A_j is the area of surface j receiving the radiant energy; A_t is the total area of all surfaces in the room.

Substituting Equation (8.26) into Equation (8.25), we have:

$$y_{ij} = \frac{4\varepsilon_i \sigma T_{ir}^{\ 3} A_i A_j}{A_t} = 5.19 \frac{A_i A_j}{A_t} \tag{8.27}$$

According to the above equations, the radiative conductance used in the thermal network can be calculated by

$$y_{ei} = 5.19 \frac{(A_{en} - A_{win}) A_i}{A_{en} + A_i}$$

$$y_{wi} = 5.19 \frac{A_{win} A_i}{A_{en} + A_i}$$

Assuming the incoming solar diffuse radiation is uniformly distributed on the interior surfaces of the external and internal walls, g_{de} and g_{di} may be calculated by

$$g_{di} = r_{sd,t} TV_{sd} \frac{A_i}{A_{en} + A_i - A_{win}} \tag{8.28}$$

$$g_{de} = r_{sd,t} TV_{sd} \frac{A_{en} - A_{win}}{A_{en} + A_i - A_{win}} \tag{8.29}$$

where $r_{sd,t}$ is the diffuse solar thermal transmittance of the window; TV_{sd} is the diffuse solar thermal transmittance of the blinds. TV_{sd} equals 1.0 if there is no blinds being used.

The solar radiation absorbed by both the window and the interior shading device should be considered. Therefore, g_{dw} may be calculated by

$$g_{dw} = g_{dw,win} + g_{dw,bl} \tag{8.30}$$

where $g_{dw,win}$ and $g_{dw,bl}$ represent the fractions of solar diffuse radiation absorbed by window and blinds, respectively.

Interior shading device can only absorb the solar radiation that passes through the window. Hence $g_{dw,bl}$ may be calculated by

$$g_{dw,bl} = r_{sd,t} S_{sd} \tag{8.31}$$

where S_{sd} is the diffuse solar absorpance of the blinds.

Beside the solar radiation from the outside, the window will also absorb a part of the solar radiation reflected from the blinds. Therefore, $g_{dw,win}$ may be calculated by

$$g_{dw,win} = r_{sd,ab}\left(1 + r_{sd,t} R_{sd}\right) \tag{8.32}$$

where R_{sd} is the diffuse solar reflectance of the blinds; $r_{sd,ab}$ is the diffuse solar absorpance of the window.

The diffuse solar absorptance $r_{sd,ab}$ and solar thermal transmittance $r_{sd,t}$ of window may be calculated by the following equations (DOE-2 Engineers Manual, 1982).

$$r_{sd,ab} = 1.08 r_{ab}(0)$$

$$r_{sd,t} = 0.87 r_t(0)$$

where $r_{ab}(0)$ and $r_t(0)$ are solar absorpance and solar thermal transmittance when solar incident angle θ_{sol} is 0°.

TV_{sd}, S_{sd} and R_{sd} are needed in the Equations (8.28)-(8.32). In Chapters 5, we developed a model for the estimation of the optical performance of the blinds. If the distribution of solar radiation over the sky hemisphere is assumed to be the same to that of the optical light, this model can be used to calculate TV_{sd}, S_{sd} and R_{sd}. TV_{sd} can be regarded as the ratio between the vertical daylight factors on the

internal and external surfaces of the blinds. Therefore, it may be calculated by

$$TV_{sd} = \frac{VDF_{i,dg}}{VDF_{o,dg}} \tag{8.33}$$

where $VDF_{i,dg}$ and $VDF_{o,dg}$ are the vertical daylight factors on the internal and external surfaces of the blinds, which are due to the sky diffuse light and ground-reflected light. They can be calculated by Equations (5.13) and (5.36).

In Chapter 5, we used the radiosity method to calculate the final luminous exitance on the glazing due to the sky diffuse light and ground-reflected light $B_{gl,dg}$. $B_{gl,dg}$ is caused by the light reflected between the blinds and the window. The reflection on the internal surface of the window glazing can be eliminated by dividing $B_{gl,dg}$ with the reflectance of the glazing, ρ_{gl}. Therefore, the diffuse reflectances of the blinds may be calculated by

$$R_{sd} = \frac{B_{gl,dg} / \rho_{gl}}{VDF_{o,dg}} \tag{8.34}$$

The sum of TV_{sd}, S_{sd} and R_{sd} should be equal to 1.0. Therefore, S_{sd} may be calculated by

$$S_{sd} = 1 - R_{sd} - TV_{sd} \tag{8.35}$$

A hybrid formulation has been developed for the symbolic thermal network analysis of buildings (Chen and Athienitis, 1993). It is based on the thermal balance laws, which is analogous to the Kirchhoff's Current Law and Kirchhoff's

Voltage Law. Based on the work of Chen (2003), a hybrid system of thermal balance equations for the thermal network in Figure 8.2 may be established in the following form

$$Ax = \begin{bmatrix} A_{11} & A_{12} \\ A_{21} & A_{22} \end{bmatrix} \begin{bmatrix} x_1 \\ x_2 \end{bmatrix} = 0 \tag{8.36}$$

where A is the coefficient matrix.

The system variable vectors are expressed by

$$x_1 = [T_{sd} \quad T_{bw} \quad T_{be} \quad T_{bi}]^T$$

$$x_2 = [Q_{aw} \quad Q_{ae} \quad Q_{ei} \quad Q_{wi} \quad Q_e \quad Q_{ai} \quad Q_{dw} \quad Q_{di} \quad Q_{de} \quad Q_{sd}]^T$$

where T is the complete tree-branch-temperature vector;

Q is the heat flow vector.

Hourly cooling load $Q_{c,sd}$ may be computed by summing up three heat flows through the branches *aw*, *ai* and *ae*.

$$Q_{c,sd} = Q_{aw} + Q_{ai} + Q_{ae}$$

The transfer function $H_{c,sd}(s)$ is the ratio of $Q_{c,sd}(s)$ to $Q_{sd}(s)$:

$$H_{c,sd}(s) = \frac{Q_{c,sd}(s)}{Q_{sd}(s)}$$

The symbolic parameters should be placed along the diagonal of the coefficient matrix. This will reduce the size of the coefficient matrix and enhance

the efficiency of generating the transfer function (Chen, 2003). Based on this principle, the partitioned coefficient matrices are given by

$$A_{11}=\begin{bmatrix} y_s & 0 & 0 & 0 \\ 0 & y_w & 0 & 0 \\ 0 & 0 & A_e Y_e & 0 \\ 0 & 0 & 0 & A_i Y_i \end{bmatrix} \quad A_{12}=\begin{bmatrix} 0 & 0 & 0 & 0 & 0 & 0 & 0 & 0 & 0 & -1 \\ 1 & 0 & 0 & -1 & 0 & 0 & -1 & 0 & 0 & 0 \\ 0 & 1 & -1 & 0 & -1 & 0 & 0 & 0 & -1 & 0 \\ 0 & 0 & 1 & 1 & 0 & 1 & 0 & -1 & 0 & 0 \end{bmatrix}$$

$$A_{21}=\begin{bmatrix} 0 & -1 & 0 & 0 \\ 0 & 0 & -1 & 0 \\ 0 & 0 & 1 & -1 \\ 0 & 1 & 0 & -1 \\ -1 & 0 & 0 & 0 \\ 0 & 0 & 0 & -1 \\ -1 & 0 & 0 & 0 \\ -1 & 0 & 0 & 0 \\ -1 & 0 & 0 & 0 \\ 0 & 0 & 0 & 0 \end{bmatrix}$$

$$A_{22}=\begin{bmatrix} 1/y_{aw} & 0 & 0 & 0 & 0 & 0 & 0 & 0 & 0 & 0 \\ 0 & 1/y_{ae} & 0 & 0 & 0 & 0 & 0 & 0 & 0 & 0 \\ 0 & 0 & 1/y_{ei} & 0 & 0 & 0 & 0 & 0 & 0 & 0 \\ 0 & 0 & 0 & 1/y_{wi} & 0 & 0 & 0 & 0 & 0 & 0 \\ 0 & 0 & 0 & 0 & Z_e/(r_{sol}A_e) & 0 & 0 & 0 & 0 & 0 \\ 0 & 0 & 0 & 0 & 0 & 1/y_{ai} & 0 & 0 & 0 & 0 \\ 0 & 0 & 0 & 0 & 0 & 0 & 1/(g_{dw}A_{win}) & 0 & 0 & 0 \\ 0 & 0 & 0 & 0 & 0 & 0 & 0 & 1/(g_{dt}A_{win}) & 0 & 0 \\ 0 & 0 & 0 & 0 & 0 & 0 & 0 & 0 & 1/(g_{de}A_{win}) & 0 \\ -1 & -1 & 0 & 0 & 0 & -1 & 0 & 0 & 0 & H_{c,sd} \end{bmatrix}$$

Substituting the previous parameters into Equation (8.36) and solving the thermal balance equation, we obtained the following transfer function:

$$\begin{aligned} H_{c,sd} &= \left(r_{sd,t}S_{sd} + r_{sd,ab} + r_{sd,ab}r_{sd,t}R_{sd}\right)A_{win}\frac{f_{dw,0}+f_{dw,1}Y_e+f_{dw,2}Y_i+f_{dw,3}Y_eY_i}{g_o+g_1Y_e+g_2Y_i+g_3Y_eY_i} \\ &+ r_{sd,t}TV_{sd}A_{win}\frac{f_{dt,0}+f_{dt,1}Y_e+f_{dt,2}Y_i}{g_o+g_1Y_e+g_2Y_i+g_3Y_eY_i} + \frac{r_{sol}}{Z_e}\frac{f_{de,0}+f_{de,1}Y_i}{g_o+g_1Y_e+g_2Y_i+g_3Y_eY_i} \end{aligned} \tag{8.37}$$

where

$$f_{de,0} = 349091856\left(A_{en}^{\ 4}A_i y_i - A_i^{\ 4}A_{win}y_i + A_i^{\ 4}A_{en}y_i - A_{en}^{\ 3}A_i A_{win}y_i\right) + 4A_{en}^{\ 4}A_i y_o y_i^{\ 2} - A_i^{\ 4}A_{win}y_i^{\ 3}$$
$$+1047275568\left(A_{en}^{\ 3}A_i^{\ 2}y_i - A_{win}A_{en}^{\ 2}A_i^{\ 2}y_i - A_{win}A_{en}A_i^{\ 3}y_i\right) + 130788\left(A_{en}^{\ 2}A_i^{\ 3}y_i^{\ 2} - A_{win}A_{en}A_i^{\ 3}y_i^{\ 2}\right)$$
$$+112104\left(A_{en}^{\ 3}A_i^{\ 2}y_o y_i - A_{en}^{\ 2}A_i^{\ 2}A_{win}y_o y_i\right) + 168156\left(A_{en}^{\ 3}A_i^{\ 2}y_i^{\ 2} - A_{en}^{\ 2}A_i^{\ 2}A_{win}y_i^{\ 2}\right) + A_{en}^{\ 5}y_i^{\ 3}$$
$$+74736\left(A_{en}^{\ 2}A_i^{\ 3}y_o y_i + A_{en}^{\ 4}A_i y_o y_i - A_{en}^{\ 3}A_{win}A_i y_o y_i\right) + 4A_{en}^{\ 4}A_i y_i^{\ 3} + 6A_{en}^{\ 3}A_i^{\ 2}y_i^{\ 3} - A_{en}^{\ 4}A_{win}y_i^{\ 3}$$
$$+18684\left(A_{en}^{\ 5}y_i^{\ 2} - A_{win}A_{en}^{\ 4}y_i y_o + A_i^{\ 4}A_{en}y_i y_o + A_{en}^{\ 5}y_i y_o - A_{win}A_i^{\ 4}y_i y_o\right) + 4A_{en}^{\ 2}A_i^{\ 3}y_o y_i^{\ 2}$$
$$-A_{win}A_{en}^{\ 4}y_i^{\ 2}y_o + 37368A_i^{\ 4}A_{en}y_i^{\ 2} - 4A_{win}A_{en}A_i^{\ 3}y_i^{\ 3} - 93420A_{win}A_{en}^{\ 3}A_i y_i^{\ 2} - 4A_{win}A_{en}A_i^{\ 3}y_i^{\ 3}$$
$$+A_i^{\ 4}A_{en}y_i^{\ 2}y_o - 6A_{win}A_{en}^{\ 2}A_i^{\ 2}y_i^{\ 3} + 4A_{en}^{\ 2}A_i^{\ 3}y_i^{\ 3} - 4A_{win}A_{en}^{\ 3}A_i y_i^{\ 3} - 6A_{win}A_{en}^{\ 2}A_i^{\ 2}y_i^{\ 2}y_o$$
$$-4A_{win}A_{en}^{\ 3}A_i^{\ 2}y_i^{\ 2}y_o$$

$$f_{de,1} = 18684\left(A_{en}^{\ 4}A_i y_i + A_{en}A_i^{\ 4}y_i + A_{win}A_{en}^{\ 3}A_i y_i - A_i^{\ 4}A_{win}y_i\right) + A_i^{\ 4}A_{en}y_i y_o + A_{en}^{\ 5}y_i y_o - A_{win}A_i^{\ 4}y_i^{\ 2}$$
$$+56052\left(A_{en}^{\ 2}A_i^{\ 3}y_i - A_{win}A_{en}A_i^{\ 3}y_i + A_{en}^{\ 3}A_i^{\ 2}y_i - A_{win}A_{en}^{\ 2}A_i^{\ 2}y_i\right) + A_i^{\ 4}A_{en}y_i^{\ 2} - A_{win}A_{en}^{\ 4}y_i y_o - A_{win}A_{en}^{\ 4}y_i^{\ 2}$$
$$+6\left(A_{en}^{\ 3}A_i^{\ 2}y_i^{\ 2} - A_{win}A_{en}^{\ 2}A_i^{\ 2}y_i^{\ 2} - A_{en}^{\ 2}A_i^{\ 2}A_{win}y_i y_o + A_{en}^{\ 3}A_i^{\ 2}y_i y_o\right) - A_{win}A_i^{\ 4}y_i y_o + A_{en}^{\ 5}y_i^{\ 2}$$
$$+4\left(A_{en}^{\ 4}A_i y_i y_o - A_{win}A_{en}A_i^{\ 3}y_i^{\ 2} - A_{win}A_{en}A_i^{\ 3}y_i y_o - A_{win}A_{en}^{\ 3}A_i y_i^{\ 2} + A_{en}^{\ 2}A_i^{\ 3}y_i^{\ 2} - A_{win}A_{en}^{\ 3}A_i y_i y_o + A_{en}^{\ 4}A_i y_i^{\ 2}\right)$$

$$f_{dt,0} = 18684\left(A_{en}^{\ 4}y_i^{\ 2} + A_i^{\ 4}y_i y_o + A_{en}^{\ 4}y_i y_o - A_{win}A_{en}^{\ 3}y_i^{\ 2} - A_{win}A_{en}^{\ 3}y_i y_o\right) + 37368\left(A_i^{\ 4}y_i^{\ 2} - A_{win}A_i^{\ 3}y_i y_o\right)$$
$$+1047275568\left(A_{en}^{\ 2}A_i^{\ 2}y_i + A_{en}A_i^{\ 3}y_i\right) + 349091856\left(A_{en}^{\ 3}A_i y_i + A_i^{\ 4}y_i - A_{win}A_{en}^{\ 2}A_i y_i\right)$$
$$-93420A_{win}\left(A_{en}A_i^{\ 2}y_i y_o + A_{en}A_i^{\ 2}y_i^{\ 2}\right) + 74736\left(A_{en}^{\ 3}A_i y_i y_o + A_{en}A_i^{\ 3}y_i y_o - A_{win}A_{en}^{\ 2}A_i y_i^{\ 2} - A_{win}A_{en}^{\ 2}A_i y_i y_o\right)$$
$$+A_{en}^{\ 4}y_o y_i^{\ 2} - 3A_{win}A_{en}^{\ 2}A_i y_i^{\ 2}y_o + 4A_{en}^{\ 3}A_i y_i^{\ 2}y_o - 3A_{win}A_i^{\ 3}y_i^{\ 3} + 6A_{en}^{\ 2}A_i^{\ 2}y_i^{\ 2}y_o - A_{win}A_i^{\ 3}y_i^{\ 3} - 3A_{win}A_{en}A_i^{\ 2}y_i^{\ 2}y_o$$
$$+1121044A_{en}^{\ 2}A_i^{\ 2}y_i y_o - 6981837151A_{win}A_{en}A_i^{\ 2}y_i - A_{win}A_{en}^{\ 3}y_i^{\ 3} + 130788A_{en}A_i^{\ 3}y_i^{\ 2} + 4A_{en}A_i^{\ 3}y_i^{\ 3} + 93420A_{en}^{\ 3}A_i y_i^{\ 2}$$
$$+168156A_{en}^{\ 2}A_i^{\ 2}y_i^{\ 2} - A_{win}A_i^{\ 3}y_i^{\ 2}y_o + A_{en}^{\ 4}y_i^{\ 3} + 4A_{en}^{\ 3}A_i y_i^{\ 3} + 6A_{en}^{\ 2}A_i^{\ 2}y_i^{\ 3} + A_i^{\ 4}y_i^{\ 2}y_o - 3A_{win}A_{en}A_i^{\ 2}y_i^{\ 3}$$
$$-A_{win}A_{en}^{\ 3}y_o y_i^{\ 2} + 4A_{en}A_i^{\ 3}y_i^{\ 2}y_o$$

$$f_{dt,1} = 18684\left(A_{en}A_i^{\ 3}y_i + A_{en}^{\ 3}A_i y_i - A_{win}A_{en}^{\ 2}A_i y_i - A_{win}A_i^{\ 3}y_i\right) + 37368\left(A_{en}^{\ 2}A_i^{\ 2}y_i - A_{win}A_{en}A_i^{\ 2}y_i\right)$$
$$+3A_{en}^{\ 3}A_i y_i^{\ 2} + 3A_{en}^{\ 2}A_i^{\ 2}y_i^{\ 2} - 3A_{win}A_{en}A_i^{\ 2}y_i y_o + 3A_{en}^{\ 2}A_i^{\ 2}y_i y_o - A_{win}A_{en}^{\ 3}y_i^{\ 2} - A_{win}A_i^{\ 3}y_i^{\ 2}$$
$$-A_{win}A_{en}^{\ 3}y_i y_o - 3A_{win}A_i A_{en}^{\ 2}y_i^{\ 2} + A_{en}A_i^{\ 3}y_i^{\ 2} + 3A_{en}^{\ 3}A_i y_i y_o - 3A_{win}A_{en}A_i^{\ 2}y_i^{\ 2} - A_{win}A_i^{\ 3}y_i y_o$$
$$+A_{en}^{\ 4}y_i y_o + A_{en}A_i^{\ 3}y_i y_o - 3_{win}A_{en}^{\ 2}A_i y_i y_o$$

$$f_{dt,2} = 18684\left(A_{win}A_i^{\ 3}y_i + A_i^{\ 4}y_i + A_{win}A_{en}^{\ 2}A_i y_i + A_{en}^{\ 2}A_i^{\ 2}y_i\right) + 37368\left(A_{en}A_i^{\ 3}y_i + A_{win}A_{en}A_i^{\ 2}y_i\right)$$
$$+3\left(A_{en}A_i^{\ 2}y_i^{\ 2} + A_{en}A_i^{\ 3}y_i^{\ 2} + A_{en}A_i^{\ 3}y_i y_o\right) + A_i^{\ 4}y_i y_o + 3A_{en}^{\ 2}A_i^{\ 2}y_i y_o + A_i^{\ 4}y_i^{\ 2} + A_{en}^{\ 3}A_i y_i^{\ 2}$$
$$+A_{en}^{\ 3}A_i y_i y_o$$

$$f_{dw,0} = 18684\left(A_i^{\ 4}y_i + A_{en}^{\ 4}y_i\right) + 74736\left(A_{en}^{\ 3}A_i y_i + A_{en}A_i^{\ 3}y_i\right) + 112104A_{en}^{\ 2}A_i^{\ 2}y_i + 6A_{en}^{\ 2}A_i^{\ 2}y_i^{\ 2}$$
$$+4\left(A_{en}^{\ 3}A_i y_i^{\ 2} + A_{en}A_i^{\ 3}y_i^{\ 2}\right) + A_i^{\ 4}y_i^{\ 2} + A_{en}^{\ 4}y_i^{\ 2}$$

$$f_{dw,1} = 1047275568\left(A_{en}^{\ 2}A_i^{\ 2}y_i + A_{en}A_i^{\ 3}y_i\right) + 349091856\left(A_i^{\ 4}y_i + A_{en}^{\ 3}A_i y_i\right) + 18684A_{en}^{\ 4}y_i^{\ 2}$$
$$+168156A_{en}^{\ 2}A_i^{\ 2}y_i^{\ 2} + A_i^{\ 4}y_i^{\ 3} + 93420A_{en}^{\ 3}A_i y_i^{\ 2} + 4A_{en}A_i^{\ 3}y_i^{\ 3} + 4A_{en}^{\ 3}A_i y_i^{\ 3} + 130788A_{en}A_i^{\ 3}y_i^{\ 2}$$
$$+37368A_i^{\ 4}y_i^{\ 2} + A_i^{\ 4}y_i^{\ 3} + 6A_{en}^{\ 2}A_i^{\ 2}y_i^{\ 3}$$

$$f_{dw,2} = A_{en}^{\ 4}y_i + 4A_{en}A_i^{\ 3}y_i + 6A_{en}^{\ 2}A_i^{\ 2}y_i + 4A_{en}^{\ 3}A_i y_i + A_i^{\ 4}y_i$$

$$f_{dw,3} = 6A_{en}^{\ 2}A_i^{\ 2}y_i^{\ 2} + 18684\left(A_i^{\ 4}y_i + A_{en}^{\ 3}A_i y_i\right) + 56052\left(A_{en}A_i^{\ 3}Y_i + A_{en}^{\ 2}A_i^{\ 2}y_i\right)$$
$$+4\left(A_{en}^{\ 3}A_i y_i^{\ 2} + A_{en}A_i^{\ 3}y_i^{\ 2}\right) + A_i^{\ 4}y_i^{\ 2} + A_{en}^{\ 4}y_i^{\ 2}$$

$$g_0 = y_i^3 A_{en}^2 + y_i^3 A_i^2 + y_o y_i^2 A_i^2 + y_o y_i^2 A_{en}^2 + 37368\left(y_i^2 A_i^2 + y_o y_i A_i A_{en}\right) + 2\left(y_o y_i^2 A_i A_{en} + y_i^3 A_{en} A_i\right)$$
$$+ 34909185\left(y_i A_{en} A_i + y_o A_{win} A_i + y_i A_i^2\right) + 18684\left(y_i^2 A_{en}^2 + y_o y_i A_i^2 + y_o y_i A_{en}^2\right) + 56052 y_i^2 A_{en} A_i$$

$$g_1 = 2 y_i^2 A_{en} A_i + 37368 y_i A_{en} A_i + y_i^2 A_i^2 + y_i^2 A_{en}^2 + 34909185\left(A_{en} A_i - A_{win} A_i\right)$$
$$+ 18684\left(y_i A_i^2 + y_i A_{en}^2 + y_o A_{en}^2\right)$$

$$g_2 = 34909185 A_i^2 + y_i^2 A_{en}^2 + 2 y_i^2 A_{en} A_i + y_i^2 A_i^2 + 18684\left(y_o A_i^2 + y_o A_i A_{en}\right) + 2 y_o y_i A_i A_{en}$$
$$+ 37368\left(y_i A_i^2 + y_i A_i A_{en}\right) + y_o y_i A_i^2 + y_o y_i A_{en}^2$$

$$g_3 = 2 y_i A_{en} A_i + 18684\left(A_i^2 + A_{en} A_i\right) + y_o A_i^2 + y_i A_i^2 + y_o A_{en}^2 + y_i A_{en}^2 + 2 y_o A_{en} A_i$$

In Equation (8.26), S_{sd}, R_{sd} and TV_{sd} may be time-dependent because occupants or the system may control the blinds to reduce solar heat gain, utilize daylighting and solve the glare problem. This violates the pre-condition for the principle of superposition. The problem may be solved by separating the time-dependent variables from the transfer function and regarding these variables as a part of the heat sources. The remaining part of the transfer function then is decomposed into three sub-transfer functions that only have time-independent variables, as shown by the following Equation.

$$Q_{c,sd} = Q_{sd,ab} H_{c,sd,ab} + Q_{sd,t} H_{c,sd,t} + Q_{sd} H_{c,sd,e} \tag{8.38}$$

where $H_{c,sd,ab}$, $H_{c,sd,t}$ and $H_{c,sd,e}$ are the sub-transfer functions; $Q_{sd,ab}$ and $Q_{sd,t}$ are the generalized heat sources. They are expressed by

$$H_{c,sd,ab} = A_{win} \frac{f_{dw,0} + f_{dw,1} Y_e + f_{dw,2} Y_i + f_{dw,3} Y_e Y_i}{g_o + g_1 Y_e + g_2 Y_i + g_3 Y_e Y_i}$$

$$H_{c,sd,t} = A_{win} \frac{f_{dt,0} + f_{dt,1} Y_e + f_{dt,2} Y_i}{g_o + g_1 Y_e + g_2 Y_i + g_3 Y_e Y_i}$$

$$H_{c,sd,e} = \frac{r_{sol}}{Z_e} \frac{f_{de,0} + f_{de,0} Y_i}{g_o + g_1 Y_e + g_2 Y_i + g_3 Y_e Y_i}$$

$$Q_{sd,ab} = Q_{sd}\left(r_{sd,t}S_{sd} + r_{sd,ab} + r_{sd,ab}r_{sd,t}R_{sd}\right)$$

$$Q_{sd,t} = Q_{sd}r_{sd,t}TV_{sd}$$

8.2.3 Symbolic transfer function of indoor air temperature to convective heat

The second symbolic transfer function is for the calculation of floating indoor air temperature when convective heat is supplied into space without air-conditioning. The thermal network for this process is shown in Figure 8.3.

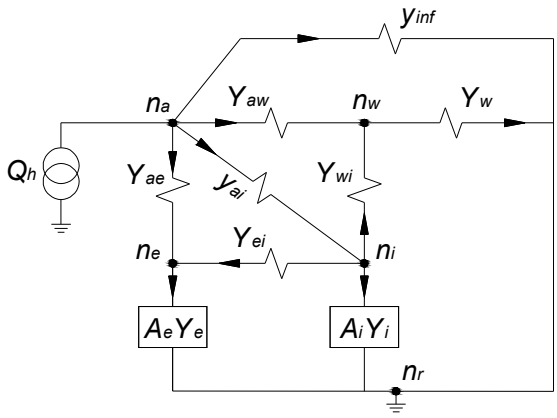

Figure 8.3. Thermal network of the room when convective heat acts only.

The system variable vectors can be expressed by

$$x_1 = \begin{bmatrix} T_{bw} & T_{be} & T_{bi} & T_{ba} \end{bmatrix}^T$$

$$x_2 = \begin{bmatrix} Q_{aw} & Q_{ae} & Q_{ei} & Q_{wi} & Q_{ai} & Q_h \end{bmatrix}^T$$

The transfer function $H_{t,h}(s)$ is the ratio of indoor air temperature $T_a(s)$ to the convective heat $Q_h(s)$:

$$H_{t,h}(s) = \frac{T_a(s)}{Q_h(s)}$$

The partitioned coefficient matrices are given by

$$A_{11}=\begin{bmatrix} y_w & 0 & 0 & 0 \\ 0 & A_eY_e & 0 & 0 \\ 0 & 0 & A_iY_i & 0 \\ 0 & 0 & 0 & y_{\inf} \end{bmatrix} \quad A_{12}=\begin{bmatrix} -1 & 0 & 0 & -1 & 0 & 0 \\ 0 & -1 & -1 & 0 & 0 & 0 \\ 0 & 0 & 1 & 1 & -1 & 0 \\ 1 & 1 & 0 & 0 & 1 & -1 \end{bmatrix}$$

$$A_{21}=\begin{bmatrix} 1 & 0 & 0 & -1 \\ 0 & 1 & 0 & -1 \\ 0 & 1 & -1 & 0 \\ 1 & 0 & -1 & 0 \\ 0 & 0 & 1 & -1 \\ 0 & 0 & 0 & -1 \end{bmatrix} \qquad A_{22}=\begin{bmatrix} 1/y_{aw} & 0 & 0 & 0 & 0 & 0 \\ 0 & 1/y_{ae} & 0 & 0 & 0 & 0 \\ 0 & 0 & 1/y_{ei} & 0 & 0 & 0 \\ 0 & 0 & 0 & 1/y_{wi} & 0 & 0 \\ 0 & 0 & 0 & 0 & 1/y_{ai} & 0 \\ 0 & 0 & 0 & 0 & 0 & H_{t,h} \end{bmatrix}$$

The transfer function $H_{t,h}(s)$ can be obtained by

$$H_{t,h}=\frac{g_o+g_1Y_e+g_2Y_i+g_3Y_eY_i}{f_{a,o}+f_{a,1}Y_e+f_{a,2}Y_i+f_{a,3}Y_eY_i}$$

$$\begin{aligned}
f_{a,0} &= 37368\left(A_i^2y_i^2y_{\inf}+A_iA_{en}y_iy_oy_{\inf}+A_{win}A_i^2y_oy_i^3\right)+56052\left(A_{win}A_{en}A_iy_oy_i^2+A_{en}A_iy_{\inf}y_i^2\right)\\
&+A_{en}^2y_i^3y_{\inf}+18684\left(A_{en}^2y_i^2y_{\inf}+A_{win}A_{en}^2y_i^2y_o+A_i^2y_iy_oy_{\inf}+A_{en}^2y_iy_oy_{\inf}\right)+A_{en}^2y_i^2y_oy_{\inf}\\
&+2A_{en}A_iy_oy_i^2y_{\inf}+349091856\left(A_{win}A_i^2y_oy_i+A_{win}A_iy_oy_{\inf}+A_{win}A_{en}A_iy_oy_i+A_i^2y_{\inf}y_i+A_{en}A_iy_{\inf}y_i\right)\\
&+56052\left(A_{win}A_{en}A_iy_oy_i^2+A_{en}A_iy_{\inf}y_i^2\right)+2A_{win}A_{en}A_iy_oy_i^3+A_{win}A_{en}^2y_i^3y_o+A_i^2y_oy_i^2y_{\inf}\\
&+2A_{en}A_iy_i^3y_{\inf}+A_{win}A_i^3y_oy_i^3+A_i^2y_i^3y_{\inf}\\
f_{a,1} &= -349091856\left(A_{win}A_iy_{\inf}+A_{win}A_i^2y_i+A_{win}A_{en}A_iy_i-A_iA_{en}y_{\inf}-A_{en}A_i^2y_i-A_{en}^2A_iy_i\right)+A_{en}A_i^2y_i^3\\
&+18684\left(A_i^2y_{\inf}y_i+A_{en}^2y_{\inf}y_i+A_{en}^3y_i^2+A_{en}^3y_iy_o+A_{en}^2y_{\inf}y_o+A_{en}A_iy_{\inf}y_o+A_{en}y_i^2y_oy_{\inf}-A_{win}A_{en}^2y_i^2\right)\\
&+37368\left(A_{en}A_i^2y_i^2+A_{en}A_iy_iy_{\inf}+A_{en}^2A_iy_iy_o-A_{win}A_i^2y_i^2\right)-56052\left(A_{win}A_{en}A_iy_i^2-A_{en}^2A_iy_i^2\right)\\
&+2A_{en}^2A_iy_oy_i^2+2A_{en}^2A_iy_i^3+A_{en}A_i^2y_oy_i^2-2A_{win}A_{en}A_iy_i^3-A_{win}A_{en}^2y_i^3+A_{en}^3y_i^3-A_{win}A_i^2y_i^3\\
&+A_{en}^3y_oy_i^2+A_{en}^2y_i^2y_{\inf}+2A_iA_{en}y_iy_oy_{\inf}+2A_iA_{en}y_i^2y_{\inf}+A_i^2y_iy_oy_{\inf}+A_{en}^2y_iy_oy_{\inf}+A_i^2y_i^2y_{\inf}\\
f_{a,2} &= -A_i^2y_i^2y_{\inf}-A_i^3y_i^2y_o-A_{en}^2A_iy_i^3-18684\left(A_i^2y_oy_{\inf}+A_{en}^2A_iy_i^2+A_iA_{en}y_oy_{\inf}+A_iA_{en}^2y_oy_i+A_i^3y_oy_i\right)\\
&-56052A_{en}A_i^2y_i^2-349091856\left(A_{en}A_i^2y_i+A_i^3y_i+A_i^2y_{\inf}\right)-37368\left(A_i^3y_i^2+A_{en}A_iy_iy_{\inf}+A_i^2y_{\inf}y_i+A_i^2A_{en}y_iy_o\right)\\
&-A_i^3y_i^3-A_{en}^2y_i^2y_{\inf}-A_{en}^2A_iy_i^2y_o-2A_{en}A_i^2y_i^3-A_{win}A_i^2y_i^2y_o-A_{win}A_{en}^2y_i^2y_o-2A_{win}A_{en}A_iy_i^2y_o\\
&-2A_{en}A_iy_iy_{\inf}y_o-2_{en}A_iy_i^2y_{\inf}-A_i^2y_oy_iy_{\inf}-A_{en}^2y_oy_iy_{\inf}-2A_{en}A_i^2y_oy_i^2\\
f_{a,3} &= 18684\left(A_iA_{en}y_{\inf}+A_i^3y_i+A_i^2y_{\inf}+A_{en}^2A_iy_i\right)+37368\,A_i^2A_{en}y_i-A_{win}A_{en}^2y_i^2-2A_{win}A_{en}A_iy_i^2\\
&-A_{win}A_i^2y_i^2+3\left(A_{en}^2A_iy_oy_i+A_{en}^2A_iy_i^2+A_{en}A_i^2y_i^2+A_{en}A_i^2y_oy_i\right)+A_i^3y_i^2+A_{en}^2y_iy_{\inf}+A_{en}^3y_oy_i\\
&+A_{en}^3y_oy_{\inf}+A_{en}^3y_i^2+2A_iA_{en}y_oy_{\inf}+2A_iA_{en}y_iy_{\inf}+A_i^3y_oy_i+A_i^2y_oy_{\inf}+A_i^2y_iy_{\inf}\\
g_{a,0} &= y_i^3A_{en}^2+y_i^3A_i^2+y_oy_i^2A_i^2+y_oy_i^2A_{en}^2+37368\left(y_i^2A_i^2+y_oy_iA_iA_{en}\right)+2\left(y_oy_i^2A_iA_{en}+y_i^3A_{en}A_i\right)\\
&+349091856\left(y_iA_{en}A_i+y_oA_{win}A_i+y_iA_i^2\right)+18684\left(y_i^2A_{en}^2+y_oy_iA_i^2+y_oy_iA_{en}^2\right)+56052y_i^2A_{en}A_i\\
g_0 &= y_i^3A_{en}^2+y_i^3A_i^2+y_oy_i^2A_i^2+y_oy_i^2A_{en}^2+37368\left(y_i^2A_i^2+y_oy_iA_iA_{en}\right)+2\left(y_oy_i^2A_iA_{en}+y_i^3A_{en}A_i\right)\\
&+349091856\left(y_iA_{en}A_i+y_oA_{win}A_i+y_iA_i^2\right)+18684\left(y_i^2A_{en}^2+y_oy_iA_i^2+y_oy_iA_{en}^2\right)+56052y_i^2A_{en}A_i
\end{aligned}$$

$$g_1 = 2y_i^{\,2}A_{en}A_i + 37368y_iA_{en}A_i + y_i^{\,2}A_i^{\,2} + y_i^{\,2}A_{en}^{\,2} + 349091856\left(A_{en}A_i - A_{win}A_i\right) + 18684\left(y_iA_i^{\,2} + y_iA_{en}^{\,2} + y_oA_{en}^{\,2}\right)$$

$$g_2 = 349091856A_i^{\,2} + y_i^{\,2}A_{en}^{\,2} + 2y_i^{\,2}A_{en}A_i + y_i^{\,2}A_i^{\,2} + 18684\left(y_oA_i^{\,2} + y_oA_iA_{en}\right) + 2y_oy_iA_iA_{en} + 37368\left(y_iA_i^{\,2} + y_iA_iA_{en}\right) + y_oy_iA_i^{\,2} + y_oy_iA_{en}^{\,2}$$

$$g_3 = 2y_iA_{en}A_i + 18684\left(A_i^{\,2} + A_{en}A_i\right) + y_oA_i^{\,2} + y_iA_i^{\,2} + y_oA_{en}^{\,2} + y_iA_{en}^{\,2} + 2y_oA_{en}A_i$$

8.3 Method for calculation of specific symbolic room response factors

The designers are usually interested in some variables for the design of a specific building. Hence, only the design variables of interest need to be kept as symbols in the symbolic transfer function, while others are taken with the selected values. The generation of specific symbolic transfer functions is demonstrated by the following example, in which A_{win} and window parameters are kept as symbols.

The dimension of a specific room considered is 6.5m (width) × 6.0m (depth) × 3.2m (height). The internal wall consists of three layers. Their materials are gypsum (1.9 cm), concrete (25 cm) and gypsum (1.9 cm). The thermal parameters of these layers are shown in Table 8.1. The wall group 38 from ASHRAE Handbook (1997) was used as the external wall. The solar absorpance of the external wall is 0.75 (Chinese Building Standard GB 50176-93). Blinds is not used in the example. Other numeric parameters are: N_{inf} = 0, c_{air} = 1.007 kJ/(kg°C) and ρ_{air} = 1.186 kg/m^3.

Table 8.1. Thermal properties of the internal wall.

Material	Conductivity W/(m°C)	Density kg/m^3	Specific heat J/(kg°C)
Gypsum	0.727	1600	837
Concrete	0.138	304	837

y_o varies with outdoor wind velocity (DOE-2 Engineers Manual, 1982). To satisfy the pre-condition for the linear and time invariant superposition, averaged y_o over the periodic time length is used. DOE-2 Engineers Manual (1982) provides the formula for the calculation of convective thermal conductance based on wind velocity. Using this formula and the weather data of Hong Kong, we calculated y_o for 8760 hours and obtained the averaged y_o, which is 15.0 W/(m^2°C). y_i is 3.15 W/(m^2°C) when the indoor air velocity is zero.

Substituting the above numeric values into the symbolic transfer functions developed previously yields

$$H_{c,sd} = \frac{1}{Z_e}\frac{f_{s,0}+f_{s,1}A_{win}}{g_0+g_1A_{win}} + 0.8r_t(0)A_{win}\frac{f_{t,0}+f_{t,1}A_{win}}{g_0+g_1A_{win}} + 1.08r_{ab}(0)A_{win}\frac{f_{ab,0}}{g_0+g_1A_{win}} \qquad (8.39)$$

where

$$g_0 = 12351.9 + 0.50Y_e + 1.0Y_i + 0.00004Y_eY_i$$

$$g_1 = 46.08 - 0.00085Y_e$$

$$f_{s,0} = 192690 + 6.418Y_i$$

$$f_{s,1} = -9263.93 - 0.3Y_i$$

$$f_{t,0} = -12351.9 + 0.357Y_e - 0.054Y_i$$

$$f_{t,1} = -106.15 + 0.00052Y_e - 0.0026Y_i$$

$$f_{ab,0} = 4174.28 + 0.151Y_e + 0.139Y_i + 2.0 \cdot 10^{-6} Y_e Y_i$$

$$H_{t,h} = -\frac{g_0 + g_1 A_{win}}{f_{a,0} + f_{a,1} A_{win}} \tag{8.40}$$

where

$$f_{a,0} = -256919.7Y_e - 169468.1Y_i - 65.0Y_e Y_i + N_{\inf}\left(-1.84 \cdot 10^9 - 74608.3Y_e - 149027.37Y_i - 5.41Y_e Y_i\right)$$

$$f_{a,1} = -2.25 \cdot 10^8 + 4174.3Y_e - 3088.7Y_i + 0.057Y_e Y_i + N_{\inf}\left(-1.84 \cdot 10^9 + 149027.4Y_e\right)$$

$$g_0 = 12351.9 + 0.50Y_e + 1.0Y_i + 0.00004\,Y_e Y_i$$

$$g_1 = 46.08 - 0.00085Y_e$$

Using the Fourier transform method developed in Chapter 7, symbolic response factors can be used by Equation (7.30). If the symbolic variables only appear at the numerator of the transfer function, the resulting symbolic response factors will have the same structure as the transfer function as the numerical coefficients at each harmonic can be directly added up. However, if the symbolic variables appear at the denominator, the symbolic fractions will have different symbolic denominators at each harmonic. The reduction of these fractions to a common denominator will lead to tedious calculation. Some pre-treatments need to be done to remove the symbolic variables from the denominator.

In Equations (8.39) and (8.40), symbolic variable A_{win} and the Laplace transform variable s appear at the denominator of the transfer function. However, only A_{win} need to be considered. That is because, when generating Fourier

transfer function, s is replaced by the production of the imaginary operation and the frequency in rad/hr, which are both constants at each harmonic. The symbol A_{win} may be removed from the denominator by (Yang and Teng, 1992).

$$\frac{1}{g_0(s)+g_1(s)A_{win}} \cong \frac{1}{g_0(s)} - \frac{g_1(s)}{g_0(s)^2}A_{win} + \frac{g_1(s)^2}{g_0(s)^3}{A_{win}}^2 + \cdots (-1)^n \frac{g_1(s)^n}{g_0(s)^{n+1}}{A_{win}}^n \tag{8.41}$$

Using Equation (8.41), Equations (8.37) and (8.38) can be rewritten by

$$\begin{aligned} H_{c,sd} \cong{}& \frac{1}{Z_e(s)}\left(f_{s,0}(s)+f_{s,1}(s)A_{win}\right)\left[\frac{1}{g_0(s)} - \frac{g_1(s)}{g_0(s)^2}A_{win} + \frac{g_1(s)^2}{g_0(s)^3}{A_{win}}^2 + \cdots (-1)^n \frac{g_1(s)^n}{g_0(s)^{n+1}}{A_{win}}^n\right] \\ &+ 0.8r_t(0)A_{win}\left[f_{t,0}(s)+f_{t,1}(s)A_{win}\right]\left[\frac{1}{g_0(s)} - \frac{g_1(s)}{g_0(s)^2}A_{win} + \frac{g_1(s)^2}{g_0(s)^3}{A_{win}}^2 + \cdots (-1)^n \frac{g_1(s)^n}{g_0(s)^{n+1}}{A_{win}}^n\right] \\ &+ 1.08r_{ab}(0)A_{win}f_{ab,0}(s)\left[\frac{1}{g_0(s)} - \frac{g_1(s)}{g_0(s)^2}A_{win} + \frac{g_1(s)^2}{g_0(s)^3}{A_{win}}^2 + \cdots (-1)^n \frac{g_1(s)^n}{g_0(s)^{n+1}}{A_{win}}^n\right] \end{aligned} \tag{8.42}$$

$$H_{t,h} \cong -\left[g_0(s)+g_1(s)A_{win}\right]\left[\frac{1}{f_{a,0}(s)} - \frac{f_{a,1}(s)}{f_{a,0}(s)^2}A_{win} + \frac{f_{a,1}(s)^2}{f_{a,0}(s)^3}{A_{win}}^2 + \cdots (-1)^n \frac{f_{a,1}(s)^n}{f_{a,0}(s)^{n+1}}{A_{win}}^n\right] \tag{8.43}$$

Although the accuracy of Equations (8.42) and (8.43) increases with the order of n, it would be better to take n to be as small as possible for calculation efficiency. To determine the suitable value of n, we examined the accuracy of the numerical response factors under different wall types, A_{win} and n values. The wall groups 6, 26, 32 and 38 from ASHRAE Handbook (1997) are used as the external wall. They represent the walls with low, median and heavy weights. Three window areas are considered, which are 6.5 m^2, 13.0 m^2 and 19.5 m^2, corresponding to *WWR* values of 31%, 63% and 94%. Our calculation results show that Equations (8.42) and (8.43) converges rapidly. Very accurate

calculation results can be obtained when $n = 2$. If the wall group 38 is used as the external wall, with the window areas of 6.5 m^2, 13.0 m^2 and 19.5 m^2, the maximum relative errors are 0.036%, 0.14% and 0.4%; and the averaged relative errors are 0.008%, 0.03% and 0.08%. Similar results are found with the wall groups 6, 26 and 32 as the external wall. Therefore, $n = 2$ can be a suitable value for calculation.

8.4 Validation

8.4.1 Validation method

First, the formulas for the direct and efficient calculation of long-term cooling load are validated with traditional hourly simulation. The room model in Section 8.3 and wall group 38 were considered. And response factors of solar radiation incident on the window are used for calculation of long-term cooling load Q_{win}. Both continuous and intermittent operations are considered. Results show the two methods give exactly the same result, as shown in Figure 8.4. This guarantees that there is no error introduced in the derivation of the formulas, and the new model will not sacrifice accuracy for efficiency.

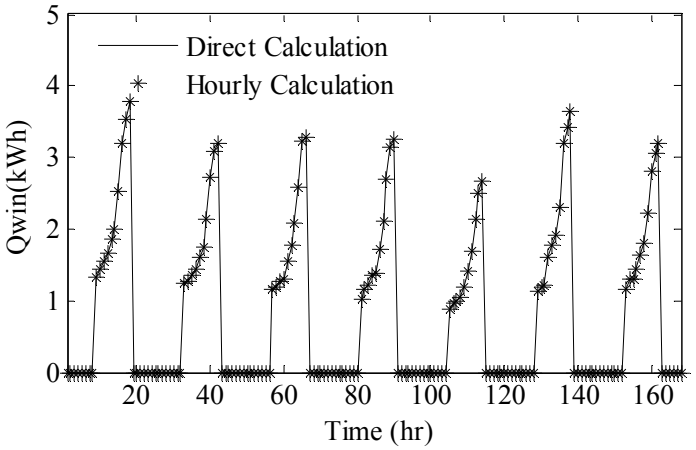

Figure 8.4 Direct calculation v.s. hourly calculation

Then, the new model is validated with DOE2, a widely used building energy simulation program. To minimize uncertainty due to errors caused by different influence parameters or sources, two approaches are used in the validation. First, all input parameters to the new model and DOE2 should be the same, thus the differences between the results are only caused by the calculation methods adopted by them. For example, the blinds system is excluded from the validation because it is treated differently in the new model and DOE2. The introduction of blinds will mix the errors due to the new thermal simulation model and the blinds simulation model. Second, calculation results due to different heat sources are validated separately. For example, to validate the cooling load due to the temperature difference between the indoor and outdoor air ($Q_{\Delta T}$), only the hourly outdoor air temperature are input to DOE2 while other heat sources are set to zero. Similar methods are used for the validation of other cooling loads, which include the cooling load due to the radiant heat gain from

lighting system ($Q_{l,rad}$) and the cooling load due to solar radiation. The validation only considers the radiant heat gain from lighting system. The convective heat gain can be directly added to the cooling load without time delay. Hence, this part of cooling load can be accurately calculated without validation. The cooling load due to solar radiation consists of two parts: the cooling load due to the solar radiation incident on the external wall (Q_{ew}) and the one due to the solar radiation incident on the window (Q_{win}).

The accuracy of the new model is quantified by mean bias error (MBE) and root mean square error (RMSE). MBE and RMSE are expressed by Equations (4.1) and (4.2).

8.4.2 Room model and operation conditions

The room model in Section 8.4.3 is used for the thermal simulation. It is assumed that the indoor air conditions in the adjacent rooms are completely identical to those in the room under consideration. Therefore, the internal wall is defined as 'adiabatic' in DOE2, which means that the internal wall can store heat but there is no heat transfer through it (DOE-2 Engineers Manual, 1982). The wall groups 6, 26 and 38 from ASHRAE Handbook (1997), which represent the walls with low, median and heavy weights, are used as the external wall. The clear glazing, which is widely used in Hong Kong, is selected as the window with absorpance $r_{ab}(0)$ = 0.18 and solar thermal transmittance $r_t(0)$ = 0.76

(ASHRAE Handbook, 2005). The installed power of the artificial lighting system is referred from the investigation results of Lam *et al*. (2004). They conducted a survey on electricity use in 20 air-conditioned office buildings in Hong Kong and their results provide average installed power of these buildings.

The adopted design parameters and operation conditions are listed below:

- Indoor air temperature set point: 24 °C;
- Installed power of the artificial lighting system: 20 W/m^2;
- Lighting special allowance factor (ASHRAE Handbook, 2005): 0.94;
- Convective ratio of the heat gain from lighting system (DOE-2 Engineers Manual, 1982): 0.33.

Both continuous and intermittent operation schedules are considered. In the continuous operation schedule, AC system is operated on all hours throughout the year. In the intermittent operation schedule, AC system is operated from 8:00 to 18:00 on all days in a year.

The weather data employed is a Typical Meteorological Year (TMY). Chan et al. (2003) published the values of weighted sum for each month of 25 years (1979-2003) in Hong Kong. Using these values, we found 12 typical meteorological months (TMM) from 1998 to 2003. The selected TMMs are listed in Table 8.2. The hourly weather data are obtained from HK observatory. HK

observatory only provides the beam and diffuse radiation data on horizontal plane. The method for the calculation of beam and diffuse radiation on the vertical wall is presented at Appendix C.

Table 8.2 Selected typical meteorological months.

January	1999	April	2001	July	2000	October	1998
February	2000	May	2000	August	2002	November	2002
March	2003	June	2003	September	2003	December	2001

8.4.3 Calculation and validation results

Under the continuous operation schedule, hourly cooling load profiles from July 1st to July 7th are presented in Figure 8.5 (NM means new model), and errors are summarized in Table 8.3. The results of the new model and DOE2 agree well with each other. The new model and DOE2 also predict the same hours at which maximum and minimum cooling loads occur. Simulation of solar cooling load is less accurate than other two cooling loads. However, most large errors occur at hours with low solar load, so will not has significant effect on annual total cooling load. If the hours with solar cooling load lower than 0.1 kWh are excluded, MBE and RMSE errors decrease to around -5% and 9.4%, respectively. The profiles of the new model are smoother than those of DOE2. The reason may be that DOE2 uses less z-transfer coefficients, which is more sensitive to the weather data on the past two hours.

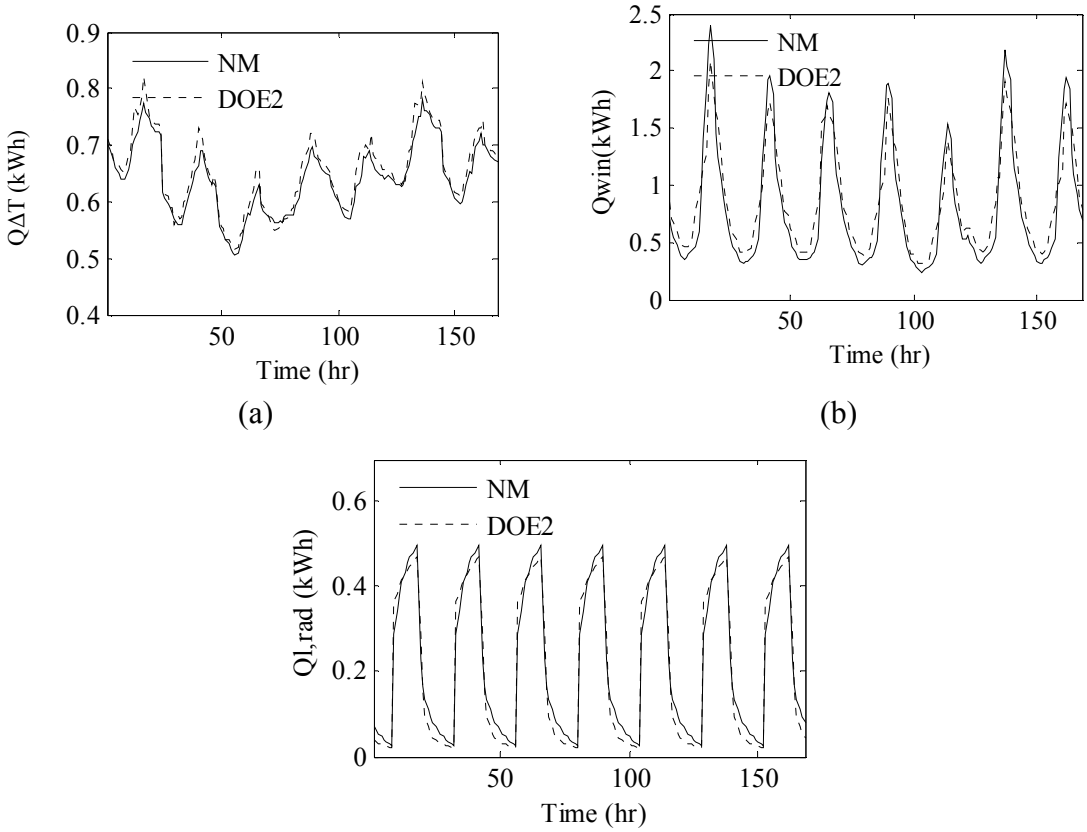

Figure 8.5 Hourly cooling load calculated by the new model and DOE2, continuous operation schedule

Table 8.3. Comparison results between DOE2 and the new model for hourly calculation, continuous operation schedule (%).

	Wall group 6		Wall group 26		Wall group 38	
	MBE	RMSE	MBE	RMSE	MBE	RMSE
$Q_{\Delta T}$	-0.76	5.93	-0.86	6.89	-0.87	7.54
Q_{win}	-1.11	4.61	-1.24	4.88	-1.21	5.14
$Q_{l,rad}$	-7.04	17.66	-7.45	17.93	-8.20	18.26

The calculation results of annual cooling load for west-facing window are shown in Figure 8.6. Using the results of DOE2 as references, the comparison results are listed in Table 8.3. It shows that the errors increase with the weight of

walls.

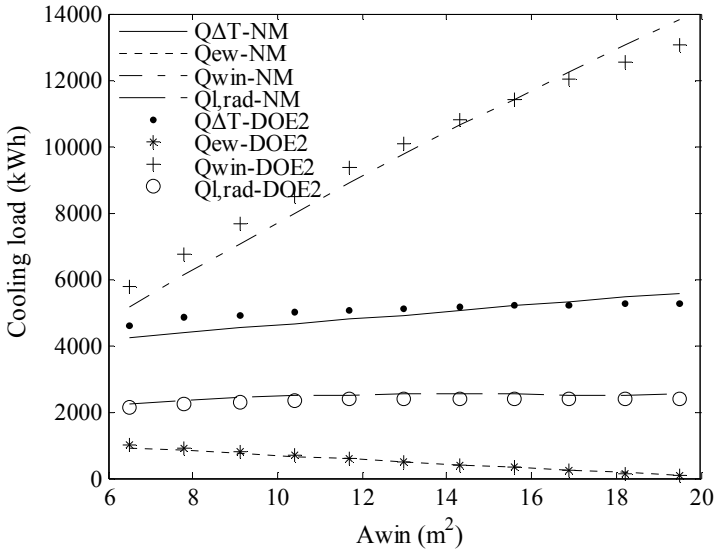

Figure 8.6. Total annual cooling loads computed by the new model and DOE2, continuous operation schedule

Table 8.4. Comparison results between DOE2 and the new model for annual simulation, continuous operation schedule (%).

	Wall group 6		Wall group 26		Wall group 38	
	MBE	RMSE	MBE	RMSE	MBE	RMSE
$Q_{\Delta T}$	-0.31	5.23	-0.39	5.44	-0.43	6.48
Q_{ew}	-1.55	4.40	-1.44	4.63	-1.81	5.55
Q_{win}	-0.33	4.41	-0.37	5.47	-0.49	6.22
$Q_{l,rad}$	-7.36	7.22	-7.9	7.99	-8.11	7.98
Total cooling load	-1.27	4.90	-1.54	5.44	-1.92	6.24

DOE2 uses 5 z-transfer coefficients for the calculation of cooling load (DOE-2 Engineers Manual, 1982). However, 5 z-transfer coefficients may be inadequate for rooms with very heavy walls. For example, we used the method described in Chapter 7 to calculate the z-transfer coefficients for the wall group 38. Calculation results show that at least 13 coefficients are needed for very accurate results. We also used the same method to generate only 5 coefficients, which must be more accurate than the 5 z-transfer coefficients used by DOE2,

due to the method used. Using the least square method described in Chapter 7, the results of simulation using 5 z-transfer coefficients given by both the least square method and DOE2 show that the error produced by DOE2 could be as large as 15.22%. Fewer coefficients are needed for walls with less weight. The wall group 6 needs only 7 coefficients, which is still more than the number adopted by DOE2. Therefore, the insufficiency of z-transfer coefficients should be one of the major sources for discrepancies between the calculation results of DOE2 and the new model.

Hourly cooling load profiles in the intermittent operation from July 1st to July 7th are presented in Figure 8.7, and errors are summarized in Table 8.6. We can see that the two methods have very similar dynamic responses to different heat sources.

The comparison between the annual cooling loads calculated by the new model and DOE2 are shown in Figure 8.8. The differences of hourly and annual cooling loads given by the new model and DOE2 are listed in Table 8.5 and 8.6, respectively. Compared with the cases continuous operation schedule, small errors can be obtained.

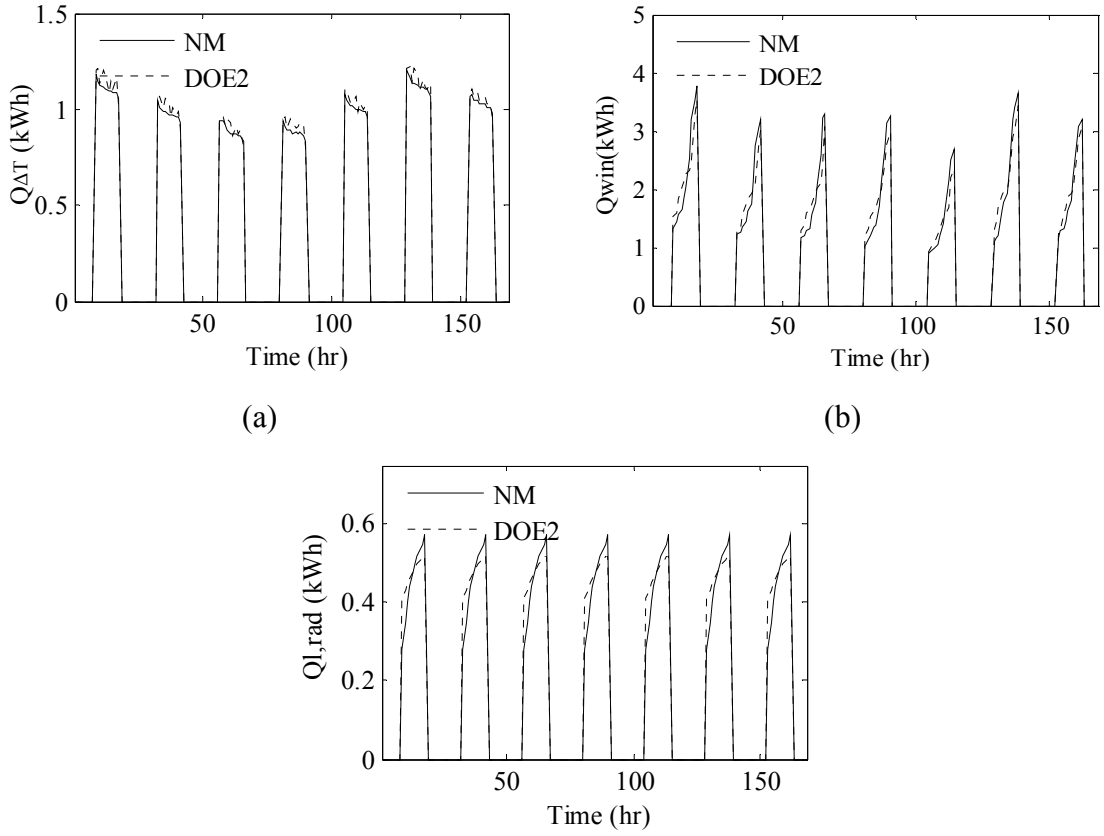

Figure 8.7 Hourly cooling load calculated by the new model and DOE2, intermittent operation schedule.

Table 8.5 Comparison results between DOE2 and the new model for hourly simulation, intermittent operation schedule (%).

	Wall group 6		Wall group 26		Wall group 38	
	MBE	RMSE	MBE	RMSE	MBE	RMSE
$Q_{\Delta T}$	-5.09	6.75	-5.31	6.94	-5.69	7.32
Q_{win}	-8.5	9.69	-9.0	9.88	-9.2	10.33
$Q_{l,rad}$	-4.85	9.84	-4.97	7.29	-5.54	7.83

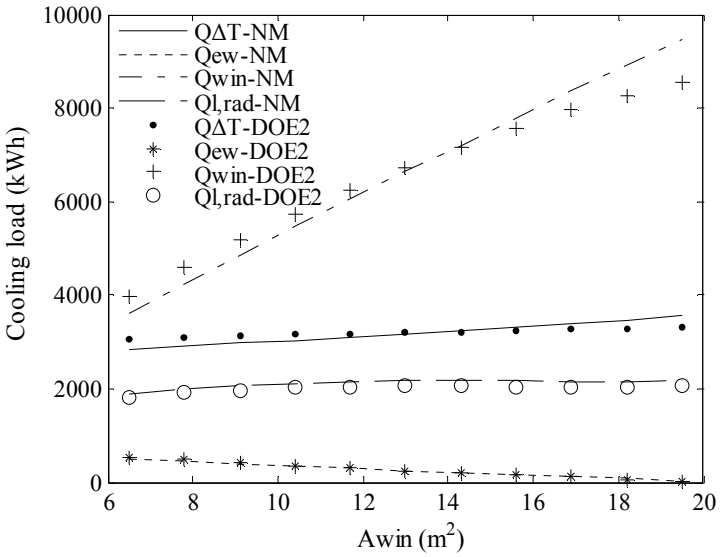

Figure 8.8 Total annual cooling loads computed by the new model and DOE2, intermittent operation schedule

Table 8.6 Comparison results between DOE2 and the new model for annual simulation, intermittent operation schedule (%).

	Wall group 6		Wall group 26		Wall group 38	
	MBE	RMSE	MBE	RMSE	MBE	RMSE
$Q_{\Delta T}$	2.62	3.11	3.88	3.97	4.84	5.31
Q_{ew}	-1.35	1.66	-1.74	2.25	-1.91	2.79
Q_{win}	-4.13	4.07	-5.64	4.31	-1.77	5.43
$Q_{l,rad}$	-4.33	8.27	-4.55	9.08	-5.26	8.98
Total cooling load	-1.34	2.09	-1.58	3.02	-2.27	3.89

8.5 Summary

This chapter develops a method for the direct evaluation of dynamic long-term cooling load without the need for hourly thermal simulation. The method is primarily based on the principle of superposition and symbolic transfer function. The principle of the method has been presented by the development of equations for continuous and intermittent operation schedules. Combined with

the thermal network analysis and the Fourier transform method developed in Chapter 7, the new method can also generate symbolic long-term cooling load, which are shown by examples. The generated symbolic cooling load consists of important design variables and can be very useful in optimal design.

The thermal simulation method was validated with DOE2, a widely used energy simulation program. The validation includes the comparison of long-term cooling loads and dynamic hourly responses to different heat sources. Both continuous and intermittent operation schedules are considered in the validation. Simulation results given by the new method agrees well with those simulated by DOE2. The discrepancies between the new method and DOE2 increase with the weight of the external wall. This may be partially attributed to the insufficiency of z-transfer coefficients used by DOE2, and partially due to the simplified room model used by the new method.

CHAPTER 9

APPLICATION EXAMPLE OF OPTIMAL DESIGN OF BUILDING FOR BOTH DAYLIGHTING AND COOLING

In the process of low-energy building design, the conceptual design stage is of great importance. Typically, decisions made in the conceptual stage may determine 80% of the energy consumption of a building (Deiman and Platt, 1993; Miles et al., 2001). Therefore, special attention needs to be paid to the conceptual design.

Simplification of data input and calculation efficiency are two equally important aspects. For the first one, all inputs may be divided into two groups based on their importance. Only the more important inputs need to be considered in the optimization, while the less important ones may be given default values based on past experiences. To enhance calculation efficiency, new models have been developed and validated for daylighting and thermal simulations in Chapters 5, 6 and 8. These models are of high accuracy and efficiency, and are very suitable for the conceptual design of a building. In this chapter, both models are adopted for the optimal design and sensitivity analysis of an example building. The optimization of building envelop is aimed at reducing the annual energy consumption E_{en}.

An office building in Hong Kong is used in the example. Both the numeration and hill-climbing methods are used in the optimization. The sensitivity analysis shows that building orientation, window to wall ratio (*WWR*), and the optical and solar thermal transmittances of windows are more influential than other parameters. Designers should pay more attention to these parameters in the optimal design.

In many previous sensitivity analyses, the sensitivity of outputs to each input parameter was evaluated by the mean influence of design parameters over their ranges. However, the application example shows that many design parameters have variable influence on E_{en}. Such design parameters include *WWR*, building orientation, optical transmittance of window, and the reflectance at the internal surface of the window. Only using the mean influence of these design parameters may lead to inaccurate or even misleading information. The sensitivity of E_{en} to these design parameters should be evaluated based on the influence over their whole ranges.

9.1 Optimization model

9.1.1 Objective function

E_{en} should include both operation and embodied energy. The operation energy consists of the lighting energy conversation E_l due to the utilization of daylighting and the cooling load related with building envelope. The cooling load

can be further divided into four components:

- Cooling load due to the temperature difference between the indoor and outdoor air ($Q_{\Delta T}$);
- Cooling load due to the solar radiation incident on the external wall (Q_{ew});
- Cooling load due to the solar radiation incident on the window system (Q_{win});
- Reduction of cooling load from artificial lighting system due to the utilization of daylighting. As the convective heat gain can be directly added to the cooling load, only the cooling load due to the radiant heat gain from lighting system need to be calculated by the thermal simulation model described in Chapter 8.

Cooling loads, electrical lighting energy and embodied energy should not be simply summed up. This is because cooling loads are not real energy consumption and the quality of electrical energy is different from that of thermal energy. Energy use in removing all cooling loads depends on the energy efficiency of the air-conditioning system. Embodied energy should be converted to electrical energy by the energy efficiency of the power plant. Therefore, the objective function may be expressed by:

$$\begin{aligned} &Min\, E_{en}(\alpha, \tau_t, T_v, \rho_i, WWR, \gamma_{bd}) = \eta_{ac}\left(Q_{\Delta T} + Q_{ew} + Q_{win} - Q_{l,rad} - Q_{l,\mathrm{cov}}\right) \\ &- E_l + \eta_p E_e \end{aligned} \tag{9.1}$$

where E_e is the embodied energy; η_{ac} and η_p are the energy efficiencies of the air-conditioning system and power plants. Their values in our study are 0.33 and

0.4, respectively. α and τ_t are the solar absorpance and solar thermal transmittance of window; T_v is the optical transmittance of window; ρ_i is the optical reflectance at the internal surface of the window; γ_{bd} is the building orientation; $Q_{l,rad}$ and $Q_{l,cov}$ are the cooling load due to radiant and convective heat gain from lighting system, respectively; E_l is the lighting energy saving from daylighting, which may be calculated by

$$E_l = N_{hr} \cdot IP \cdot A_{floor} P_l \tag{9.2}$$

where N_{hr} is the number of occupied hours in a year; IP is the installed power of the artificial lighting system used for the required illuminance intensity (W/m^2); A_{floor} is the total floor area (m^2); P_l is the reduction ratio of artificial lighting energy consumption due to daylighting utilization. It can be determined by the daylighting model developed in Chapters 5 and 6.

$Q_{l,cov}$ and $Q_{l,rad}$ may be calculated by

$$Q_{l,\mathrm{cov}} = r_c F_{sa} E_l$$

$$Q_{l,rad} = (1 - r_c) F_{sa} E_l$$

where r_c is the ratio of the convective heat gain from lighting system; F_{sa} is the special allowance factor, which represents the ratio of the heat gain that goes to the conditioned space (ASHRAE Handbook, 2005). The values of F_{sa} for different lighting systems may be found from ASHRAE Handbook (2005).

Intermittent operation schedule is used in our calculation. In this schedule,

AC system is operated on between 9:00 to 19:00 on weekdays. Using the thermal simulation model described in Chapter 8, the cooling loads due to different heat sources may be calculated by

$$Q_c = Q_{c,h} + Q_{c,1} + Q_{c,2} + Q_{c,3} + Q_{c,4} \tag{9.3}$$

The meanings of $Q_{c,h}$, $Q_{c,1}$ and $Q_{c,2}$ have been described in Chapter 8. $Q_{c,3}$ is the cooling load due to the impact of no cooling service during 9:00 to 19:00 on weekends, and the indoor air temperature is kept constant during occupied hours. $Q_{c,4}$ is the additional cooling load caused by indoor air temperature increases due to the imaginarily supplied convective heat during all unoccupied hours. $Q_{c,3}$ and $Q_{c,4}$ can be calculated by Equations (9.4) and (9.5), which are derived by the same principle applied to $Q_{c,1}$ and $Q_{c,2}$, respectively.

$$\begin{aligned} Q_{c,3} = \sum_{l_{p2}=0}^{167} SUM_{p,3}(n_2 - 23 - l'_{p2}) Y_{c,a}(0) \Bigg\{ + \sum_{i'_1=0}^{\infty} \sum_{i'=0}^{n_2-n_1} Y_{pm2,ca}(168'_1 - n_2 + i' - 1) \Bigg[\sum_{k'=0}^{n_2-n_1-i'} Y_{a,c}(k') Y_p(l'_{p2} - k' - i') \\ + \sum_{k'=0}^{n_2-n_1} Y_{p,ac}(k' - i') Y_p(l'_{p2} - k') \sum_{k'=0}^{n_2-n_1} Y_{p,ac}(k' - i') Y_p(l'_{p2} - k' - 24) + \sum_{k'=0}^{n_2-n_1} Y_{p,ac}(k' - i' + 24 \cdot 6) Y_p(l'_{p2} - k') \Bigg] \Bigg\} \end{aligned} \tag{9.4}$$

$$
\begin{aligned}
Q_{c,4} = \sum_{l_{p3}=0}^{167} SUM_{p,4}\left(n_1 - 23 - l'_{p3}\right)\Bigg\{ & + \sum_{i'_1=0}^{\infty}\sum_{i'=0}^{n_2-n_1} Y_{pm2,ca}\left(168i'_1 - n_2 + i' - 1\right) \\
& \cdot \sum_{k'=0}^{n_2-n_1-i'} Y_{a,c}\left(k'\right)\Bigg[\sum_{i=1}^{24+n_1-n_2} Y_{pm2,ac}\left(n_2 - n_1 + i - i' - k'\right)Y_p\left(l'_{p3} - i\right) \\
& + \sum_{i=1}^{24+n_1-n_2} Y_{pm3,ca}\left(n_2 - n_1 + i - i' - k'\right)\sum_{k=0}^{24+n_1-n_2-i} Y_{a,c}\left(k\right)Y_p\left(l'_{p3} - k - i\right) \\
& + \sum_{i=1}^{24+n_1-n_2} Y_{pm3,ca}\left(n_2 - n_1 + i - i' - k'\right)\sum_{k=0}^{24+n_1-n_2} Y_{p,ac}\left(k - i + 24\right)Y_p\left(l'_{p3} - k - 24\right)\Bigg] \\
& + \sum_{i'_1=0}^{\infty}\sum_{i'=0}^{n_2-n_1} Y_{pm2,ca}\left(168i'_1 - n_2 + i' - 1\right)\sum_{k'=0}^{n_2-n_1} Y_{p,ac}\left(k' - i'\right)\Bigg[\sum_{i=1}^{24+n_1-n_2} Y_{pm2,ac}\left(n_2 - n_1 + i - i' - k'\right)Y_p\left(l'_{p3} - i\right) \\
& + \sum_{i=1}^{24+n_1-n_2} Y_{pm3,ca}\left(n_2 - n_1 + i - i' - k'\right)\sum_{k=0}^{24+n_1-n_2-i} Y_{a,c}\left(k\right)Y_p\left(l'_{p3} - k - i\right) \\
& + \sum_{i=1}^{24+n_1-n_2} Y_{pm3,ca}\left(n_2 - n_1 + i - i' - k'\right)\sum_{k=0}^{24+n_1-n_2} Y_{p,ac}\left(k - i + 24\right)Y_p\left(l'_{p3} - k - 24\right)\Bigg] \\
& + \sum_{i'_1=0}^{\infty}\sum_{i'=0}^{n_2-n_1} Y_{pm2,ca}\left(168i'_1 - n_2 + i' - 1\right)\sum_{k'=0}^{n_2-n_1} Y_{p,ac}\left(k' - i' + 24\cdot 6\right)\Bigg[\sum_{i=1}^{24+n_1-n_2} Y_{pm2,ac}\left(n_2 - n_1 + i - i' - k'\right)Y_p\left(l'_{p3} - i\right) \\
& + \sum_{i=1}^{24+n_1-n_2} Y_{pm3,ca}\left(n_2 - n_1 + i - i' - k'\right)\sum_{k=0}^{24+n_1-n_2-i} Y_{a,c}\left(k\right)Y_p\left(l'_{p3} - k - i\right) \\
& + \sum_{i=1}^{24+n_1-n_2} Y_{pm3,ca}\left(n_2 - n_1 + i - i' - k'\right)\sum_{k=0}^{24+n_1-n_2} Y_{p,ac}\left(k - i + 24\right)Y_p\left(l'_{p3} - k - 24\right)\Bigg] \\
& + \sum_{i'_1=0}^{\infty}\sum_{i'=0}^{n_2-n_1} Y_{pm2,ca}\left(168i'_1 - n_2 + i' - 1\right)\sum_{k'=0}^{n_2-n_1} Y_p\left(l'_{p2} - k' - 24\right)\Bigg[\sum_{i=1}^{24+n_1-n_2} Y_{pm2,ac}\left(n_2 - n_1 + i - i' - k'\right)Y_p\left(l'_{p3} - i - 24\right) \\
& + \sum_{i=1}^{24+n_1-n_2} Y_{pm3,ca}\left(n_2 - n_1 + i - i' - k'\right)\sum_{k=0}^{24+n_1-n_2-i} Y_{a,c}\left(k\right)Y_p\left(l'_{p3} - k - i - 24\right) \\
& + \sum_{i=1}^{24+n_1-n_2} Y_{pm3,ca}\left(n_2 - n_1 + i - i' - k'\right)\sum_{k=0}^{24+n_1-n_2} Y_{p,ac}\left(k - i + 24\right)Y_p\left(l'_{p3} - k - 48\right)\Bigg]\Bigg\}
\end{aligned}
\tag{9.5}
$$

In Equations (9.4) and (9.5), Y represents the response factor of a heat source; $Y_{c,a}$ is the response factor for calculation of cooling load due to indoor air temperature; and $Y_{a,c}$ is the response factor for calculation of indoor air temperature due to convective heat gain. Other response factors in Equations (9.4) and (9.5) are summations of some Y; $SUM_{p,3}$ and $SUM_{p,4}$ are the summations of some hourly heat gains. They can be calculated by

$$
Y_p\left(j\right) = \sum_{j_1=0}^{\infty} Y\left(168\,j_1 + j\right) \qquad\qquad j = 0, 1, 2, \ldots, 167
$$

$$Y_{pm,ca}(i) = \sum_{w_3=0}^{6}\sum_{i_1=0}^{\infty}\sum_{m=n_1+1}^{n_2} Y_{c,a}(168i_1 + 24w_3 + m + i) \qquad i = 0, 1, 2, \ldots, 167$$

$$Y_{pm,ac}(i) = \sum_{w_3=0}^{6}\sum_{i_1=0}^{\infty}\sum_{m=n_1+1}^{n_2} Y_{a,c}(168i_1 + 24w_3 + m + i) \qquad i = 0, 1, 2, \ldots, 167$$

$$Y_{p,ac}(i) = \sum_{i=0}^{\infty} Y_{a,c}(i) = \sum_{i_1=0}^{\infty}\sum_{w_3=0}^{6} Y_{a,c}(168i_1 + 24w_3 + i) \qquad i = 0, 1, 2, \ldots, 167$$

$$Y_{pm2,ca}(i) = \sum_{i_e=0}^{1}\sum_{m'_1=1}^{5}\sum_{m'=n_1+1}^{n_2} Y_{c,a}(24m'_1 + 24i_e + m' + i) \qquad i = 0, 1, 2, \ldots, 167$$

$$Y_{pm3,ca}(i) = \sum_{i_e=0}^{1}\sum_{w_3=0}^{6}\sum_{i_1=0}^{\infty} Y_{c,a}(168i_1 + 24i_e + 24w_3 + i) \qquad i = 0, 1, 2, \ldots, 167$$

$$SUM_{p,3}(j) = \sum_{i_e=0}^{1}\sum_{i=0}^{51} S(168i - 24i_e + j) \qquad j = 0, 1, 2, \ldots, 167$$

$$SUM_{p,4}(j) = \sum_{i_e=0}^{1}\sum_{w_3=0}^{6}\sum_{i=0}^{51} S(168i - 24i_e - 24w_3 + j) \qquad j = 0, 1, 2, \ldots, 167$$

where S means a heat source.

l'_{p2} depends on n_2-23-l_{p2} and is computed by

$$l'_{p2} = \begin{cases} l_{p2} & n_2 - 23 - l_{p2} \geq 0 \\ l_{p2} - 168 & n_2 - 23 - l_{p2} < 0 \end{cases}$$

l'_{p3} depends on n_1-23-l_p and is computed by

$$l'_{p3} = \begin{cases} l_{p3} & n_1 - 23 - l_{p3} \geq 0 \\ l_{p3} - 168 & n_1 - 23 - l_{p3} < 0 \end{cases}$$

A great amount of embodied energy is used for buildings, and should not be ignored. The embodied energy for the building envelope may be calculated by:

$$E_e = A_{win} E_{e,win} + (A_{en} - A_{win}) E_{e,ew} \qquad (9.9)$$

where A_{win} and A_{en} are the area of the window and the envelope (m^2), which

include both the window and the external wall; $E_{e,win}$ and $E_{e,ew}$ are the embodied energy for unit area of window and the external wall (kWh/m^2), respectively.

The embodied energy may be classified into three primary categories: energy used in manufacturing (E_m), transporting (E_t) and processing (E_p) the building materials and components. Since all the other terms in equation (9.1) represent operation energy on the basis of annual energy use, the total embodied energy use should also be distributed to each year in the life span of buildings. Hence, thermal embodied energy use E_e may be expressed by

$$E_e = \left(E_m + E_t + E_p\right) / n_{life} \tag{9.6}$$

where n_{life} is the number of years for the average life span of the building. The lifespan of buildings is assumed to be 80 years in this study.

The detailed method for estimating these three energy uses have been given by Chen *et al*. (2001), and will not be tediously repeated here.

9.1.2 Building model

An office building considered in the optimization has two opposite orientations, and each orientation consists of 10 identical rooms, as shown in Figure 9.1. The rooms have the same parameters as the room model used for the validation of the thermal simulation model in Chapter 8. Hence, they will not be tediously described here. Wall group 38 from Spitler and Fisher (1999) is

selected as exterior wall. Information for calculation of embodied energy is shown in Table 9.1 (Chen et al, 2001). The life span of the building is assumed to be 50 years.

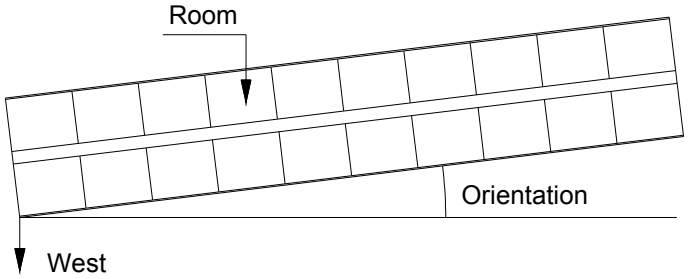

Figure 9.1 Plan of the office building used in the optimization

Table 9.1 Information for calculation of embodied energy.

	et (MJ/kg)	λ	μ	ρ (kg/m3)
Aluminum	191	0.025	1.3	2700
Glass	16.3	0	1.3	2600
Concrete	2.0	0.025	1.0	2243
Vinyl	6.1	0.025	1.0	920

In the above table, *et* is energy required for manufacturing the building materials; λ is a factor for waste of the materials; μ is a replacement factor for building elements.

Previous common practice using one reference point in daylighting simulations may result in the largely overestimated or under-estimated energy performance (Tian, *et al*., 2010). This may mislead the energy analysis and thermal design of buildings. Therefore, the working space is evenly divided into three zones; each zone is served by a row of electrical lights simultaneously controlled. Three reference points, located at the center of each zone respectively

as shown in Figure 9.2, are used for illuminance control. All three reference points are placed at the height of 0.8m above the floor. The artificial lighting will be supplemented whenever the daylighting illuminance at the reference point is lower than the design illuminance, which is 500 Lux. Continuous dimming control have been widely used for artificial lighting control. Hence, it is considered in the simulation. The dimming ballasts can be dimmed from 100% light output with 100% power input to 0% light output with 10% power input (Choi *et al*., 2005).

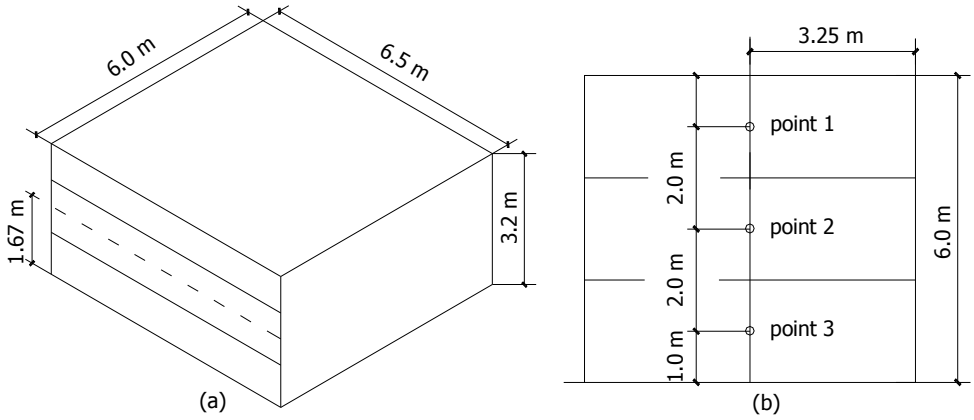

Figure 9.2 Schematic plan of the room of the office building,
(a) Room model, (b) floor plan.

When the beam light is incident on the window, the venetian blinds are used to prevent beam light from entering the building to avoid glare and high contrast (Athienitis and Tzempelikos, 2002). The tilt angle of the blinds is adjusted based on the solar position. The method for calculating the tilt angle is presented at Appendix D. At hours without beam light, the blinds will be retracted to let more daylight enter the building to reduce artificial lighting.

9.1.3 Variables and constraints

Variables considered in the optimization include window type, building orientation and window-to-wall ratio (*WWR*). As the office building has two identical opposite facades, only the building orientation ranging from 0° to 180° need to be considered. As shown in Figure 9.1, building orientation = 0°, 90° and 180° represents the buildings facing west (and east), south (and north) and east (and west), respectively. The interval of building orientation is 10°. *WWR* ranges from 0.0 to 1.0, with an interval of 0.05. Referring to results from our previous survey on windows currently used in Hong Kong, 12 types of windows are considered in the optimization. These windows include those commonly used as well as some windows not widely used in Hong Kong. Table 9.2 lists the parameters of these windows. These data was obtained from WINDOW 5.2a, a computer program recommended by National Fenestration Rating Council, an organization in the US that administers the rating and labeling system for the energy performance of windows, doors, skylights, and attachment product (http://www.nfrc.orh/).

Table 9.2 Windows used in the optimization.

Window types	Frame	Glass Thickness (mm)	α	τ_t	T_v	ρ_i
Optifloat Clear (Clear8)	Aluminum	8.0	0.06	0.67	0.78	0.08
Optifloat Clear (ClearV8)	Vinyl	8.0	0.05	0.67	0.78	0.08
Optifloat Clear (Clear15.6)	Aluminum	15.6	0.16	0.48	0.73	0.07
Optifloat Clear (ClearV15.6)	Vinyl	15.6	0.14	0.48	0.73	0.07
Optical Bronze (Bronze8)	Aluminum	8.0	0.13	0.37	0.40	0.05
Optical Bronze (Bronze12.5)	Aluminum	12.5	0.13	0.24	0.26	0.05
Blue-Green (BG)	Aluminum	5.9	0.28	0.30	0.68	0.07
Advantage Evergreen (AE)	Aluminum	5.9	0.14	0.28	0.43	0.08
Energy Advantage Low-E (EAL)	Aluminum	5.6	0.14	0.56	0.74	0.11
Reflective Low-E on Clear (RL)	Aluminum	5.7	0.10	0.27	0.53	0.28
Reflective Low-E on Clear (RLV)	Vinyl	5.7	0.08	0.27	0.53	0.29
Blue Low-E on Clear (BL)	Aluminum	5.7	0.12	0.24	0.38	0.17

9.2 Weather data

The weather data employed is a Typical Meteorological Year (TMY), which has been described in Chapter 8. The daylighting simulation model needs hourly outdoor illuminances as inputs. According to the hourly outdoor radiations from Hong Kong observatory, we calculated the hourly outdoor illuminances by using the Chung's luminous efficacy model (1992), which is developed based on the weather data of Hong Kong. The hourly solar positions were calculated by the model described at ASHRAE Handbook (2005).

9.3 Optimization and calculation results

Two assumptions are made in the optimization. First, rooms at the corner of the building, which have two external walls, have no significant effect on the whole building. Second, all floors are completely identical. The heat transfer through the building roof and the ground floor is ignored.

Both numeration and hill-climbing methods are used in the optimization. The numeration method is used for the optimization of the windows. For each window, the hill-climbing method is used to find the optimal combination of building orientation and *WWR*. The hill-climbing method is a local-search algorithm. It starts with an arbitrary original solution, and attempts to find a better solution by incrementally changing a single variable of the solution. If the change produces a better solution, the change is made to the new solution. The process repeats until no further improvements can be found. The hill-climbing method is not good for objective functions that have both global and local optimal values as it often fails to locate the global optimal solution by sticking to a local optimal one (Rich and Knight, 1991). Our pre-examination of the objective function shows that, for all window types, there is only one global optimal solution over the whole range, as shown in Figure 9.3. Therefore, the hill-climbing method can be safely used without the problem of local optimal solution.

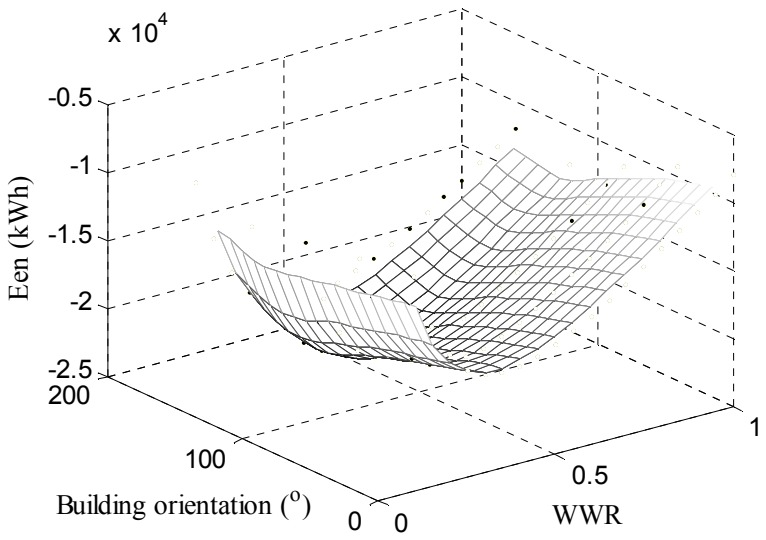

Figure 9.3 E_{en} under different *WWRs* and building orientations, RLV.

For all windows, the hill climbing method starts at the arbitrary original solution with *WWR* = 0.5 and building orientation = 90º. At the arbitrary original solution, there are 4 possible paths to be considered, as shown in Figure 9.3. At the first step, the hill climbing method compares the values of E_{en} at the original solution and the 4 neighborhood solutions. If more than one neighborhood solutions can produce lower E_{en} than the original solution, the one with the least energy consumption will be selected as the solution for the next step. The following steps are similar except that only 3 neighborhood solutions need to be calculated because the path that the current solution comes from need not to be reconsidered.

For each window, there are 18 building orientations × 21 *WWRs* = 378 design alternatives. The utilization of hill-climbing method greatly reduces the

number of design alternatives to be calculated. For these two windows, only 22 and 31 design alternatives need to be calculated, which account for 5.8% and 8.2% of the total design alternatives.

Optimization results show that the minimum and maximum E_{en} can be obtained under the following combinations of design variables.

Table 9.3 Combinations of design variables that yield minimum and maximum E_{en}.

	Minimum E_{en}	Maximum E_{en}
Window type	RLV	Bronze15.6
WWR	0.35	1.0
Building orientation	120°	20°

Figure 9.4 shows how the key influence design parameter *WWR* impacts E_{en}. Two types of window are included. One window is Clear8, which is widely used in practice; and the other is RLV, which is the optimal window from Table 9.3. The building orientation is 120°, which is also the optimal orientation. For both windows, there is an optimal *WWR* where most energy can be saved. The energy savings increase with *WWR* from 0 to the optimal *WWR* and then decrease with further increase of *WWR*. The optimal *WWRs* of Clear8 and RLV are 0.2 and 0.35, respectively. With Clear8, the building envelope becomes energy consumer when *WWR* is greater than 0.6. The building envelope with RLV can always save energy with any *WWR* value from 0.0 to 1.0.

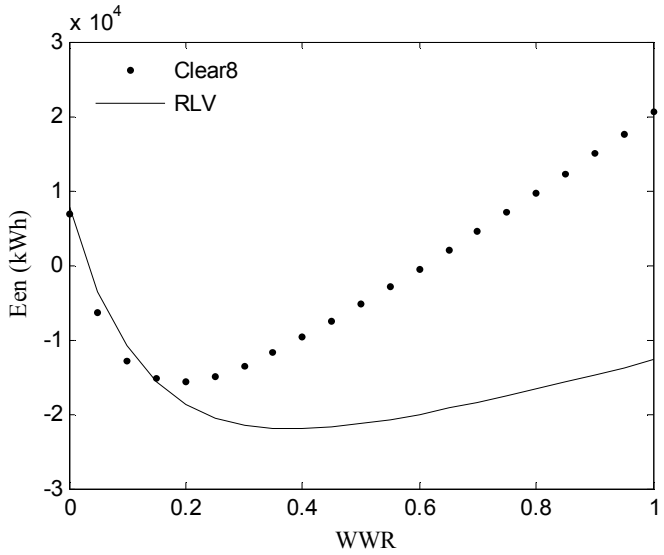

Figure 9.4 Annual energy consumption related with building envelope vs. *WWR*.

For all windows, the minimum and maximum E_{en} occur at the building orientations of 120º and 20º, respectively. Two examples are shown in Figure 9.5, in which the optimal *WWR*s of Clear8 and RLV are used. Table 9.3 summarizes the energy savings of all windows at their optimal *WWRs*. Examination of Table 9.4 indicates that the window type is also a high influence factor. The energy saving of RLV can be 40% larger than that of Clear8 at the optimal building orientation of 120º.

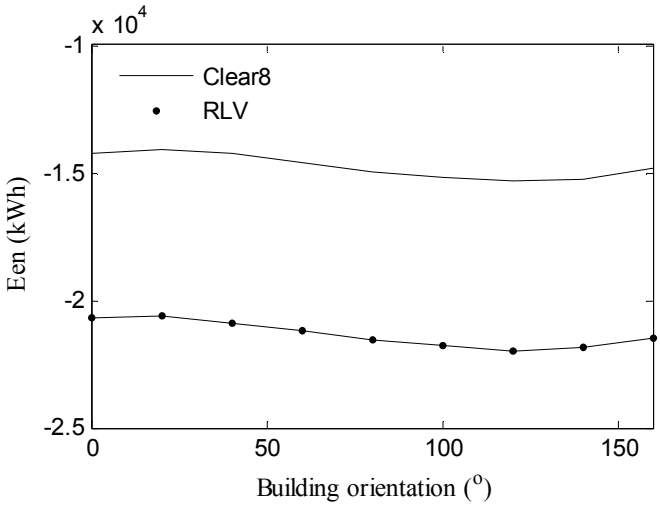

Figure 9.5 Annual energy consumption related with building envelope vs. building orientation.

Table 9.4 Energy savings at the optimal *WWR*.

Window type	20°		120°	
	Optimal *WWR*	Energy saving (kWh)	Optimal *WWR*	Energy saving (kWh)
Clear8	0.20	13281	0.20	14953
ClearV8	0.20	13290	0.20	14573
Clear15.6	0.25	16397	0.20	17793
ClearV15.6	0.25	16416	0.20	17812
Bronze8	0.40	13746	0.35	15285
Bronze12.5	0.65	14810	0.50	16378
BG	0.35	17556	0.30	18306
AE	0.50	17622	0.40	18933
EAL	0.25	14915	0.20	16340
RL	0.40	19570	0.35	20852
RLV	0.40	19722	0.35	20890
BL	0.50	18278	0.45	19541

Figure 9.6 shows a breakdown of the energy uses and savings from the window RLV. We can see that $Q_{c,win}$, E_e, and the energy saving from daylighting (including the savings from both lighting and cooling energy) account for most of the total energy consumption related with the building envelope.

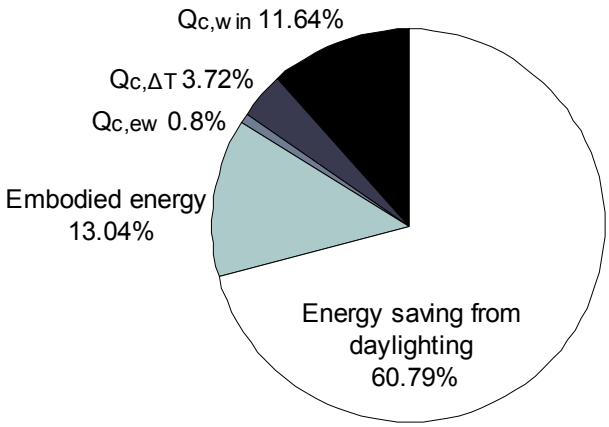

Figure 9.6 Breakdown of the energy uses of the envelope with window RLV, *WWR* = 0.4, building orientation = 120°.

9.4 Sensitivity analysis

The optimal solution obtained from Section 9.3 is used as the reference case. The sensitivity of E_{en} to different design variables is evaluated based on the variation of one design variable from the reference value, while all other design variables are held at the constant reference values. The sensitivity of E_{en} is evaluated by the influence coefficient *IC*, which is determined by the finite-difference approximation method (Saltelli *et al*., 2000):

$$IC = \frac{\partial E_{en}}{\partial v_j} \approx \frac{E_{en}\left(v_j + \Delta v\right) - E_{en}\left(v_j\right)}{\Delta v} \tag{9.7}$$

where *v* represents a design variable.

9.4.1 Sensitivity analysis of building orientation

The *IC* of building orientation is not uniformly distributed, as shown in Figure 9.7. It ranges from -292.6 to 200.7 with the averaged value of -142.6.

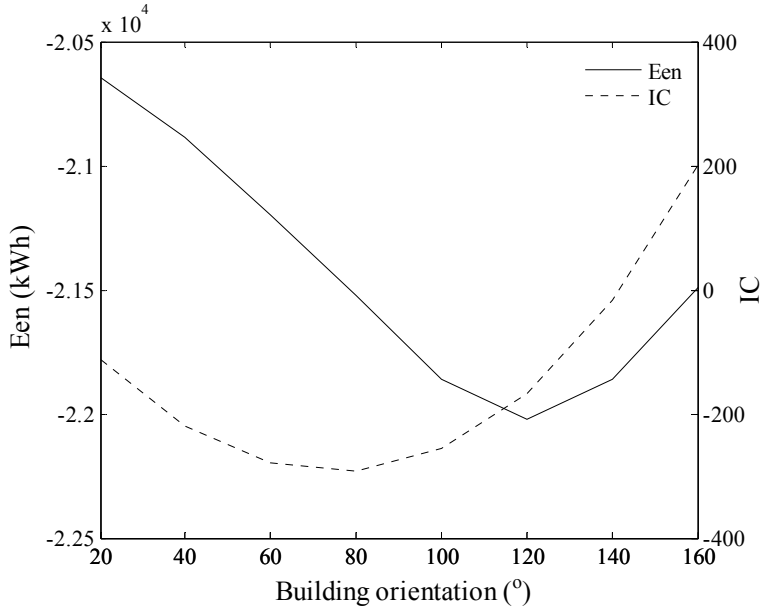

Figure 9.7 E_{en} and IC vs. building orientation.

Lower E_{en} can be obtained at the building orientation of 120° because the building facade receive less beam radiation at this orientation. Compared with diffuse radiation, beam radiation has less energy saving potential. The reason is that the intensity of beam radiation may be much higher than that of diffuse radiation under many sky conditions, thus results in large cooling load. For example, the analysis of the weather data of Hong Kong shows that the hourly beam solar radiation on building facade may be 5-7 times higher than diffuse solar radiation under clear sky condition. Therefore, blinds have to be more frequently utilized, which may result in great reduction in the energy saving from daylighting.

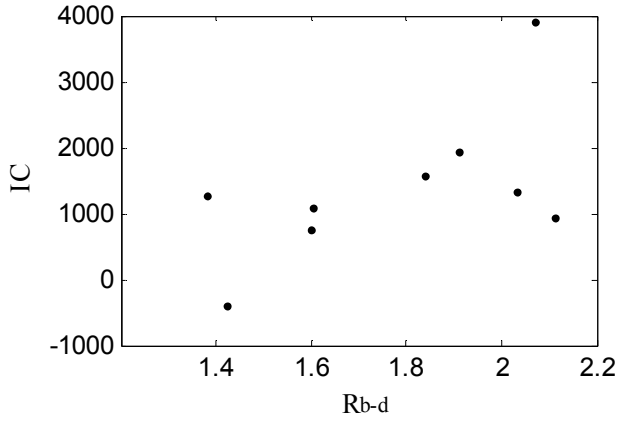

Figure 9.8 *IC* of $R_{b\text{-}d}$ on E_{en}

Sensitivity analysis was conducted to study the sensitivity of E_{en} to $R_{b\text{-}d}$, which is the ratio between annual total beam and diffuse radiation incident on the facade of the building. The considered window type is RLV and *WWR* equals 0.35, which are the optimal values obtained from Section 9.4. *ICs* of $R_{b\text{-}d}$ on E_{en} are shown in Figure 9.8. We can see that $R_{b\text{-}d}$ has positive influence on E_{en} under most cases, which means high $R_{b\text{-}d}$ leads to large energy consumption.

9.4.2 Sensitivity analysis of WWR

Figure 9.9 shows the distribution of *IC* over the range of *WWR*. We can see that E_{en} is more sensitive to *WWR* that ranges from 0.0 and 0.2. *IC* of *WWR* is not uniformly distributed over the whole range of *WWR*. It ranges from -225043 to 2008 with the averaged value of -2049.6. In some previous works (Lam *et al*. 2008; Heiselberg *et al*., 2009), averaged sensitivity is use to evaluate the influence of design parameters on the output. This method is not suitable for the analysis of *WWR*. If only the average *IC* is provided to the designer, designer may get a wrong impression that the window area should be as large as possible

to save more energy, which may lead to large energy consumption.

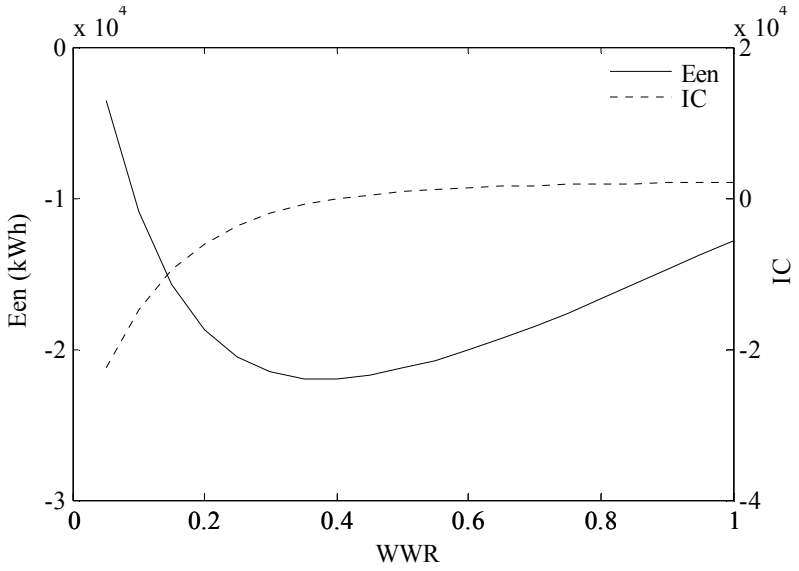

Figure 9.9 E_{en} and *IC* vs. *WWR*.

Table 9.3 summarizes the optimal *WWRs* for different windows. From it we found the optimal *WWR* decreases with the optical transmittance. That is because, with higher optical transmittance, more light can enter the building through unit area of window. Then the required daylight to reach the saturation status, where most of the reference points have daylight illuminance higher than the design illuminance, can be achieved with small window area. Table 9.3 also shows that the building orientation of 20º has higher optimal *WWR* than the building orientation of 120º. Our analysis with the weather data of Hong Kong indicates that the building orientation of 20º receives more solar beam radiation. Therefore, the blinds system has to be more frequently used to reduce solar heat gain. The utilization of blinds may greatly reduce the amount of daylight that enters the building through unit area of window. Thus larger window area need to be

adopted to achieve higher lighting energy saving.

9.4.3 Sensitivity of window type

We imagined four window types to study the influence of different window parameters on E_{en},. Among these imagined windows, $RLV_1(\tau_t)$, $RLV_2(\alpha)$, $RLV_3(T_v)$ and $RLV_4(\rho_i)$ have variable τ_t, α, T_v and ρ_i while all other parameters are the same as those of RLV. All window parameters range from 0.0 to 1.0 with an internal of 0.1. Then the influence of different window parameters on E_{en} can be evaluated by comparing results of the imagined windows and that of RLV.

The influence of T_v and ρ_i on E_{en} are shown in Figures 9.7 and 9.8. As T_v increases, E_{en} becomes less and less sensitive to T_v. This is because the lighting saving increases quickly with the increase of T_v at the beginning and then gradually approaches to a saturation status, where most of the indoor reference points have daylight illuminance higher than the required level. After this status, the surplus daylighting has few effects on lighting energy saving, but may add some cooling loads.

Similar to *WWR*, the influence of T_v on E_{en} is not uniformly distributed. Comparison between Figures 9.10 and 9.11 shows that ρ_i has much less influence than T_v.

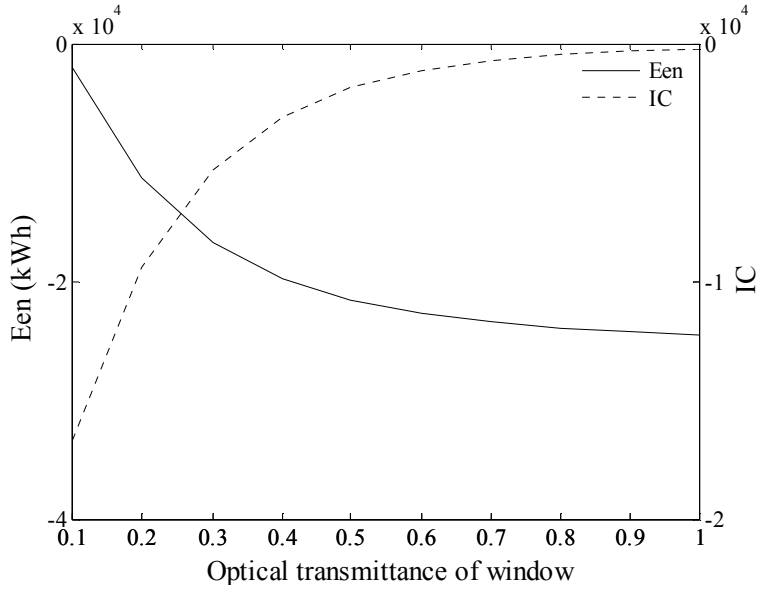

Figure 9.10 E_{en} and IC vs. T_v.

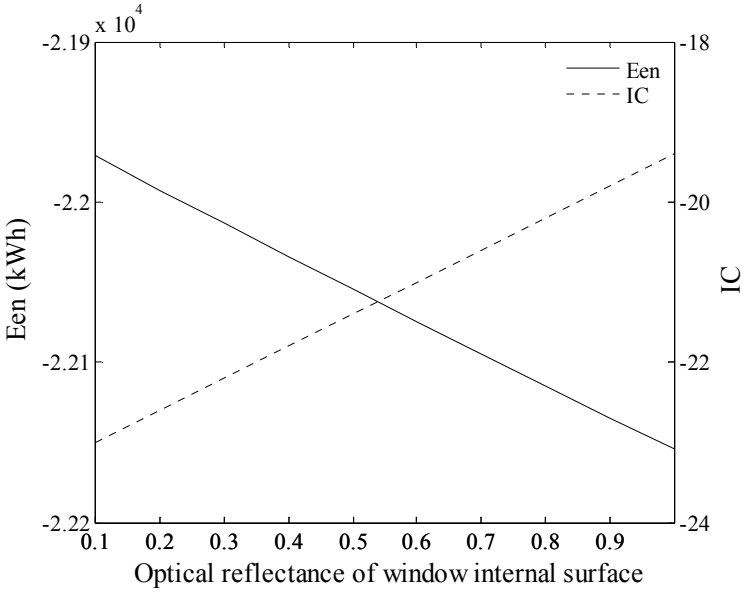

Figure 9.11 E_{en} and IC vs. ρ_i.

The influence of τ_t on E_{en} is shown in Figure 9.12. Unlike the case with variable T_v and ρ_i, there is a linear relationship between E_{en} and τ_t, which results in a constant value of IC over the whole range of τ_t. The influence of α on E_{en} is shown in Figure 9.13. The analysis results are very similar to those of ρ_i. Comparison between Figures 9.12 and 9.13 shows that τ_t has much more

influence than α.

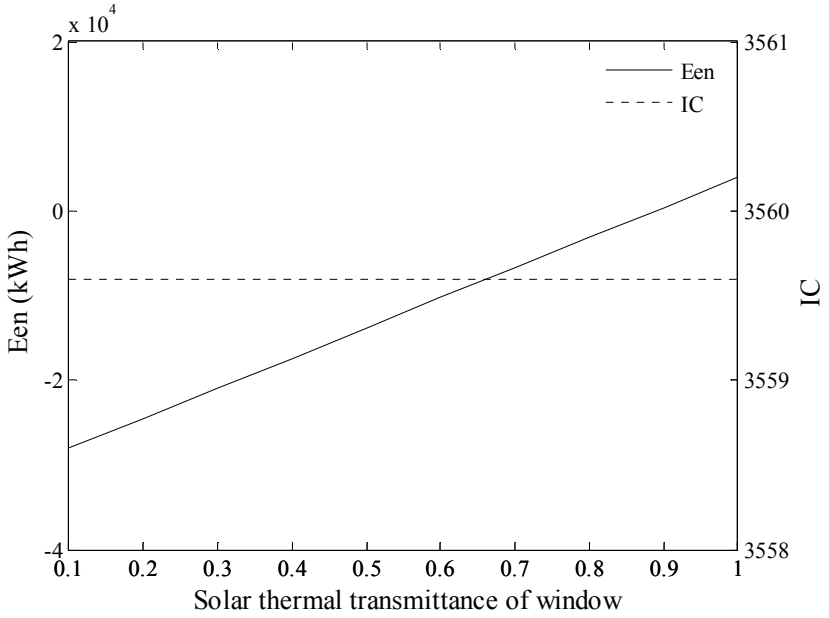

Figure 9.12 E_{en} and IC vs. τ_t.

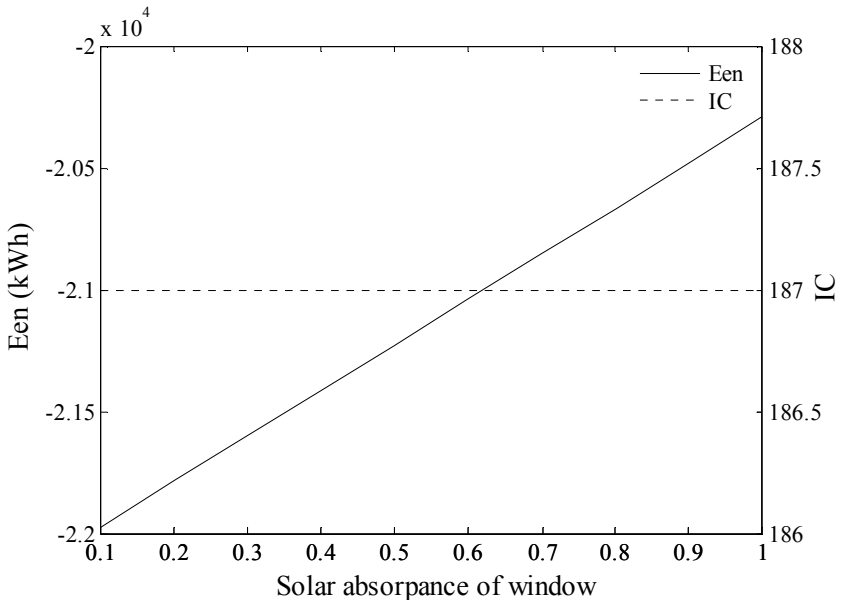

Figure 9.13 E_{en} and IC vs. α.

9.5 Summary

Based on an office building in Hong Kong as an example, the dayligting and thermal simulation models developed in Chapters 5, 6 and 8 are used for the

optimal design and sensitivity analysis of long-term energy consumption related with building envelope. The numeration method is used for the optimization of windows, and the hill-climbing method is used to find the optimal combination of building orientation and *WWR*. The hill-climbing method is used because our pre-examination of the objective function shows that there is only one global optimal value over the whole range. Therefore, the problem of sticking to local optimal values can be avoided. Hill-climbing method greatly reduces the amount of calculation. Less than 10% of the totally 378 design alternatives need to be calculated to achieve the optimal solution.

The sensitivity analysis shows that the solar thermal transmittance and absorpance of windows have constant influential coefficient *IC* over their whole range; while other design parameters have variable influence on E_{en}. For example, *WWR* and optical transmittance are more influential at small values. Building orientation has large influence on E_{en} because it determines the amount of beam and diffuse solar radiation incident on the building facade. E_{en} increases with the ratio between annual total beam and diffuse radiation incident on the building facade. Generally, E_{en} is more sensitive to building orientation, *WWR*, and the optical and solar thermal transmittance of windows. Designer should pay more attention to these design parameters in the optimal design.

Previous common practice using the mean influence of design parameters

to evaluate the sensitivity of outputs to each parameter may lead to inaccurate or even misleading information if there is a non-linear relationship between the output and the design parameters. For example, our sensitivity analysis shows that the *IC* of *WWR* ranges from -10703 to 1437 with the averaged value of -676.25. If only the average *IC* is provided to the designer, designer may get a wrong impression that the window area should be as large as possible to save more energy, which may lead to large energy consumption. Similar problems occur with building orientation, optical transmittance of window and the reflectance at the internal surface of the window. The sensitivity of E_{en} to these design parameters should be evaluated based on the influence over their whole ranges.

CHAPTER 10

CONCLUSIONS AND RECOMMENDATIONS

10.1 Conclusions

The optimal design of a building in the initial design stage involves detailed evaluation of the impacts of many design variations and design alternatives, which requires a great amount of calculations. This thesis presents a methodology that integrates accurate and efficient models for daylighting and thermal simulations. First, the accuracy of daylighting simulations with venetian blinds by DOE2 and Adeline and the assumptions adopted in them were examined by experiments conducted in a full-scale classroom. Experimental results show that the assumptions adopted by DOE2 and Adeline may result in large errors. Therefore, a mathematical daylighting simulation model was developed for reasonable prediction of indoor daylight illuminance with venetian blinds. The new model is based on geometric optics, radiosity method and radiation transfer. It considers the different features of daylights passing through blinds. The new model carefully calculates the reflections among the blinds, window glazing and indoor surfaces. Thus the balance of light during the reflections can be guaranteed. The model is of very high computational efficiency, and is particularly useful for optimal design and parametric analysis. The new model has been validated with experiments. Validation results show that the new model is slightly less accurate than Radiance, but much more accurate than

Adeline, DOE2 and EnergyPlus.

A new method has been developed for the direct and rigorous calculation of response factors of multilayered slabs. This method is based on fast Fourier transform (FFT), hence it does not have the errors due to missed roots during numerically searching for the poles of the image function of solutions to heat conduction through multilayered slabs. Z-transfer coefficients have been generated by the least square method with the accurate response factors. Validation results show that cooling loads computed with the same number of z-transfer coefficients obtained by this method are much more accurate than those by the conventional method.

A novel method has been developed for the direct calculation of life-cycle, annual or seasonal cooling loads without the need for hourly simulations. The method is primarily based on the principle of superposition, symbolic network analysis as well as FFT. The principle of the method has been presented and applied to a simple example in Hong Kong. With the symbolic response factors obtained by the FFT method, the new method can generate the symbolic functions of long-term cooling loads, keeping important design parameters as symbols. This could significantly facilitate the optimal design and parametric analysis of buildings. The new model has been validated by the thermal simulations of DOE2.

The new methodology has been applied in the optimal design of a side-lit building in Hong Kong. The optimization of building envelope is aimed at reducing the annual energy consumption related with room envelope, and to minimize the operation and embodied energy use. The design variables include building orientation, window-to-wall ratio (*WWR*), and window type. As the objective function does not have local optimal solution, hill-climbing method was used in the optimization, which greatly reduces the number of calculations. Optimization results show that selected design variables greatly impact the energy performance. A sensitivity analysis is conducted to investigate the influence of each design variable on the building energy performance. Results show that the solar thermal transmittance and absorpance of the window have constant influence on the building energy consumption, while *WWR* and the optical transmittance of the window have variable influence. *WWR*, building orientation, the optical and solar thermal transmittances of the window are more influential than other design parameters.

10.2 Further investigation

The model for the simulation of blinds developed in Chapters 5 and 6 only considers flat slats with diffuse-reflecting surfaces. More research work should be conducted to simulate the curved slats and specular-reflecting surfaces. Geometric analysis may be used to calculate direct transmittance of diffuse sky

light. For curved slats with diffuse-reflecting surfaces, the daylight factor on slats, and the view factors between adjacent slats may be functions of slat curvature, tilt angle and dimension of the blinds. These functions may be derived through the geometrical analysis similar to that for flat slats. Then the radiostiy method can be used to simulate the multi-reflections of light between slats. For slats with specular-reflecting surface, the amount and directions of the light that passes through the blinds after the multi-reflections among slats may be determined through the analysis of both the incident angle of the incoming light and the number of reflections between adjacent slats.

Data input and computational efficiency are two equally important aspects in the optimization of building envelopes at the initial design stage. The former aspect has not been well dealt with in this study. An expert system may be further developed to automatically provide all the essential data and design variable ranges and the calculation mode based on the intentions of building designers, which can significantly avoid heavy loads in inputting the detailed data required for the optimization. This expert system is then integrated with the computer method developed in this thesis to form a full solution to the initial design and optimization of building envelopes.

REFERENCES

ADELINE 1.0, 1994, Acronym for Advanced Daylighting and Electric Lighting Integrated New Environment, a product of the International Energy Agency (IEA) Solar Heating and Cooling Program, Task 12: Building Energy Analysis and Design Tools for Solar Applications.

Al-Homoud M.S., 2001, Computer-aided building energy analysis techniques, Building and Environment 36, p421-433.

Anton H., 2005, Elementary Linear Algebra, Hoboken, N.J., : John Wiley & Sons, Inc.

Aleo F., Sciuto S., Viadana R., 1994, Solar transmission measurements in outdoor conditions of non-homogeneous shading device, in: Proceedings of the European Conference on Energy Performance and Indoor Climate in Buildings, Lyon, France.

Andersen A., Rubin M., Powles R., Scartezzini J.L., 2005, Bi-directional transmission properties of Venetian blinds: experimental assessment compared to ray-tracing calculation, Solar Energy 78, p187-198.

ASHRAE Handbook of fundamentals, 1993, Atlanta, USA: American Society of Heating, Refrigeration and Air-Conditioning Engineers, Inc.

ASHRAE Handbook of fundamentals, 1997, Atlanta, USA: American Society of Heating, Refrigeration and Air-Conditioning Engineers, Inc.

ASHRAE Handbook of fundamentals, 2001, Atlanta, USA: American Society of Heating, Refrigeration and Air-Conditioning Engineers, Inc.

ASHRAE Handbook of fundamentals, 2005, Atlanta, USA: American Society of Heating, Refrigeration and Air-Conditioning Engineers, Inc.

Athienitis A.K., 1987, Discrete Fourier series models for building anxiliary energy loads based on network formulation techniques, Solar Energy 39(3), p203-210.

Athienitis A.K., Tzempelikos A., 2002, A methodology for simulation of daylight room illuminance distribution and light dimming for a room with a controlled shading device, Solar Energy 72 (4), p271-281.

Bodart M., De Herde A., 2002, Global energy savings in offices buildings by the use of daylighting, Energy and Buildings 34, p421-429.

Breitenbach J., Lart S., Langle I., Rosenfeld J.L.J., 2001, Optical and thermal performance of glazing with integral venetian blinds. Energy and Building 2001; 33, p433-442.

Brigham E.O., 2002, The Fast Fourier Transform, New York: Prentice-Hall.

Bryan H.J., Clear R.D., 1981, Calculating interior daylight illumination with a programmable hand calculation, Journal of the Illuminating Engineering Society 10.4, p219-227.

Building energy data book, 2003, Department of Energy, US.

Chan A.L.S., Chow T.T., Fong S.K.F., Lin J.Z., 2003, Generation of a typical meteorological year for Hong Kong, Energy Conversion and Management, 47, p87-96.

Chantraarisalai C., Fisher D.E., 2004, Comparative analysis of one-dimensional

slat-type blind models, In: Proceedings of SimBuild, Boulder, Colorado, USA, p1-10.

Chen T.Y., Athienitis A.K., 1993, Computer generation of semi-symbolic thermal network functions of buildings, Building and Environment, 28(3), p301-309.

Chen T.Y., 1997, A Methodology for Thermal Analysis and Predictive Control of Building Envelope Heating Systems, Ph.D Thesis, Concordia University, Montreal.

Chen T.Y., Burnett J., Chau C.K., 2001, Analysis of embodied energy use in the residential building of Hong Kong, Energy Conversion and Management 47, p87-96.

Chen T.Y., 2003, A method for the direct generation of comprehensive numerical solar building transfer functions, Solar Energy 74, p123-132.

Choi U.S., Johnson R., Selkowitz S., 1984, The impact of daylighting on peak electrical demand, Energy and Building 6, p387-399.

Chung T.M., 1992, A study of luminous efficacy of daylight in Hong Kong, Energy and Buildings 19, p45-50.

CIE, 1973, Standardisation of luminance distribution on clear skies, Publication No 22, CIE, Paris.

CIE-TC-3-33, 2004, Test cases to assess the accuracy of lighting computer programs, First draft, Commission Internationale de l'Eclairage, Vienne.

Clarke J.A., 2001, Energy simulation in building design, Butterworth-Heinemann.

Cofaigh E.O., Fitzgerald E., Alcock E., McNicholl R., Peltonen V., Marucco A., 1999, A green Vitruvius-principles and practice of sustainable architecture decisions, Building Research & Information 27(1), p20-34.

Crawkey, D.B., Lawrie L.K., Winkelmann F.C., Buhl W.F., Huang Y.J., Pedersen C.O., Strand R.K., Liesen R.J., Fisher D.E., Witte M.J., Glazer J., 2001, EnergyPlus: creating a new-generation building energy simulation program, Energy and Buildings 33 (4), p319-331.

Davies M.G., 1973, The thermal admittance of layered walls, Building Science 8, p207-220.

Davies M.G., 1996, A time-domain estimation of wall conduction transfer function coefficients, ASHRAE Transactions 102(1), p328-343.

Davies M.G., 1997, Wall transient heat flow using time-domain analysis, Building and Environment 32(5), p427-446.

Deiman. E.P., Platt H.T., 1993, Cost information in succeeding stages of the design process. Advanced Technologies, p327.

Desoer C.A., Kuh E.S., 1969, Basic Circuit Theory, McGraw-Hill, New York.

DOE-2 Engineers Manual, 1982, Lawrence Berkeley Laboratory, University of California, Berleley, CA 94720 and Los Alamos National Laboratory, Los Alamos, NM 87545.

Eicker U., Solar Technologies for Buildings, Wiley, New York, 2003.

Energy efficiency trends in Canada 1990-2001, 2003, Ottawa: Natural Resources Canada.

EnergyPlus Engineering Reference, Lawrence Berkeley National Laboratory, Ernest Orlando, 2010.

Frank P.I., David P.D., 2002, Fundamentals of Heat and Mass Transfer, John Willey&Sons.

Freewan A.A., Shao L., Riffat S., 2008, Optimizing performance of the lightshelf by modifying ceiling geometry in highly luminous climates, Solar Energy 82, p343-353.

Galasiu A.D., Atif M.R., 2002, Applicability of daylighting computer modeling in real case studies: comparison between measured and simulated daylight availability and lighting consumption, Building and Environment 37, p363-377.

Galasiu A.D., Atif M.R., MacDonald R.A., 2004, Impact of blinds on daylight-linked dimming and automatic on/off lighting controls, Solar Energy 76, p523-544.

Ghisi E., Tinker J.A., 2005, An ideal window area concept for energy efficient integration of daylight and artificial light in building, Building and Environment 40, p51-61.

Gui X.M., Li C.H., Chai C.Z., 1993, Handbook of Mathematics, Shanghai Popular Science Press, Shanghai.

Harris S.M., McQuiston F.C., 1988, A study to categorize walls and roofs on the basis of thermal response, ASHRAE Transactions 94(2), p688-714.

Heiselberg P., Brohus H., Hesselholt A., Rasmussen H., Seinre E., Thomas S.,

2009, Application of sensitivity analysis in design of sustainable buildings, Renewable Energy 34, p2030-2036.

Hittle D.C., 1979, Building loads analysis and system thermodynamic (BLAST) programs, Version 2.0: Users Manual. Technical Report E-153, US Army Construction Engineering Research Laboratory (USACERL), Champaign, IL.

Hittle D.C., Bishop R., 1983, An improved root-finding procedure for use in calculating transient heat flow through multilayer slabs, Internal Journal of Heat and Mass Transfer 26(1), p1685-1693.

Hopkinson R.G., Petherbridge P., Longmore J., 1966, Daylighting, Heineman, London.

Hviid C.A., Nielsen T.R., Svendsen S., 2008, Simple tool to evaluate the impact of daylight on building energy consumption, Solar Energy 82, p787-798.

Incropera E.P., Dewitt D.P., Bergman T.L., Lavine A.S., 2007, Fundamentals of Heat and Mass Transfer, Hoboken, NJ: John Wiley.

Jiten K., 1984, Dictionary of Geometry, Shanghai, China: Shanghai Jiao Yu Publisher.

Kerrisk J.F., Schnurr N.M., Moore J.E., Hunn B.D., 1981, Custom weighting-factor method for thermal load calculations in the DOE-2 computer program, ASHRAE Transactions 87, p569-584.

Klein S.A., Beckman W.A., Mitchell J.W., 1994, TRNSYS – a transient system simulation program, Solar Energy Laboratory, University of Wisconsin –

Madision, Madison, USA.

Kotey N.A., Wright J.L., 2006, Simplified solar optical calculations for windows with venetian blinds, In: Proceedings of 31st Annual Meeting of the Solar Energy Society of Canada, Inc, Montreal, August.

Krarti M., Erickson P.M., Hillman T.C., 2005, A simplified method to estimate energy savings of artificial lighting use from daylighting, Building and Environment 40, p747-754.

Lam J.C., Li D.H.W., 1999, An analysis of daylighting and solar hear for cooling-dominated office buildings, Solar Energy 65 (4), p251-262.

Lam J.C., Chan R.Y.C., Tsang C.L., Li D.H.W., 2004, Electricity use characteristics of purpose-built office buildings in subtropical climates, Energy Conversion and Management 45 (6), 829-844.

Lam J.C., Wan K.K.W., Yang L., 2008, Sensitivity analysis and energy conservation measures implications, Energy Conversion and Management 49, p3170-3177.

LBNL, 1982, DOE-2 Engineer manual – Version 2.1A, LBNL, University of California Berkeley.

Lee E.S., Selkowitz S.E., 1995, The design and evaluation of integrated envelope and lighting control strategies for commercial building, ASHRAE Transaction 101(1), p326-342.

Li D.H.W., Lau C.C.S., Lam J.C., 2004, Predicting daylight illuminance by computer simulation techniques, Lighting research and technology 36 (2),

p113-129.

Littlefair P.J., 1994, A comparison of sky luminance models with measured data for Garston, United Kingdom, Solar Energy 53(4), p315-322.

Mardaljevic J., 1995, Validation of a lighting simulation program under real sky conditions, Lighting Research and Technology 27 (4), p181-188.

Mardaljevic J., 2000, Simulation of annual daylighting profiles for internal illuminance, Lighting Research & Technology 32(3), p111-118.

Mardaljevic J., 2001, The BRE-IDMP dataset: a new benchmark for the validation of illuminane prediction techniques, Lighting Research & Technology 33(2), p117-136.

Miles J.C., Sisk G.M., Moore C.J., 2001, The conceptual design of commercial building using a genetic algorithm, Computers and Structures 79, p1583-1592.

Moon P., Spencer D.E., 1942, Illumination from a non-uniform sky, Illuminating Engineering 37, p707-726.

Ne'eman E., Hopkinson R.G., 1970, Critical minimum acceptable window size: a study of window design and provision of a view, Lighting Research and Technology 2(1), p17-27.

Ouarchi R., Krarti M., 2006, Building shape optimization using neural network and genetic algorithm approach, ASHRAE Transactions 112, p484-491.

Ouyang K., Haghighat F., 1991, A procedure for calculating thermal response factors of multilayer walls – state space method, Building and Environment

26(2), p173-177.

Park C., Clark D.R., Kelly G.E., 1986, HVACSIM+ building systems and equipment simulation program: building loads calculation, NBSIR 86-3331, National Bureau of Standards.

Parmelee G.V., Aubele W.W., 1952, The shading of sun glass: an analysis of the effect of uniformly spaces flat opaque slats. ASHVE Transactions 58, p377-398.

Perez R., Seals R., Michalsky J., 1993, All-weather model for sky luminance distribution – preliminary configuration and validation, Solar Energy 50(3), p235-245.

Pipes L.A., 1957, Matrix analysis of heat transfer problems, Journal of the Franklin Institute 263, p195-206.

Pfrommer P., Lomas K.J., Kupke C., 1996, Solar radiation transport through slat-type blinds: a new model and its application for thermal simulation of buildings. Solar Energy 57(2), p77-91.

Phillips C.L., Parr J.M., 1999, Signals, Systems, and Transforms. Prentice-Hall, Inc.

Rabl A., Riahle A., 1992, Energy signature model for commercial buildings: test with measured data and interpretation, Energy and Buildings 19, p143-154.

Radiance Material Library, Lawrence Berkeley National Laboratory, Ernest Orlando, 2010.

Rea M.S., 2000, The IESNA lighting handbook: reference&application, New York: Illuminating Engineering Society of North America.

Reinhart C.F., Walkenhorst O., 2001, Validation of dynamic RADIANCE-based daylight simulations for a test office with external blinds, Energy and Buildings 33, p683-697.

Reinhart C.F., Andersen M., 2006, Development and validation of a Radiance model for a translucent panel, Energy and Buildings 38, p890-904.

Reinhart C.F., Fitz A., 2006, Finding from a survey on the current use of daylighting simulations in building design, Energy and Buildings 38, p824-835.

Rich E., Knight K., 1991, Artificial Intelligence, New York: McGraw-Hill.

Saltelli A., Chan K., Scott E.M., 2000, Sensitivity Analysis, Chichester; New York: Wiley.

Sillion F.X., Puech C., 1994, Radiosity&Global Illuminance, Morgan Kaufmann Publishers, INC, San Francisco, California.

Sowell E.F., Hittle D.C., 1995, Evolution of building energy simulation methodology. ASHRAE Transactions 101(1), p850-855.

Spitler J.D., Fisher D.E., 1999, Development of periodic response factors for use with the radiant time series method, ASHRAE Transactions 105(2), p491-502.

Stephenson D.G., Mitalas G.P., 1967, Room thermal response factors, ASHRAE Transactions 73, pIII 1.1-1.7.

Stephenson D.G., Mitalas G.P., 1971, Calculation of heat conduction transfer functions for multilayer slabs, ASHRAE Transactions 77(2), p117-126.

Strand R., Winkelmann F., Buhl F., Huang J., Liesen R., Pedersen C., Fisher D., Taylor R., Crawley D., Lawrie L., 1999, Enhancing and extending the capabilities of the building heat balance simulation technique for use in energyplus, Proceedings of Building Simulation' 99, Vol II, Kyoto, Japan, September 1999, p653-657.

Szermann M., Stoffel J., 1999, ADELINE 3.0, SUPERLINK/RADLINK Technical Manual, Fraunhofer-Institut für Bauphysik, 70569 Stuttgart, Germany.

Tavares P.F.A.F., Martins A.M.O.G., 2007, Energy efficient building design using sensitivity analysis - A case study, Energy and Buildings 39, p23-31.

Tian C., Chen T.Y., 2009, Experimental validation of daylight simulation tools, RADIANCE, Adeline and DOE2, 3rd International Conference on Experiments/Process/System Modeling/Simulation & Optimization, Athens, Greece.

Tian C., Chen T.Y., Yang H.X., Chung T.M., 2010, A generalized window energy rating system for typical office buildings, Solar Energy 84, p1232-1243.

Tregenza P.R., Waters I.M., 1983, Daylight coefficients, Lighting Research & Technology 15(2), p65-71.

Tuhus-Dubrow D., Krarti M., 2010, Genetic-algorithm based approach to optimize building envelope design for residential buildings, Building and

Environment 45, p1574-1581.

Tzempelikos A., 2008, The impact of venetian blind geometry and tilt angle on view, direct light transmission and interior illuminance, Solar Energy 82, p1172-1191.

Ward G.J., Rubinstein M., 1988, A new technique for computer simulation of illuminated spaces, Journal of the Illuminating Engineering society 1, p80-91.

Ward G.J., Shakespeare R., 1998, Rendering with Radiance: the art and science of lighting visualization, San Francisco, California: Morgan Kaufmann.

WinDat, 2006, Window Information System software (WIS), WinDat Thematic Network, TNO Bouw, Netherlands.

Winkelmann F.C., Selkowitz S., 1985, Daylighting simulation in the DOE-2 building energy analysis program, Energy and Buildings 8, p271-286.

Yan Q.S., Zhao Q.Z., 1986, Building Thermal Process, China Architecture & Building Press.

Yang S.M., 1980, Heat Transfer, Higher Education Press, Beijing.

Yang W.L., Teng G.L., 1992, Higher Mathematics, Tianjin: Tianjin University Press.

Zhao Z.M., 1984, Handbook of Lighting Engineering, Tianjin: Tianjin Science and Technology Press.

APPENDICES

APPENDIX A

CALCULATION OF THE TEMPAREAURE INCREASE DURING THE OCCUPIED HOURS

Let $Y_{a,c}$ be the response factor for the calculation of temperature increase due to a heat source. At the occupied hour n_1+1 (the first occupied hour), the temperature increase $\Delta T_{a,on}$ may be calculated by:

$$\begin{aligned}
&\Delta T_{a,on}(n_1+1)=\sum_{i=0}^{\infty}Y_{a,c}(i)Q_{c,c}(n_1+1-i)\\
&=0+Y_{a,c}(1)Q_{c,c}(n_1+1-1)+Y_{a,c}(2)Q_{c,c}(n_1+1-2)+\cdots+Y_{a,c}(24+n_1-n_2)Q_{c,c}(n_1+1-24-n_1+n_2)+0+\cdots+0\\
&+0+Y_{a,c}(24+1)Q_{c,c}(n_1+1-24-1)+Y_{a,c}(24+2)Q_{c,c}(n_1+1-24-2)+\cdots+Y_{a,c}(48+n_1-n_2)Q_{c,c}(n_1+1-48-n_1+n_2)+0+\cdots+0\\
&+0+Y_{a,c}(48+1)Q_{c,c}(n_1+1-48-1)+Y_{a,c}(48+2)Q_{c,c}(n_1+1-48-2)+\cdots+Y_{a,c}(72+n_1-n_2)Q_{c,c}(n_1+1-72-n_1+n_2)+0\\
&+\cdots\\
&=\sum_{i_1=0}^{\infty}\sum_{i=1}^{24+n_1-n_2}Y_{a,c}(24i_1+i)Q_{c,c}(-24i_1-i+n_1+1)
\end{aligned}\tag{A.1}$$

Using the same method, $\Delta T_{a,on}$ at hour n_1+2 (second occupied hour) and n_2 (last working hour) may be calculated by:

$$\Delta T_{a,on}(n_1+2)=\sum_{i_1=0}^{\infty}\sum_{i=1}^{24+n_1-n_2}Y_{a,c}(24i_1+i+1)Q_{c,c}(-24i_1-i+n_1+1)\tag{A.2}$$

$$\Delta T_{a,on}(n_2)=\sum_{i_1=0}^{\infty}\sum_{i=1}^{24+n_1-n_2}Y_{a,c}(24i_1+i+n_2-n_1-1)Q_{c,c}(-24i_1-i+n_1+1)\tag{A.3}$$

Equations (A.1), (A.2) and (A.3) are very similar, only differ in the order number of $Y_{a,c}$. Then they may be generalized as:

$$\Delta T_{a,on}(m)=\sum_{i_d=0}^{\infty}\sum_{i=1}^{24+n_1-n_2}Y_{a,c}(24i_d+i-n_1+m-1)Q_{c,h}(-24i_d-i+n_1+1)\tag{A.4}$$

where $m = n_1$+1, n_1+2, …, n_2.

APPENDIX B

CALCULATION OF THERMAL ADMITTANCE AND IMPEDANCE

On the basis of the Laplace transformation of the partial differential equation governing one-dimensional dynamic heat conduction, a homogeneous slab can be represented by a two port thermal network (Davies, 1973) as shown below.

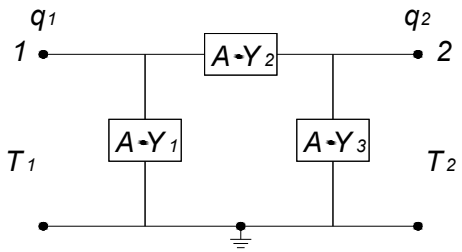

Figure B.1 Delta-connected thermal network of a homogeneous slab.

where A is the area of the slab, Y_1, Y_2 and Y_3 are thermal admittances of the unit area of a homogeneous slab.

The three thermal admittances Y_1, Y_2 and Y_3 may be expressed as:

$$Y_1(s) = Y_3(s) = \frac{\cosh\left(\sqrt{s/a}l\right) - 1}{\sinh\left(\sqrt{s/a}l\right) / \left(\lambda\sqrt{s/a}\right)}$$

$$Y_2(s) = \frac{1}{\sinh\left(\sqrt{s/a}l\right) / \left(\lambda\sqrt{s/a}\right)}$$

where s is the Laplace variable; a is the thermal diffusivity; l is the slab thickness; λ is the conductivity of the slab material and A is the area of the slab.

The three thermal admittances Y_1, Y_2 and Y_3 of a double-layered wall may be

calculated by recursive formulas as follows (Chen, 1997):

$$Y_2^*(s) = \frac{Y_2 Y_2^{'}}{Y_2 + Y_3 + Y_1^{'} + Y_2^{'}} \tag{B.1}$$

$$Y_1^*(s) = Y_1 + \frac{Y_2\left(Y_3 + Y_1^{'}\right)}{Y_2 + Y_3 + Y_1^{'} + Y_2^{'}} \tag{B.2}$$

$$Y_3^*(s) = Y_3^{'} + \frac{Y_2^{'}\left(Y_3 + Y_1^{'}\right)}{Y_2 + Y_3 + Y_1^{'} + Y_2^{'}} \tag{B.3}$$

where Y and Y' represent the thermal admittance of each homogeneous layer of a two-layered wall; Y^* is the combined thermal admittance of the two-layered wall. Equations (B.1)-(B.3) can be used recursively for determining the overall admittances of a multi-layered wall.

Figure B.2 shows the sub-network of the external wall solar diffuse radiation active. A_e is the area of the external wall; T_{sd} is the imaginary solar diffuse temperature; r_{sol} is the solar absorpance of the external wall and y_o is the exterior convective coefficient. According to the Norton's theorem, Figure B.2 can be transformed to the Norton equivalent network shown in Figure B.3.

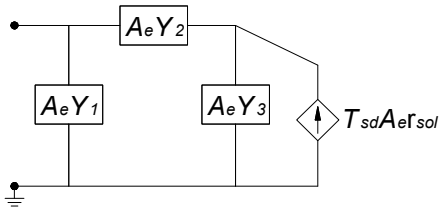

Figure B.2 Sub-network of the external wall with solar diffuse radiation active alone.

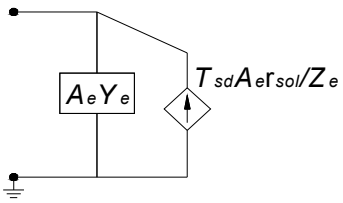

Figure A.3 Norton equivalent network of the external wall with solar diffuse radiation active alone.

The Norton equivalent thermal admittance Y_e and the transfer-impedance Z_e can be calculated by:

$$Y_e = Y_1 + \frac{Y_2(Y_3 + y_o)}{y_o + Y_2 + Y_3}$$

$$Z_e = \frac{y_o + Y_2 + Y_3}{Y_2}$$

The internal wall is assumed as symmetric and there is no heat flows through the central layer. Therefore, if the internal wall consists of $2n$+1layers, we only need to consider the n and half layers on the outside of the wall. Using the recursive Equations (B.1)-(B.3), we can have the combined thermal admittances of the n layers (Y_n^*) before the central layer. These admittances and a half of the central layer is shown in Figure B.4.

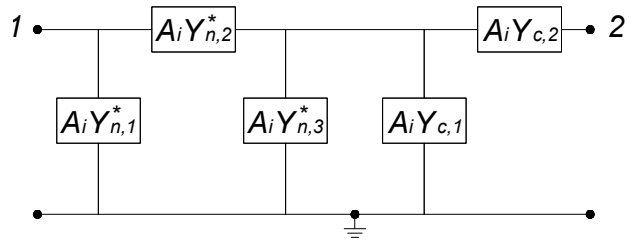

Figure B.4 The first n layers and a half of the central layer of the internal wall.

In Figure B.4, A_i is the area of the internal wall; $Y_{n,1}^*$, $Y_{n,2}^*$ and $Y_{n,3}^*$ are the combined thermal admittances of the n layers before the central layer; $Y_{c,1}$ and $Y_{c,2}$ are the thermal admittances of the central layer.

According to the Norton's theorem (Desoer and Kuh, 1969), Figure B.4 can be transformed to the Norton equivalent network shown in Figure B.5.

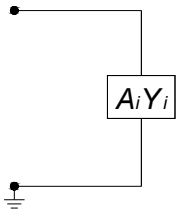

Figure B.5 Norton equivalent network of the internal wall.

where Y_i is the equivalent thermal admittance.

Similar to Y_e, Y_i can be calculated by:

$$Y_i = Y_{n,1}^* + \frac{Y_{n,2}^* \left(Y_{n,3}^* + Y_{c,1} \right)}{Y_{c,1} + Y_{n,2}^* + Y_{n,3}^*}$$

APPENDIX C

CALCULATION OF DIFFERENT HEAT SOURCES

The solar beam radiation incident on the vertical external wall facing the sun consists of two parts. The first part directly comes from the sun without any reflection; and the second part reaches the wall after the reflection on the outdoor ground. Therefore, Q_{sb} may be calculated by (ASHRAE Handbook, 2005)

$$Q_{sb} = \frac{IR_{h,b} \cos\theta_{sol}}{\sin\alpha_{sol}} + 0.5 IR_{h,b} \rho_{gr} \tag{C.1}$$

where $IR_{h,b}$ is the solar beam radiation on unobstructed horizontal plane in (W/m^2); ρ_{gr} is the ground reflectivity; θ_{sol} is solar incident angle on the external wall (º), which may be calculated by

$$\cos\theta_{sol} = \cos\alpha_{sol} \cos(\gamma_{rm} - \gamma_{sol})$$

with α_{sol} and γ_{sol} are solar altitude and azimuth (º); γ_{rm} is the building orientation (º).

The external wall not facing the sun can only receive the beam radiation reflected from the ground. Hence, Q_{sb} may be calculated by (ASHRAE Handbook, 2005)

$$Q_{sb} = 0.5 IR_{h,b} \rho_{gr} \tag{C.2}$$

Similar to Q_{sb}, the solar diffuse radiation on the vertical external wall Q_{sd} consists of the part directly coming from the sky and the part coming from the reflection on ground. It may be calculated by (ASHRAE Handbook, 2005)

$$Q_{sd} = IR_{h,d} R_d + 0.5 IR_{h,d} \rho_{gr} \tag{C.3}$$

where $IR_{h,d}$ is the diffuse solar radiation on unobstructed horizontal plane (W/m^2); R_d is the ratio of sky diffuse on vertical surface to sky diffuse on horizontal surface, which may be calculated by (ASHRAE Handbook, 2005)

$$R_d = \begin{cases} 0.55 + 0.437\cos\theta_{sol} + 0.313\cos\theta^2{}_{sol} & \text{for } \cos\theta_{sol} > -0.2 \\ 0.45 & \text{for } \cos\theta_{sol} \le -0.2 \end{cases} \tag{C.4}$$

The solar absorpance and solar thermal transmittance under different solar incident angles for windows with single glazing can be calculated by following equations (DOE-2 Engineers Manual, 1982).

$$r_{sb,ab}(\theta_{sol}) = r_{ab}(0)\left(1.564\cos^3\theta_{sol} - 3.957\cos^2\theta_{sol} + 3.48\cos\theta_{sol} - 0.083\right) \tag{C.5}$$

$$r_{sb,t}(\theta_{sol}) = r_t(0)\left(\frac{0.197}{0.111 + \cos\theta_{sol}} - 0.577\cos\theta_{sol} + 1.748\right) \tag{C.6}$$

where $r_{sb,ab}(\theta_{sol})$ and $r_{sb,t}(\theta_{sol})$ are the absorpance and thermal transmittance of the solar beam irradiance; $r_{ab}(0)$ and $r_t(0)$ are solar absorpance and solar thermal transmittance when the solar incident angle is 0°.

The diffuse solar absorpance $r_{sd,ab}$ and thermal transmittance $r_{sd,t}$ may be calculated by (DOE-2 Engineers Manual, 1982)

$$r_{sd,ab} = 1.08 r_{ab}(0) \tag{C.7}$$

$$r_{sd,t} = 0.87 r_t(0) \tag{C.8}$$

APPENDIX D

CALCULATION OF THE TILT ANGLE OF BLINDS THAT BLOCKS BEAM SUNLIGHT

According to our study in chapter 6, if the blinds just block the beam light, the blinds tilt angle β must satisfy the following equation:

$$\frac{\cos\gamma'_{sol}}{L'\left(\tan\alpha_{sol}\cos\beta+\sin\beta\cos\gamma'_{sol}\right)}=1 \tag{D.1}$$

where L' is the ratio between slat width and the distance between adjacent slats; α_{sol} is the solar altitude (º); γ'_{sol} is the difference between solar azimuth γ_{sol} and the window orientation γ_{win} (º), i.e. $\gamma'_{sol.} = \gamma_{sol} - \gamma_{win}$.

Equation (D.1) may be rewritten by:

$$\frac{\tan\alpha_{sol}}{\cos\gamma'_{sol}}\cos\beta+\sin\beta=\frac{1}{L'} \tag{D.2}$$

with

$$\sin\beta=\frac{2\tan\left(\beta/2\right)}{1+\tan^2\left(\beta/2\right)} \tag{D.3}$$

$$\cos\beta=\frac{1-\tan^2\left(\beta/2\right)}{1+\tan^2\left(\beta/2\right)} \tag{D.4}$$

Substituting Equations (D.3) and (D.4) into Equation (D.2), we have:

$$\frac{\tan\alpha_{sol}}{\cos\gamma'_{sol}}\left[1-\tan^2\left(\beta/2\right)\right]+2\tan\left(\beta/2\right)=\frac{1}{L'}\left[1+\tan^2\left(\beta/2\right)\right] \tag{D.5}$$

Rearrangement of Equation (D.5) yields:

$$t_1 \tan^2\left(\beta/2\right) - 2\tan\left(\beta/2\right) + t_2 = 0 \tag{D.6}$$

where

$$t_1 = \frac{1}{L'} + \frac{\tan\alpha_{sol}}{\cos\gamma'_{sol}}$$

$$t_2 = \frac{1}{L'} - \frac{\tan\alpha_{sol}}{\cos\gamma'_{sol}}$$

Solving Equation (D.6), we have two tilt angles that can block the beam light:

$$\beta_1 = 2\arctan\left(\frac{1+\sqrt{1-t_1t_2}}{t_1}\right) \tag{D.7}$$

$$\beta_2 = 2\arctan\left(\frac{1-\sqrt{1-t_1t_2}}{t_1}\right) \tag{D.8}$$

Equations (D.7) and (D.8) show that the tilt angle β_1 is always larger than β_2. In practice, we hope the tilt angle to be as small as possible, so more diffuse skylight can enter the room to replace the artificial lighting. Therefore, the smaller tilt angle β_2 is adopted in our daylighting simulations.